# CHEMICAL STRUCTURE ANALYSIS OF COAL HYDROGENATION PRODUCTS —— DISTRIBUTION OF STRUCTURAL PARAMETERS AND APPLICATION OF $^{13}C$ NMR TO STRUCTURAL ANALYSIS

Y. Maekawa, S. Ueda, Y. Hasegawa, Y. Nakata,
S. Yokoyama and Y. Yoshida

Government Industrial Development Laboratory, Hokkaido, Agency of Industrial Science and Technology, MITI, Japan
41-2, Higashi-Tsukisamu, Toyohiraku, Sapporo, Japan —— 061-01

In order to study the chemical structure of coal, Yubari coal ( C : 86.1, H : 6.2, N : 1.5, S : 0.3, O : 5.9 ) was subjected to mild hydrogenation with red mud catalyst under a reaction temperature of 400°C and 200 atm. of hydrogen pressure[1]. Under these conditions, it was found from previous studies[2] that the main reaction of decrease of the molecular weight is the cleavage of linkages of the structural units and the decomposition of structural units is limited.

The hydrogenation was conducted in a 5L rotating autoclave with an inner vessel set at a uniform temperature zone. The reaction time was changed 8 times from 26 to 206 min. ( exp. No. 502 - 509 ). The solvent soluble products were extracted with n-haxane, benzene and pyridine successively, which resulted in 5 fractions; oil-1 ( n-hexane solubles at room temperature ), oil-2 ( n-hexane solubles extracted by Soxhlet extractor ), asphaltene ( benzene solubles ), Py-1 ( pyridine solubles at room temperature ), Py-2 ( pyridine solubles extracted by Soxhlet extractor ). Regarding these hydrogenation reaction products, ultimate analysis, high resolution proton NMR spectroscopy and molecular weight measurement were carried out and the chemical reaction in Yubari coal in the course of hydrogenation was followed. From the above, structural analysis of the average structural unit of Yubari coal was conducted and reported[3].

This was followed by fractionation of the oil-2 ( Exp. No. 503, reaction time : 206 min. ) which corresponds to the mixture mainly consists of monomers of structural units[3], by GPC and each fraction was measured for $^1H$-NMR, $^{13}C$-NMR spectra, molecular weight and ultimate compositions. The structural parameters determined from the above fractions and the distribution of the structure of structural units were studied. At the same time, attempts to apply $^{13}C$-NMR spectroscopy to the structural analysis of coal hydrogenation products was carried out in this work.

## RESULTS AND DISCUSSION

### DISTRIBUTION OF STRUCTURAL PARAMETERS OF COAL HYDROGENATION PRODUCTS

For the fractionation of No. 503, oil-2 ( 503-O-2 ), 100 cm respectively of SG -1 ( theoretical plates / foot-T.P.F. = 1250 ) ( Shimadzu Seisakusho Ltd ) and SG-2 ( T.P.F = 1360 ) column were applied. $CHCl_3$ was used as the solvent, and the eluent flow rate was set at 1.5 ml. / min.. The eluted sample was divided into 15 fractions and the respective elution volume, yield ( against total eluted ), ultimate composition and molecular weight were shown in Table 1. Elution after 440 ml was colorless and it was recognized that elution was completed.

The $^1H$-NMR spectra of 503-O-2 and fractions separated from 503-O-2 were obtained on a GEOL JNM-PFT-100 spectrometer and shown in figure 1. The determination of chemical shifts of various functional hydrogens was carried out after the method of Bartle et al[4] and hydrogen distribution was calculated from figure 1. The percentage distribution of Ho, Hα, Ha in fractions separated from 503-O-2 by GPC were shown in figure 2. Based on the values of Table 1 and from the hydrogen

TABLE 1. - Yield, ultimate composition and molecular weight of fractions separated from 503-0-2 by GPC

| Fractionated sample No. | Range of elution volume ml. | Yield wt. % | Ultimate analysis C | H | N | O | S | M.W. (Mv) |
|---|---|---|---|---|---|---|---|---|
| 503-0-2 | - | - | 87.5 | 7.1 | 2.0 | 3.2 | 0.8 | 390 |
| Fr. 3 | 92 - 96 | 0.75 | 87.5 | 8.1 | 1.3 | 4.2 | - | 540 |
| Fr. 4 | 97 - 100 | 2.51 | 88.4 | 8.2 | 1.1 | 3.9 | - | 930 |
| Fr. 5 | 101 - 104 | 4.27 | 87.4 | 7.5 | 1.2 | 3.6 | - | 490 |
| Fr. 6 | 105 - 108 | 7.54 | 87.8 | 8.2 | 1.3 | 3.6 | - | 670 |
| Fr. 7 | 109 - 112 | 7.04 | 87.5 | 7.5 | 1.7 | 3.5 | - | 620 |
| Fr. 8 | 113 - 116 | 8.54 | 86.7 | 7.6 | 1.7 | 4.1 | - | 540 |
| Fr. 9 | 117 - 120 | 8.29 | 86.8 | 7.4 | 1.8 | 4.6 | - | 510 |
| Fr.10 | 121 - 128 | 17.84 | 86.8 | 7.1 | 1.8 | 3.8 | - | 360 |
| Fr.11 | 129 - 148 | 26.38 | 87.6 | 6.8 | 1.8 | 4.0 | - | 340 |
| Fr.12 | 149 - 168 | 7.29 | 85.8 | 6.5 | 2.4 | 5.8 | - | 270 |
| Fr.13 | 169 - 200 | 2.76 | 80.1 | 8.8 | 3.0 | - | - | 250 |
| Fr.14 | 201 - 252 | 1.76 | - | - | - | 17.0 | - | 310 |
| Fr.15 | 253 - 440 | 5.03 | 72.5 | 8.2 | 0.0 | 21.0 | - | 380 |

TABLE 2. - Structural parameters of fractions separated from 503-0-2 by GPC

| Samples | fa | Hau/ca | Ho/Hα | σT | σCH3*1 | σal'*2 | σCH2*3 | σo*4 |
|---|---|---|---|---|---|---|---|---|
| 503-0-2 | 0.69 | 0.75 | 1.2 | 0.40 | 0.04 | 0.23 | 0.08 | 0.05 |
| Fr. 4 | 0.57 | 0.61 | 2.8 | 0.45 | | 0.32 | 0.03 | 0.10 |
| Fr. 5 | 0.64 | 0.64 | 2.8 | 0.43 | 0.07 | 0.20 | 0.08 | 0.08 |
| Fr. 6 | 0.59 | 0.66 | 3.4 | 0.45 | 0.08 | 0.22 | 0.08 | 0.08 |
| Fr. 7 | 0.64 | 0.69 | 1.8 | 0.47 | 0.06 | 0.26 | 0.08 | 0.07 |
| Fr. 8 | 0.63 | 0.71 | 2.0 | 0.47 | 0.06 | 0.24 | 0.10 | 0.08 |
| Fr. 9 | 0.65 | 0.72 | 1.6 | 0.47 | 0.05 | 0.26 | 0.07 | 0.09 |
| Fr.10 | 0.68 | 0.68 | 1.6 | 0.43 | 0.05 | 0.24 | 0.06 | 0.07 |
| Fr.11 | 0.72 | 0.72 | 1.1 | 0.39 | 0.05 | 0.23 | 0.05 | 0.07 |
| Fr.12 | 0.76 | 0.75 | 1.1 | 0.34 | 0.06 | 0.16 | 0.04 | 0.09 |

*1 Substitution by $CH_3$ groups α to rings
*2 Substitution by aliphatic chain (except*1)
*3 Substitution by $CH_2$ groups α to two rings
*4 Substitution by oxygene containing groups

distribution calculated from figure 1, the structural parameters were calculated by partially modified Brown-Ladner method[3] and shown in Table 2. Regarding elution by GPC, as seen in theoretical work and experimental results conducted hitherto, it was recognized roughly that elution occurred in the order of high molecule to lower molecules. Thus from the parameter Hau/ca which is inversely proportional to the number of aromatic rings, a decrease of the number of aromatic rings in the order

of Fr. 4, 5, 6 of the initial elution is seen whereas in Fr.7 - 11 an approximately similar Hau/ca value is seen, namely, in Fr.7 - 11 which comprises the majority of 503-0-2 ( approx. 70% ) the aromatic ring size is approximately the same. Therefore, while the aromatic rings of structural units of 503-0-2 show a slightly sporadic presence, the majority is approximately the same and it may be surmized that the aromatic rings of the original Yubari coal are unified.

## APPLICATION OF $^{13}C$-NMR TO COAL HYDROGENATION PRODUCTS STRUCTURAL ANALYSIS

The $^{13}C$-NMR spectra of 503-0-2 and part of fractions which gave comparatively large yield are shown in Fig. 3. For the measurement of these spectra a JEOL, JNM-PFT 100 NMR spectrometer was applied. Decoupling of the protons was achieved with decoupler and spectra was accumulated by repetition of scanning ( 10000 - 30000 times ) to improve the signal to noise ratio.

$^{13}C$-NMR spectra are greatly simplified a signal enhancement due to the operation of $^{13}C$-$^{1}H$ overhauser effect is possible. The magnitude of the overhauser enhancement ordinarily differs for different $^{13}C$-Nuclei, and the spectra as is, generally can not be applied to quantitative analysis. Further the value of spin-latice relaxation time ($T_1$) shows different values with different $^{13}C$-Nuclei, and in a quantitative analysis, it is necessary to take sufficient longer pulse repetition time. In order to clarify the influense of the above two on the spectra, the $^{13}C$-NMR spectra in measured by changing the repetition time of the pulse and the ratio of Ca (aromatic carbon) against Cp (aliphatic carbon) is calculated from the intensity of the spectra. This is shown in Table 3.

TABLE 3. - Ca/Cp ratio of Yubari coal hydrogenation products under various pulse repetition times

| Samples | Pulse repetition time, sec. | Ca% | Cp% | Ca/Cp |
|---|---|---|---|---|
| Fr.11 | 0.8 | 0.668 | 0.332 | 2.0 |
| Fr.11 | 2.0 | 0.655 | 0.345 | 1.9 |
| 503-0-2 | 1.0 | 0.615 | 0.385 | 1.6 |
| 503-0-2 | 1.5 | 0.649 | 0.351 | 1.9 |
| 503-0-2 | 2.0 | 0.635 | 0.365 | 1.7 |
| 503-A | 1.0 | 0.689 | 0.311 | 2.2 |
| 503-A | 1.5 | 0.689 | 0.311 | 2.2 |

From the esults in Table 3, with regard to the sample used in the present work, no influence of the pulse repetition time was recognized or the Ca/Cp ratio, and at 0.8 sec of pulse repetition time already a quantitative spectra was obtained.

Regarding this it has been stated that this $^{13}C$-$^{1}H$ overhauser polarization might be eliminated by the presence of a paramagnetic species[5]. Inasmuch as a free radical exsists in the sample used in the present work, it is surmized that a similar effect exsists.

Based on this, it is possible to make a direct calculation of aromaticity (fa') using the spectra of Fig. 3. When this value and the fa value of Table 2 calculated from the assumption of x=y=2 lead from $^{1}H$-NMR are compared the fa/fa' value in Table 4 are both in the vicinity of 1.2, this indicated that the assumption x=y=2 is an over estimation. In the case of Fr.10, if the following is taken namely if x=y=1.5, fa is calculated as fa=0.60, which resembles fa' to a considerable extent.

In Fig. 3, the peaks are clearly identified the aromatic carbon (Ca) may be

subdivided into 4 species namely $Ca_1$, $Da_2$, $Ca_3$ and $Ca_4$ while the aliphatic carbon (Cp) may be subdivided into 9 species namely $Cp_1$, $Cp_2$, $Cp_3$, $Cp_4$, $Cp_5$, $Cp_6$, $Cp_7$, $Cp_8$ and $Cp_9$, while the data of the chemical shift in $^{13}C$-NMR is still insufficient, it may be surmized from the data collection[6] that $Cp_4$, $Cp_5$, $Cp_6$ are intimately related to the carbon of the chain β or father from ring $Cp_1$, $Cp_2$, $Cp_3$,are closely related to the α carbon atoms $Cp_8$, $Cp_9$ is closely related to the end methyl carbon atoms of the chains and $Cp_7$ is closely related to the α methyl carbon atoms.

TABLE 4. - Aromaticities of fractions separated from 503-0-2 by GPC

| Samples | fa*[1] | fa'*[2] | fa/fa' |
|---|---|---|---|
| 503-0-2 | 0.69 | 0.63 | 1.1 |
| Fr. 8 | 0.63 | 0.63 | 1.0 |
| Fr. 9 | 0.65 | 0.53 | 1.2 |
| Fr.10 | 0.68 | 0.57 | 1.2 |
| Fr.11 | 0.72 | 0.67 | 1.1 |
| Fr.12 | 0.76 | 0.65 | 1.2 |

fa*[1] Calculated from $^{1}H$-NMR spectra
fa*[2] Calculated from $^{13}C$-NMR spectra

From the ratio of $Cp_1$ - $Cp_3$ and $Cp_4$ - $Cp_6$, $Cp_8$, $Cp_9$ the mean chain length is obtained. This was compared with Hα/Hα + 1 and presented in Table 5 as shown a fairly good coincidence is seen. Further based on the above it may be surmized that the assumption x=y is feasible. Still further since x and y have a value close to 1.5 in the present sample, on the chain including the substitution on the naphthenic ring there would be a considerable branching of the chain.

TABLE 5. - Average carbon numbers of chains on fractions separated from 503-0-2 by GPC

| Samples | 503-0-2 | Fr.8 | Fr.9 | Fr.10 | Fr.11 | Fr.12 |
|---|---|---|---|---|---|---|
| Hα/Hα + 1 | 2.2 | 3.0 | 2.6 | 2.6 | 2.1 | 2.1 |
| $\frac{Cp_4\text{-}Cp_6,\ Cp_8,\ Cp_9}{Cp_1\text{-}Cp_3} + 1$ | 1.8 | 2.0 | 2.0 | 1.5 | 1.9 | 2.2 |

For a still further detailed study of the chemical shift of the $^{13}C$-NMR spectra, it is the intent of the author to continue work along this line.

## LITERATURE CITED


1) Y. Maekawa, S. Ueda, Y. Hasegawa, S. Yokoyama, E. Hiroki, Y. Yoshida, J. Fuel Soc. Japan, 49, 908 (1970)
2) Y. Maekawa, K. Shimokawa, T. Ishii, G. Takeya, J. Fuel Soc. Japan, 46, 927 (1967)
3) Y. Maekawa, S. Ueda, S. Yokoyama, Y. Hasegawa, Y. Nakata, Y. Yoshida, J. Fuel Soc, Japan, 53, 987 (1974)
4) R. D. Bartle, D. W. Jones, Fuel, 49, 21 (1969)
5) G. N. La Mar, J. Am. Chem. Soc., 93, 1040 (1971)
6) "13C FT NMR Spectra" Vol. 1, Vol. 2, Vol. 3, JEOL LTD., L. F. Johnson, W. C. Jankowski "Carbon-13 NMR Spectra" A. Wiley-Interscience publication (1972)

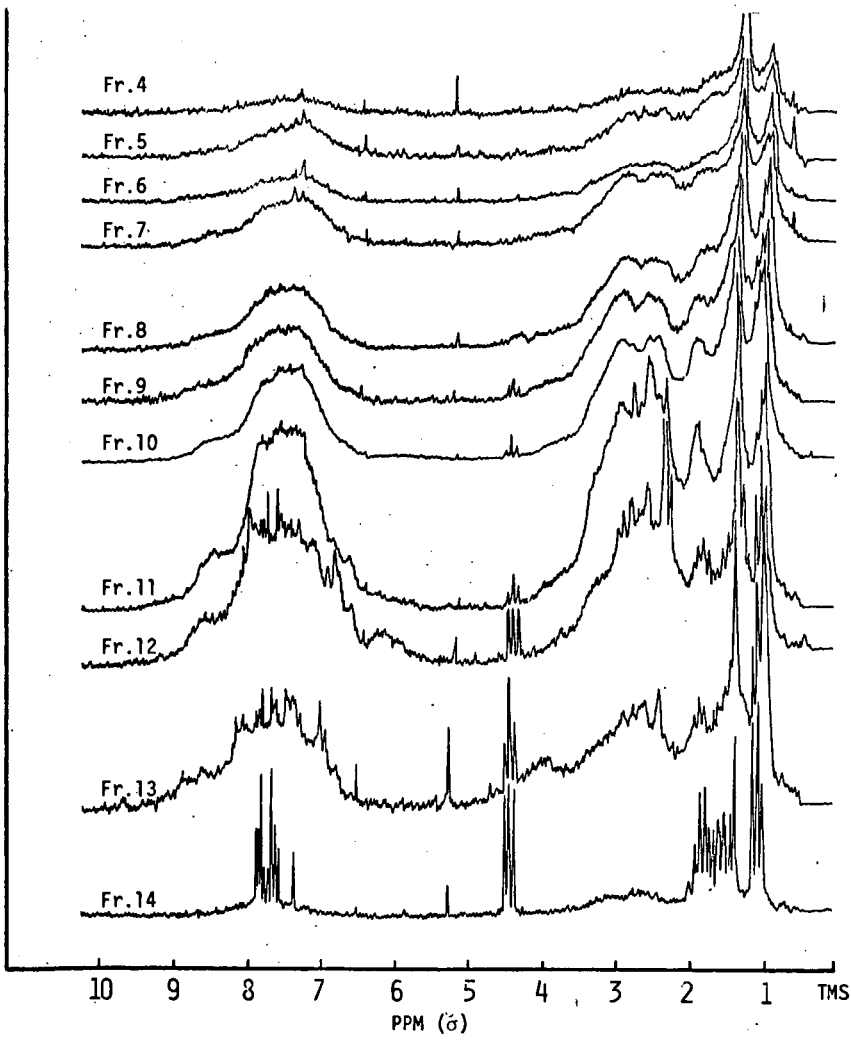


FIGURE 1 - $^{1}$H-NMR spectra of fractions separated from 503-0-2 by GPC

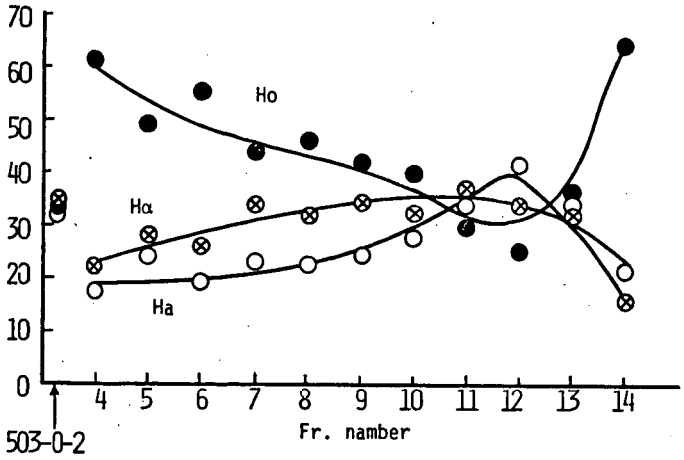


FIGURE 2 - Percentage hydrogen distribution in fractions separated from 503-0-2 by GPC

Ho : Hydrogen on β or farther from ring carbon
Hα : Hydrogen on α-carbon atoms
Ha : Aromatic hydrogen

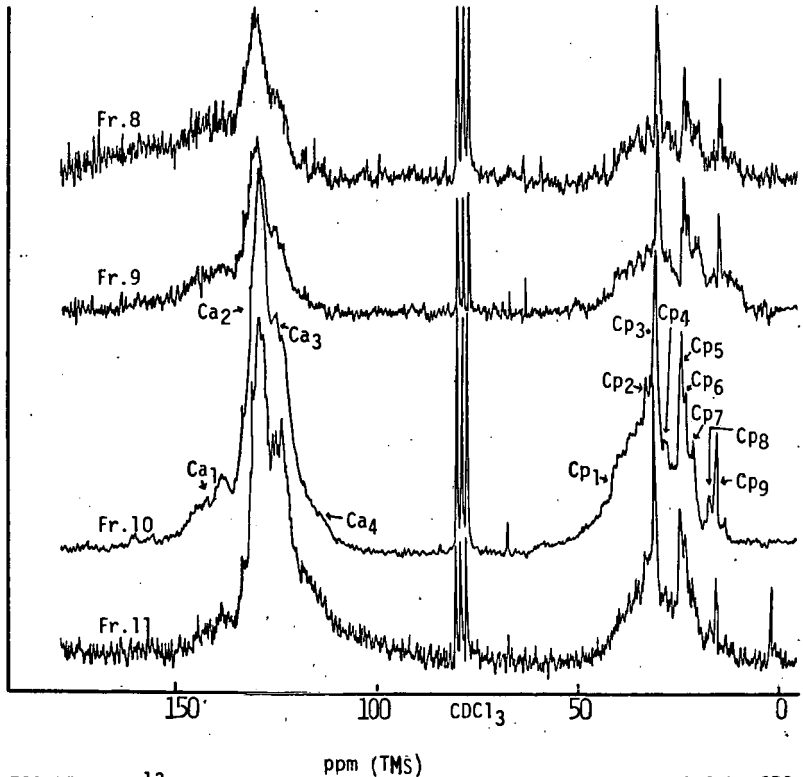


FIGURE 3 - $^{13}C$ NMR spectra of fractions separated from 503-0-2 by GPC

# Devolatilization of Coal and Zinc Chloride - Impregnated Coal in a Nitric Oxide Atmosphere

David M. Bodily, Sheldon H. D. Lee, Wendell H. Wiser

University of Utah, Salt Lake City, Utah

## Introduction

Zinc chloride acts as a catalyst for the hydrogenation of coal[1,2]. It has been proposed as a coal hydrogenation catalyst in a number of processes, but development of these processes has been hindered by corrosion and recovery problems of the zinc chloride. Zielke, et.al.[3,4] have reported on the catalytic activity of massive amounts of zinc chloride for hydrocracking coal, coal extracts and polynuclear aromatic compounds. Studies at the University of Utah[5,6] have shown the effectiveness of lesser amounts of impregnated zinc chloride for catalyzing coal hydrogenation. Conversions of up to 85% were obtained at residence times estimated to be one to six seconds. Dry coal was rapidly heated in an entrained-flow reactor. Coal is very reactive to hydrogenation in the presence of zinc chloride. However, the mechanism of catalysis is not understood and is an important and interesting problem for study.

Studies have shown that zinc chloride interacts with coal upon heating and produces important structural changes[7,8]. Pyrolysis of $ZnCl_2$-impregnated coals in inert atmospheres results in dehydrogenation of hydroaromatic groups in the coal and a decrease in the evolution of tars and gases. Hydrogen is evolved below 400°C when $ZnCl_2$ is present, but not in the absence of $ZnCl_2$. The hydrogen has been shown to come primarily from hydroaromatic groups. Dehydrogenation at relatively low temperatures results in supression of tar and gas evolution at higher temperatures. The acidic properties of zinc chloride on the coal surface disappear upon heating. Impregnated samples show large increases in surface area, enlargement of the capillary pores and hydrogen chemisorption properties upon heat treatment. The nature of intermediates formed by the $ZnCl_2$ during these reactions is of interest because of its possible roll in coal hydrogenation reactions. A Friedel-Crafts type acid intermediate has been proposed for hydrogenation with large amounts of zinc chloride[3]. In this report, the importance of free radical reactions is studied. Nitric oxide is used as a radical scavenger to terminate chain-propagation reactions.

## Experimental

A microbalance was used to continuously record the weight of coal samples during heating at 5°C/min. and during isothermal experiments. Nitrogen or a 0.1 mole percent mixture of nitric oxide in nitrogen flowed through the reactor during the reaction at a rate of 0.2 l/min. Hiawatha, Utah coal was used in these experiments (high volatile bituminous, 43.1% VM on dry basis, 79.5% C, 5.2% H, 1.6% N, 0.6% S, 13.0% O). Impregnated samples were prepared by mixing coal with aqueous solutions of $ZnCl_2$ and evaporating the water[8].

## Results and Discussion

Thermogravimetric analysis results are shown in figure 1. Hiawatha coal shows a typical weight loss curve in nitrogen atmospheres. The evolution of tar and gases is supressed by impregnation of 12% $ZnCl_2$. The effect of nitric oxide is to further decrease the loss of weight for both the coal and the impregnated coal. Above 500°C, there is considerable oxidation of the samples by the nitric oxide. The results of isothermal experiments at 400°C are shown in figure 2. A similar result is noted to that of the thermogravimetric analysis. The coal shows the loss of volatile matter in nitrogen atmospheres, while the impregnated coal shows a much

lower weight loss. The effect of the nitric oxide is to inhibit the pyrolysis reactions which lead to volatile products. The weight loss of the impregnated samples includes the loss of $ZnCl_2$. A result similar to that obtained with $ZnCl_2$ is obtained when $SnCl_2 \cdot 2H_2O$ is impregnated on the coal surface. Results of isothermal experiments are listed in table 1.

Table 1

Isothermal Weight Losses at 400°C

| Sample | Atmosphere | Weight loss, % |
|---|---|---|
| Coal | $N_2$ | 27.5 |
| Coal | $NO/N_2$ | 23.0 |
| Effect of NO | | 4.5 |
| Coal/12% $ZnCl_2$ | $N_2$ | 14.3 |
| Coal/12% $ZnCl_2$ | $NO/N_2$ | 10.1 |
| Effect of NO | | 4.2 |
| Coal/20% $SnCl_2$ | $N_2$ | 10.4 |
| Coal/20% $SnCl_2$ | $NO/N_2$ | 5.0 |
| Effect of NO | | 5.4 |

Berkowitz and Dammeyer[9] studied the low-temperature carbonization of coal in the presence of nitric oxide and concluded that nitric oxide retarded thermal decomposition of the coal and inhibited secondary polymerization of tar when present at the start of pyrolysis. den Hertog and Berkowitz[10] reported an enhancement of decomposition due to nitric oxide. The partial pressure and flow rate of NO were much greater in these experiments.

Nitric oxide inhibits the devolatilization of coal, presumably by terminating free radical chain reactions. Zinc chloride and stannous chloride also inhibit the devolatilization of coal, but the effects of $ZnCl_2$ and $SnCl_2$ are independent of NO inhibition as shown in table 1. It can be concluded that $ZnCl_2$ and $SnCl_2$ reactions do not involve free radical chains in coal pyrolysis.

## References


1. Weller, S., Pelipetz, M. G., Friedman, S., and Storch, H. H., Ind. Eng. Chem., 42, 330 (1950).

2. Pelipetz, M. G. Kuhn, E. M., Friedman, S., and Storch, H. H., Ind. Eng. Chem., 40, 1259 (1948).

3. Zielke, C. W., Struck, R. T., Evans, J. M., Constanza, C. P., and Gorin, E., Ind. Eng. Chem., Process Des. Develop., 5, 151 (1966).

4. Zielke, C. W., Struck, R. T., Evans, J. M., Constanza, C. P. and Gorin, E., Ind. Eng. Chem., Process Des. Develop., 5, 158 (1966).

5. Wood, R. E., Anderson, L. L., and Hill, G. R., Colorado School Mines Quart., 65, 201 (1970).

6. Wood, R. E., and Wiser, W. H., to be published.

7. Matsuura, K., Bodily, D. M., and Wiser, W. H., Preprints Fuel Div., Am. Chem. Soc., 19, No. 1, 157 (1974).

8. Bodily, D. M., Lee, S. H. D., and Wiser, W. H., Preprints Fuel Div., Am. Chem. Soc., 19, No. 1, 163 (1974).

9. Berkowitz, N., and Dammeyer, W., Fuel, 35, 19 (1956).

10. den Hertog, W., and Berkowitz, N., Fuel, 39, 125 (1960).

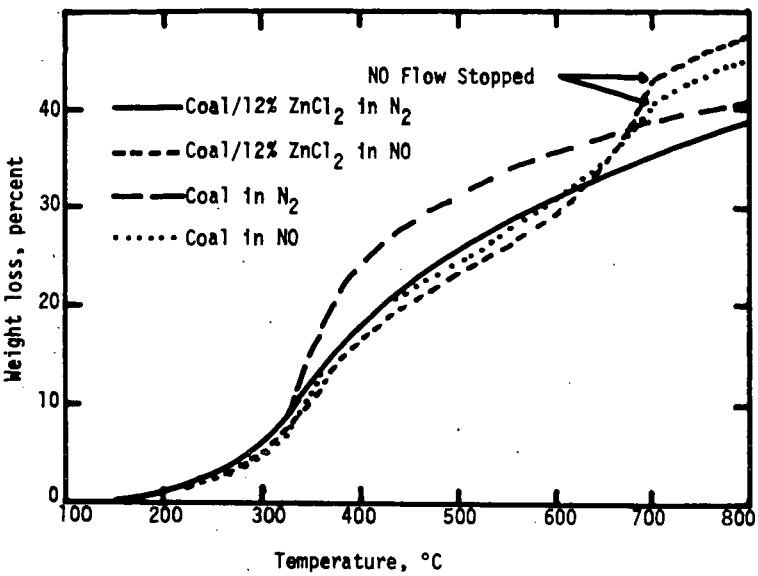


Figure 1. Thermogravimetric Analysis

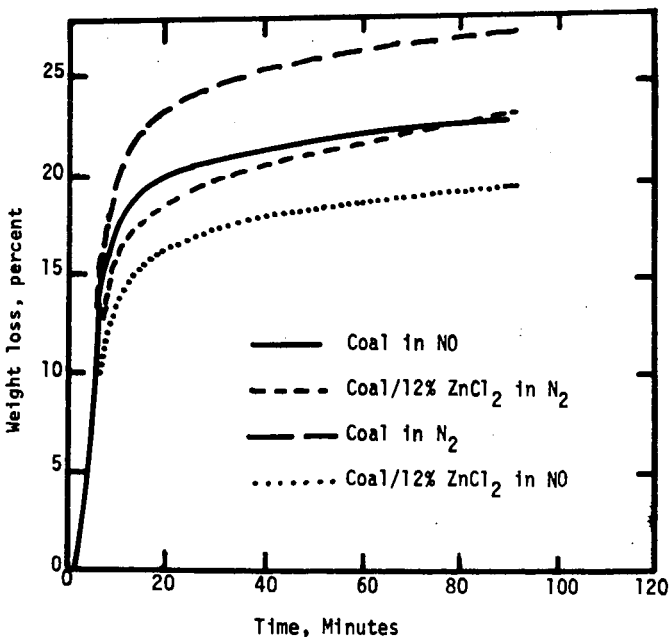


Figure 2. Isothermal Pyrolysis

HYPOCHLORITE OXIDATION OF MODEL COAL COMPOUNDS: STRUCTURAL AND MECHANISTIC INFERENCES. G. L. Tingey, J. R. Morrey, J. A. Campbell, and J. A. Franz, Battelle Memorial Institute, Pacific Northwest Laboratories, Richland, WA. 99352

The traditional view that coal consists primarily of varying degrees of aromatic structure has recently been challenged by Chakrabartty, et al., (Fuel, 53, 240 (1974)), who conclude from results of the hypochlorite oxidation of coal and from a study of hypochlorite oxidation of model compounds (from which aromatic and polynuclear aromatic carbon-carbon bonds are generally found to be inert to oxidation) that extensive aromatic structure cannot represent the structure of certain coals. We present the results of reactions of the hypochlorite oxidant with polynuclear aromatic compounds neglected in the above mentioned study to reach the opposite conclusion, i.e., that suitably substituted polynuclear aromatics are indeed labile to oxidation, and that extensive aromatic structure cannot be ruled out on the basis of results of hypochlorite oxidation. The results of hypochlorite oxidations of pyrene hydroquinone and quinone model systems and several coals are presented, and mechanisms for the mild dissolution of aromatic structure are discussed.

# INFERENCES ON THE STRUCTURE OF COAL: $^{13}C$ NMR AND IR SPECTROSCOPY



J. A. Franz*, J. R. Morrey*, J. A. Campbell*, G. L. Tingey*
R. J. Pugmire† and D. M. Grant†

*Battelle Memorial Institute, Pacific Northwest Laboratory, Richland, WA. 99352
and † Department of Chemistry, University of Utah, Salt Lake City, UT

## INTRODUCTION

The low solubility of coal in suitable nmr solvents (1) has limited high resolution nmr studies of coal to solvent extracts not necessarily representative of coal structure, or to extreme techniques (pyrolytic hydrogenation, high temperature distillation) which cast doubt on the structural memory of the resulting solutions. Nondestructive wideline nmr (2,3) produces little or no useful spectral information due to severe loss of resolution and fine structure. The same objections hold for infrared studies; the nondescript complexity of ir spectra of coal has made them useful in only the most qualitative sense. A mild technique for the dissolution of coal with minimal loss of structural memory is thus vital for the successful application of nmr and ir to coal-structure elucidation. The acid-catalyzed depolymerization of coal by phenol, used by Ouchi and Brooks (4) to dissolve 87% of a depolymerized Yallourn brown coal sample in methanol, appeared highly attractive for this purpose. We present the first account, to our knowledge, of the application of $^{13}C$ nmr and ir spectroscopy for monitoring the successive dissolution of coal under mild conditions. Spectroscopic results, analytical and radiochemical data are presented which depict the structural changes occurring during depolymerization and permit tentative identification of structural types.

## EXPERIMENTAL

SUCCESSIVE DEPOLYMERIZATION OF KNIFE RIVER COAL. A procedure similar to that of Ouchi (4, 5) was used for the depolymerization of Knife River coal whose elemental analysis can be found in Table II. Knife River coal (Beulah, Mercer Co., North Dakota) is classified as a lignite. After drying, elemental analysis and calorimetry permit assignment to the A.S.T.M. rank of high-volatile bituminous C. In a typical experiment, coal (10.7 g, dry basis), phenol (55.6 g), and p-toluenesulfonic acid (PTSA) were combined in a 3-neck, round-bottom flask equipped with mechanical stirrer, heating mantle, thermometer, and reflux condenser. Heating and stirring was begun without the reflux condenser until water contained in the coal and PTSA was driven off. The reflux condenser was attached, and the reaction proceeded at 185° for 6 hr. Phenol was removed by steam distillation. The resulting powder was filtered and washed thoroughly with water to remove PTSA and dried at $10^{-1}$ Torr and 125° for 10 hr. Soxhlet extraction of the depolymerized coal with methanol yielded a methanol soluble material (MeOH extract #1, nmr-1, ir-1a) and an insoluble material (residue #1, ir-1b). The procedure was repeated twice, substituting the insoluble residue after methanol extraction each time for coal. Results are summarized in Table 1.

Table 1 - Summary of Successive Depolymerization Steps

| Step No. | Wt Initial Mat'l | Wt Depolymerisate | Wt Extract | Wt Residue | Corrected Wt Extract‡ | Accumulated % Coal Extracted‡ |
|---|---|---|---|---|---|---|
| 1 | 10.70 | 13.26 | 4.97[a] | 8.29[b] | 2.30 | 21.5 |
| 2 | 8.29 | 10.93 | 4.37[c] | 6.62[d] | 2.72 | 46.9 |
| 3 | 6.62 | 8.85 | 3.01[e] | 5.87[f] | 1.66 | 62.4 |
| 1A | 4.1056 | 5.9913 | 2.24 | 3.76 | 1.12 | 27.3 |

‡Correction based on assumption that 59.3% of the phenol taken up during depolymerization is MeOH soluble. This percentage derives from the $^{14}C$ experiment described below. a-nmr-1, ir-1a; b-ir-1b; c-nmr-2, ir-2a; d-ir-2b; e-nmr-3, ir-3a; f-ir-3b.

DEPOLYMERIZATION OF KNIFE RIVER COAL USING 1-$^{14}$C PHENOL. In experiment 1A of Table 1, a sample of Knife River coal, 4.1056 g (dry basis) was stirred with a mixture of p-toluenesulfonic acid (PTSA) (5.79 g) and 50.7 g of phenol exhibiting $3.9 \pm 0.1 \times 10^6$ disintegrations $min^{-1}$ $g^{-1}$ (determined by scintillation counting) for 6 hr at 185° (reflux temperature of phenol). Unreacted phenol was removed by steam distillation, the resulting powder was filtered and washed thoroughly with water to remove PTSA. The depolymerized coal exhibited $12.3 \pm 0.2 \times 10^5$ d $min^{-1}$ $g^{-1}$ of activity. Extraction with methanol left an insoluble residue exhibiting $7.4 \pm 0.1 \times 10^5$ d $min^{-1}$ $g^{-1}$ activity and a methanol soluble fraction exhibiting $18.1 \pm 0.3 \times 10^5$ d $min^{-1}$ $g^{-1}$ activity. $^{14}$C combustion analysis established 0.71 g phenol contained in the residue, and 1.04 g of phenol contained in the extract. Elemental analyses were performed by the Schwarzkopf Analytical Laboratories.

Table 2 - Elemental Analyses

| Sample | C | H | N | S | O | Atomic H/C | Corrected H/C† |
|---|---|---|---|---|---|---|---|
| Knife River coal | 61.84 | 4.12 | 0.49 | 0.70 | 29.31 | 0.785 | |
| Successive Depolymerization | | | | | | | |
| MeOH Extract #1 | 75.54 | 4.82 | 0.35 | 1.84 | 16.52 | .758 | 0.474 |
| MeOH Extract #2 | 73.40 | 4.70 | 0.35 | 3.53 | 15.65 | .761 | 0.604 |
| MeOH Extract #3 | 75.06 | 5.92 | 0.09 | 2.75 | 16.45 | .939 | 0.880 |
| Residue #1 | 73.28 | 4.16 | 0.58 | 2.37 | 16.36 | .675 | 0.579 |
| Residue #2 | 71.85 | 3.84 | 0.35 | 1.35 | 14.86 | .634 | 0.740 |
| Residue #3 | 71.88 | 4.03 | 0.40 | 1.50 | 14.23 | .668 | 0.600 |

†The corrected H/C ratio was calculated using the distributive results of the $^{14}$C experiment to correct for phenol uptake by both residue and extract. It was assumed that 40.7% of the phenol remained in the residue and the remainder went with the extract in each successive depolymerization. Of course, this assumption must be accepted only with reservation.

$^{13}$C NMR SPECTRA AND IR SPECTRA. Proton-decoupled $^{13}$C nmr spectra were determined at the University of Utah with a Varian Associates XL-100 FTNMR Spectrometer operating at 25.16 MHz. Dioxane was used as an internal lock signal. Methanol solutions of Extracts 1, 2, and 3 contained no nonbonded phenol (gc analysis) and no PTSA (by addition of authentic sample to nmr tube). Infrared spectra were determined by a computer-coupled Perkin-Elmer model 521 Spectrometer. KBr pellets containing 0.5% sample concentration by weight were used. See Figure 1 for $^{13}$C nmr spectra and Figures 2 and 3 for ir spectra.

## DISCUSSION

The $^{13}$C nmr spectra of Extracts 1, 2, and 3 are shown in Figure 1. Since the depolymerization procedure incorporated bonded phenol into the coal structure, there is some uncertainty as to the percent of coal actually dissolved. However, at least 45% of the original coal was depolymerized and extracted assuming the worst case that all of the phenol ended up in the extracts. The actual quantity is greater since the weight gain on depolymerization occurs by incorporation of phenol in both residue and extract. To estimate the partitioning of phenol between residue and extract, $^{14}$C-labeled phenol was used in a depolymerization. If the distribution of phenol determined in the labeling experiment can be extrapolated to later stages of a successive depolymerization, then up to 62% of coal structure is contained in the methanol extracts. Reliable data for such an extrapolation must await further labeling studies. Nevertheless, a significant portion of the coal structure has been successfully dissolved.

The general features of the $^{13}$C nmr and ir spectra of Knife River coal residues and extracts indicate an aromatic system with high phenolic/hydroxylic OH content,

modest aliphatic structure, and very little carbonyl content. The overall features of the ir spectrum of the original coal (ir-4) are retained on depolymerization, in accordance with the observations of Ouchi (5) using brown coal. Elemental analysis reveals a substantial drop in oxygen content, in the first depolymerization step, attributed (4) to dehydration reactions of the type

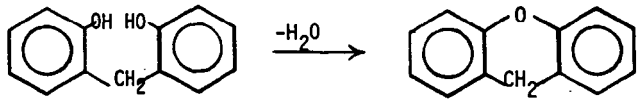


A four to five-fold increase in aliphatic CH content occurs in the methanol extracts from the first to third depolymerization. This is indicated by the increase in CH aliphatic stretching bands from 2800 to 3000 $cm^{-1}$ in ir spectra ir-1a through ir-3a. At the same time, the aromatic C=C stretching bond at ~1600 $cm^{-1}$ decreases from extract 1 to 3. The increase in aliphatic CH is accompanied by a significant increase in the H/C ratio (from elemental analysis) in the extracts of successive depolymerizations. The apparent change in aliphatic content in residues 1-3 appears to be small, and carbonyl content (~1750 $cm^{-1}$) is concentrated in the residues. All of these observations parallel those of Ouchi (5) who found that aliphatic structure increases in the extracts, and that the residues show an increasingly dense network of aromatic structure.

The $^{13}C$ nmr spectra (Figure 1) of Extracts 1-3 show a similar pattern. Nmr-1 of Extract #1 shows a complex aromatic structure (4200-2800 Hz, 167-111 ppm) with a much smaller complement of aliphatic structure, most apparent in the region 900-300 Hz (36-12 ppm). Aliphatic resonances at ca. 830 Hz (33 ppm) in nmr 1-3 can be tentatively assigned to aliphatic methine and/or methylene bridge carbons ($Ar_2CH_2$ or $Ar_3CH$). The resonances at ca.600 Hz (23.9 ppm) can be assigned to methyl groups attached to aromatic nuclei (6,7). No long-chain aliphatic, olefinic or carbonyl resonances are detectable.

The nmr spectra of successive extracts show a decrease in aromatic/aliphatic content, in agreement with infrared and analytical data. The aromatic regions become progressively simpler with successive extracts. At the third stage, the aromatic region of the spectrum suggests a highly specific reaction and extraction sequence, yielding a mixture of highly similar structures. Nmr-2 is consistent with the general structures 1 or 2: The quaternary carbons A (3945 Hz, 156.8 ppm) and

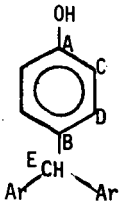


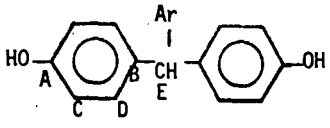


B (3630 Hz, 144.3 ppm) are unaffected in an off-resonance experiment, while aromatic methines C (3255 Hz, 129.4 ppm), and D (2925 Hz, 116.2 ppm) and aliphatic methine E (820 Hz, 32.6 ppm) become doublets. Complex structure surrounding the doublet in the off-resonance experiment provides evidence for aromatic methylene groups as well as methine E at 33 ppm.

In addition, a quaternary aliphatic carbon appears at 1095 Hz (43.5 ppm) in nmr-3. Precise structural assignment has not been made at the time of writing. Detectable aromatic structure probably associated with this resonance has not been identified.

The genesis of structures 1 and/or 2 (Ar = coal-derived structure) may be consistent with an increasingly endothermic depolymerization reaction reflected in a much greater specificity in point of attack on the coal structure. Structure 2 may result from displacement of two aromatic moieties from a ArCH group. A closely related reaction has been used to extract methylene groups from model compounds (Ar, $CH_2Ar_2$) and from coal:[8]

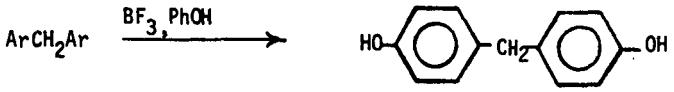


## SUMMARY

A modified method of Ouchi and Heredy for depolymerizing coal shows great promise for obtaining substantial fractions in true solutions. These solutions can be used in high resolution $^{13}C$ nmr studies and in infrared studies to elucidate the basic structures of coals.

The technique has been demonstrated for a high-volatile bituminous C coal. We are currently pursuing this research in an attempt to obtain structural information, particularly with emphasis on the functional groups in coal and their effect on its reactivity.

## REFERENCES

1. D. W. Van Krevelen, "Coal; Typology, Chemistry, Physics, Constitution," Elsevier Publishing Co., New York, N. Y., 1961, p. 177.
2. H. L. Retcofsky and R. A. Friedel, J. Phys. Chem., 77, 68 (1973).
3. H. L. Retcofsky and R. A. Friedel, Anal. Chem. 43, 485 (1971).
4. K. Ouchi and J. D. Brooks, Fuel, 46, 367 (1968).
5. K. Ouchi, Fuel, 46, 319 (1968).
6. G. C. Levy and G. L. Nelson, "Carbon-13 Nuclear Magnetic Resonance for Organic Chemists," John Wiley & Sons, New York, N. Y., 1972.
7. L. F. Johnson and W. C. Jankowski, "Carbon-13 NMR Spectra: A Collection of Assigned, Coded, and Indexed Spectra," John Wiley & Sons, New York, N. Y., 1972.
8. L. A. Heredy, A. E. Kostyo, and M. B. Neuworth, Fuel, 43, 414 (1964).

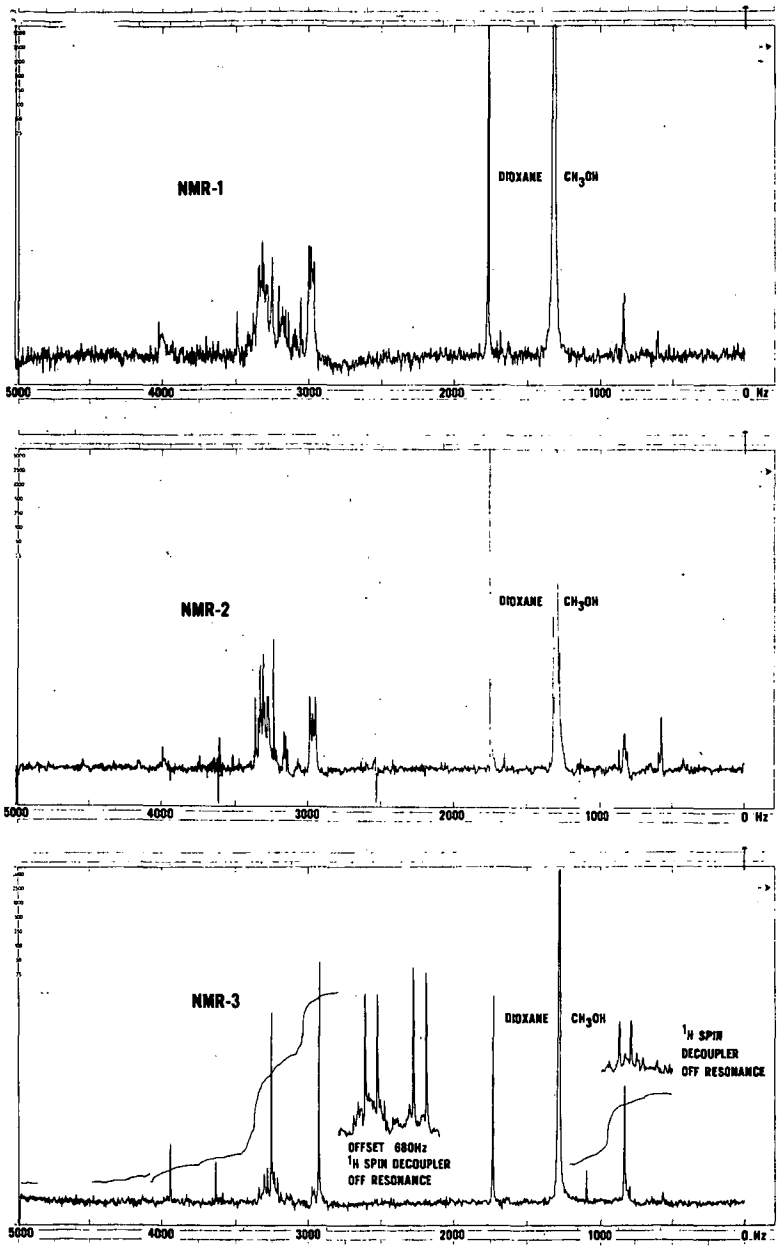


Figure 1. $^{13}C$ NMR Spectra of $CH_3OH$-soluble Fractions from the Successive Depolymerization of Knife River Coal.

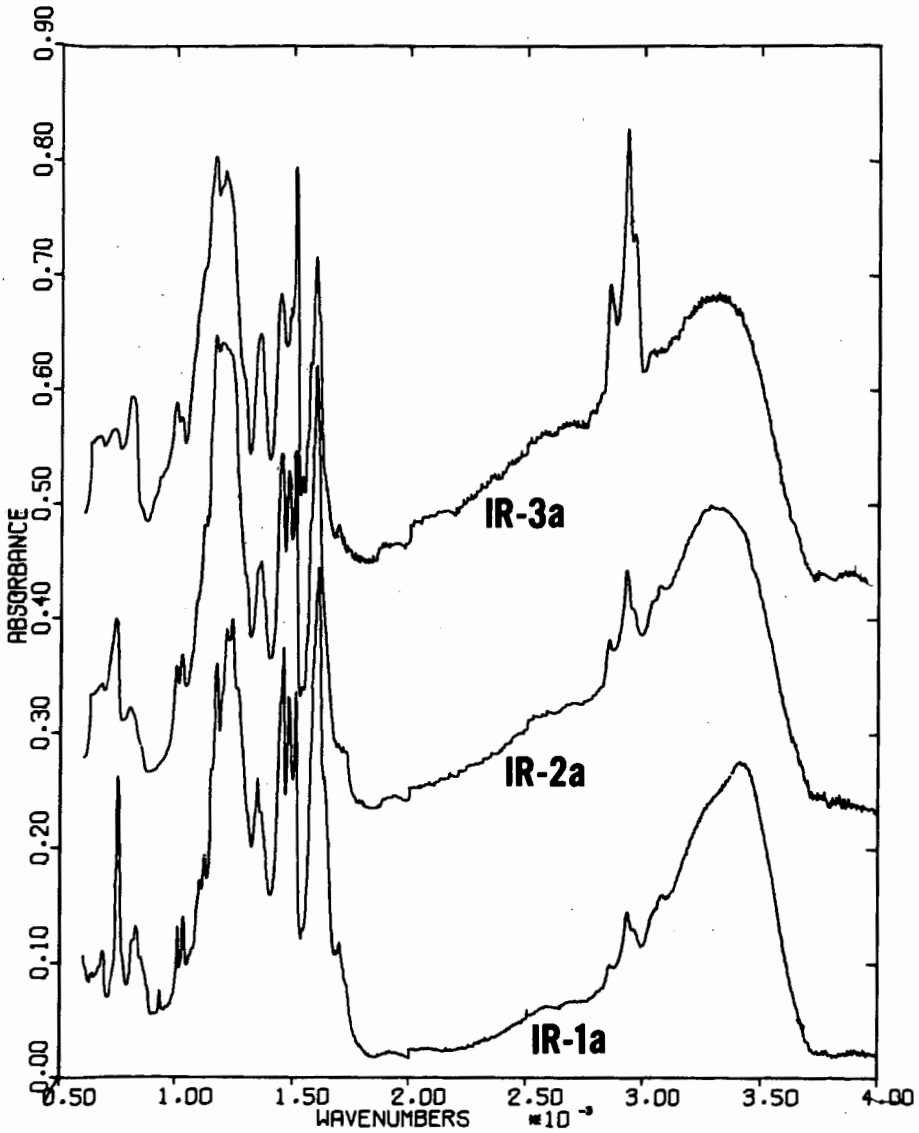


Figure 2. Infrared Spectra of $CH_3OH$ Fractions from the Successive Depolymerization of Knife River Coal.

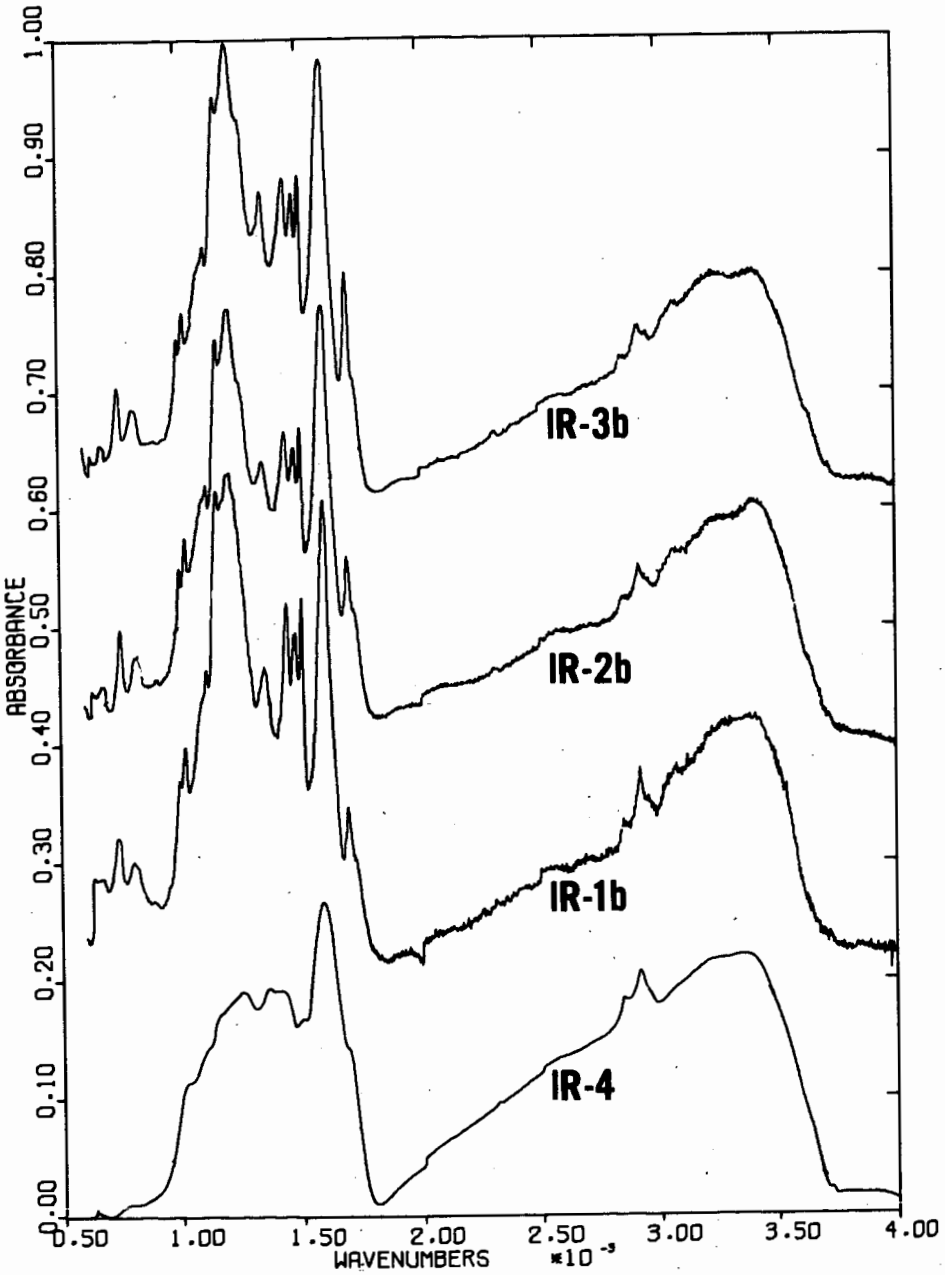


Figure 3. Infrared Spectra of Residues from the Successive Depolymerization of Knife River Coal (ir-1b, 2b, 3b) and of Knife River Coal (ir-4).

# DIFFERENTIAL SCANNING CALORIMETRY STUDIES ON COAL HYDROGENATION

O. P. Mahajan, A. Tomita, J. R. Nelson and P. L. Walker, Jr.

Department of Material Sciences
The Pennsylvania State University
University Park, Pennsylvania 16802

## INTRODUCTION

There is considerable interest in the production of high BTU gas by coal hydrogenation. The Hydrane process (1), recently developed by the U.S. Bureau of Mines, involves direct hydrogenation of raw coals. The present study on coal hydrogenation using the differential scanning calorimetry (DSC) approach is intended to provide some information on the reactivity of representative U.S. raw coals. Twenty U.S. raw coals of different rank have been selected for the present study, in which heats of reaction at 800 psig of hydrogen and temperatures up to 570°C have been measured. The effect of demineralization of coals upon heats of reaction has also been studied.

## EXPERIMENTAL

A DuPont pressure DSC cell was used in conjunction with a cell base Module I and a 990 Thermal Analyzer to determine thermal effects involved during hydrogenation of coals. DSC scans for various coals (40x70 U.S. standard mesh) were obtained from 200 to 570°C at a linear heating rate of 5.4°C/min. Details of experimental procedure and calculations have been described elsewhere (2).

## RESULTS AND DISCUSSION

Heats of hydrogenation of different coals, expressed as cal per unit weight of starting coal, are given in Table 1. Throughout the discussion which follows, carbon contents of coal are given on a dry-ash-free (daf) basis. The heat of hydrogenation ($-\Delta H$) increases, in general, with decrease in coal rank; the value varying from about 7 cal per gram, exothermic, for anthracite to about 150 cal per gram, exothermic, for lignites.

Weight losses at 570°C for various coals are included in Table 1. It is seen that weight loss decreases, in general, with increase in coal rank. However, in the case of PSOC 24, weight loss is far greater than that expected from its rank. Weight losses at 570°C for various coals are plotted against integral exothermic heats in Figure 1. It is seen that, except in the case of PSOC 24 and 95, data points for the rest of the coals fit on two straight lines of different slopes; the two lines intersect each other at a weight loss of about 45%. Considering the data in Table 1, it is seen that weight losses up to 45% are characteristic of coals with a carbon content greater than about 82%. For such coals, each one per cent of weight loss is seen to correspond to evolution of about 1.4 cal per gram weight of starting coal. This value increases to about 2 cal per gram for coals with carbon contents less than 82%.

The higher weight loss observed in the case of PSOC 24 may be due to the presence of a beneficial catalytic impurity. Out of all the samples investigated, PSOC 24 has the highest pyritic sulphur content (4.95%, daf); this may be responsible for its enhanced reactivity. However, in the case of PSOC 290 which has a pyritic sulphur content of 3.18% (daf), weight loss corresponds to that expected on the basis of its rank. DSC and TGA runs on the two coals were also made after partial removal of pyrite by a flotation technique using a halogenated hydrocarbon of density 2.85 g/cc. Following partial removal of pyrite, both coals exhibit a significant decrease in weight loss as well as exothermic heat (Table 2). These results suggest that pyrite or its reduction products, namely pyrrhotite or iron, catalyze hydrogenation.

Transition temperatures, that is the temperatures corresponding to the onset of the exotherms, are plotted as a function of carbon content in Figure 2. The transition temperature is strongly rank dependent, varying from about 230-250°C for lignites to about 535°C for anthracite. The plot in Figure 2 consists of four distinct parts. Coals associated with 63-75% carbon have about the same transition temperature. A sharp increase in transition temperature (about 200°C) occurs in 75-80% carbon range. Thereafter, up to about 90% carbon, the transition temperature increases only slightly. A further increase in transition temperature occurs beyond 90% carbon. It is noteworthy that variation of transition temperature with carbon content follows essentially the same trend as variation of average layer diameter and number of atoms per layer with carbon content (3).

The effect of demineralization on transition temperatures and exothermic heats for eight coals is illustrated by data in Table 1. It is seen that in the case of coals with carbon content less than 80%, demineralization increases the transition temperature and decreases the exothermic heat of reaction. This behavior again suggests that mineral matter associated with such coals catalyzes hydrogenation. However, in the case of coals with carbon contents greater than about 80%, removal of mineral matter decreases the transition temperature and increases the heat of hydrogenation. This is probably due to the fact that in such coals mineral matter removal opens up new feeder pores, thus increasing the accessibility of hydrogen into the pore structure. The development of additional porosity and enhanced accessibility to active sites more than offsets a decrease in reactivity which might result from the removal of catalytically active mineral matter. This is consistent with previous studies on the reactivity of coal chars with air (4). That is, mineral matter removal from lignites decreased gasification rates whereas mineral matter removal from an LV bituminous coal increased gasification rates.

ACKNOWLEDGEMENTS

This study was supported by NSF-RANN under Grant No. GI-38974. Professor W. Spackman supplied the coals used in the study.

REFERENCES

1. Feldmann, H. F., Wen, C. Y., Simons, W. H. and Yavorsky, P. M., 71st AIChE Nat. Meeting, Feb. 20-23, 1972.

2. Mahajan, O. P., Tomita, A. and Walker, P. L., Jr., Fuel, Communicated.

3. Cartz, L. and Hirsch, P. B., Phil. Trans. Roy. Soc., Lond., A252, 557 (1960).

4. Jenkins, R. G., Nandi, S. P., and Walker, P. L., Jr., Fuel, 52, 288 (1973).

TABLE 1

HEATS OF HYDROGENATION

| PSOC Sample No. | ASTM Rank | State | Coal analysis, % Ash (dry) | VM (daf) | C (daf) | Wt Loss at 570°C % (daf) | -ΔH, cal/g (daf) Raw | Demin | Transition Temp, °C Raw | Demin |
|---|---|---|---|---|---|---|---|---|---|---|
| 85 | Anthracite | Pa. | 8.3 | 7.7 | 91.3 | 8.7 | 6.9 | - | 536 | - |
| 130 | MV | W.Va. | 6.4 | 23.0 | 90.6 | 24.7 | 48.0 | - | 450 | - |
| 127 | LV | Pa. | 5.7 | 20.6 | 89.6 | 24.3 | 36.4 | 42.5 | 478 | 457 |
| 135 | MV | Ala. | 5.0 | 24.9 | 88.4 | 26.8 | 30.9 | 41.7 | 487 | 462 |
| 137 | MV | Ala. | 7.1 | 26.4 | 86.9 | 34.4 | 37.3 | - | 468 | - |
| 4 | HVA | Ky. | 2.1 | 38.3 | 83.8 | 40.3 | 57.4 | - | 446 | - |
| 95 | HVA | Wash. | 21.1 | 42.1 | 81.6 | 46.9 | 37.1 | 63.9 | 468 | 455 |
| 24 | HVB | Ill. | 11.8 | 41.9 | 80.1 | 73.6 | 66.2 | 52.7 | 340 | 445 |
| 290 | HVB | Ill. | 13.9 | 47.2 | 79.7 | 53.2 | 68.2 | - | 412 | - |
| 197 | HVC | Ohio | 12.4 | 42.0 | 78.9 | 50.4 | 79.7 | - | 315 | - |
| 151 | HVC | N.M. | 5.1 | 45.7 | 77.8 | 55.3 | 85.6 | - | 421 | - |
| 22 | HVC | Ill. | 10.1 | 42.8 | 78.8 | 55.4 | 83.8 | 59.6 | 324 | 431 |
| 190 | Sbb-B | Ill. | 8.5 | 41.5 | 75.6 | 59.3 | 111.5 | 51.5 | 285 | 457 |
| 97 | Sbb-A | Wyo. | 9.8 | 54.4 | 75.0 | 57.1 | 94.6 | - | 343 | - |
| 138 | Lignite | Tex. | 10.3 | 47.1 | 74.3 | 66.7 | 120.6 | 89.2 | 230 | 363 |
| 100 | Sbb-C | Wyo. | 5.0 | 60.7 | 72.1 | 57.0 | 125.7 | - | 232 | - |
| 93 | Lignite | Mon. | 10.7 | 51.6 | 71.9 | 56.6 | 122.2 | - | 266 | - |
| 141 | Lignite | Tex. | 9.0 | 49.2 | 71.7 | 66.1 | 120.4 | - | 246 | - |
| 87 | Lignite | N.D. | 8.2 | 54.2 | 71.2 | 70.8 | 151.6 | 123.1 | 232 | 272 |
| 89 | Lignite | N.D. | 11.6 | 57.3 | 63.3 | 74.5 | 153.1 | - | 256 | - |

TABLE 2

EFFECT OF PYRITE REMOVAL ON EXOTHERMIC HEAT AND WEIGHT LOSS DURING HYDROGENATION

| PSOC Sample No. | Pyritic S % (dry) | Wt Loss at 570°C % (daf) | -ΔH cal/g (daf) |
|---|---|---|---|
| 24 | 4.95 | 73.6 | 66.2 |
| 24 (d < 2.85g/cc) | 3.56 | 56.7 | 61.8 |
| 290 | 3.18 | 53.2 | 68.2 |
| 290 (d < 2.85 g/cc) | 1.87 | 47.0 | 40.7 |

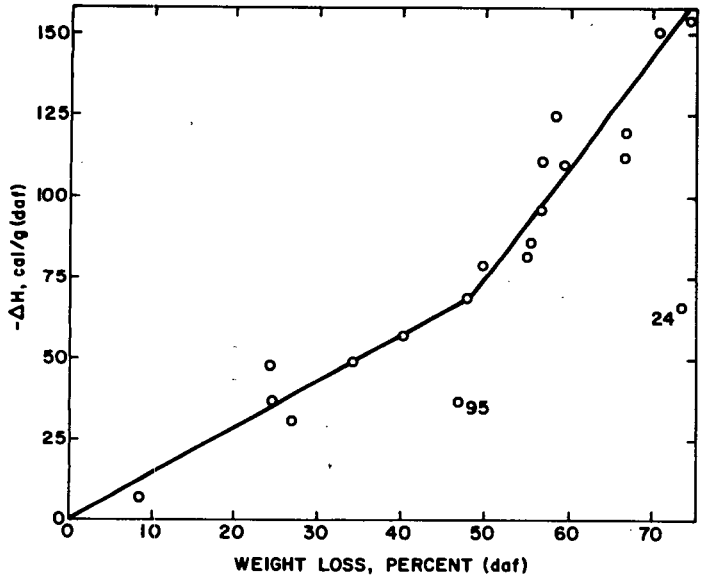


Figure 1 Exothermic Heat in Relation to Weight Loss During Hydrogenation.

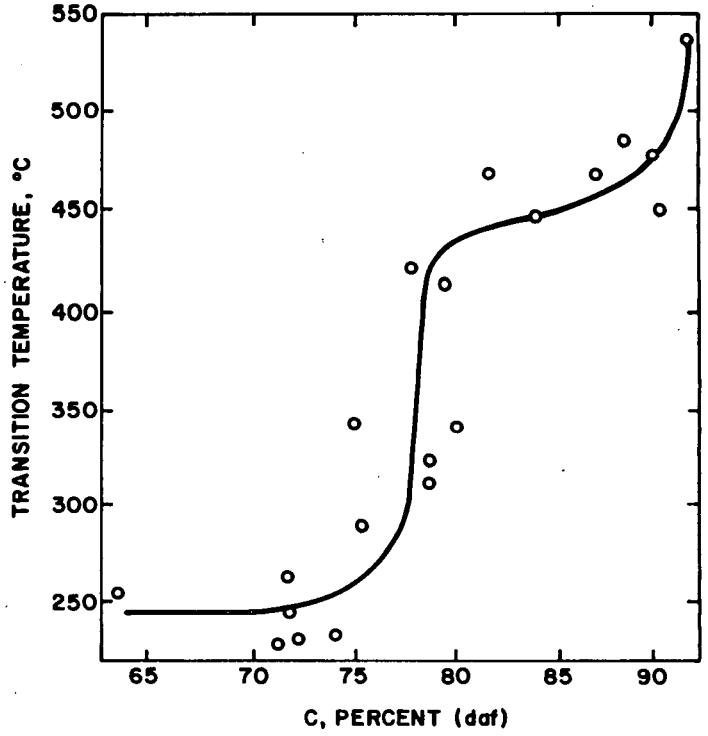


Figure 2 Transition Temperature in Relation to Carbon Content of Coals.

# PRODUCTS OF FLASH HYDROGENATION OF ILLINOIS NO. 6 COAL

Robert A. Graff
Samuel Dobner
Arthur M. Squires

Clean Fuels Institute
Department of Chemical Engineering
The City College of the City University of New York
New York, New York 10031

The chemical structure of coal is still a matter of continuing speculation. All workers do agree, however, that it is indeed a fairly fragile structure which can easily be transformed into species of higher molecular weight.(1) The process is thought to be the result of the competitive reactions of fragmentation and polymerization of portions of the coal structure. Rapid heating to above 500°C improves selectivity toward lighter products by accelerating fragmentation and volatilization during the early stages of polymerization. Hydrogen acts to stabilize the light species formed by terminating free radicals which might otherwise polymerize.

Forty years ago Dent had established that raw coal can give substantial yields of gaseous hydrocarbons at high temperatures and hydrogen pressures (2-5). His work was later confirmed by researchers at Purdue University (6-9) and the Institute of Gas Technology (10).

In an effort to obtain data at shorter solids contact time, the U.S. Bureau of Mines developed a captive sample technique for rapidly heating coal to temperature (in about 2 to 4 minutes) (11,12). Other workers have also investigated the flash heating (5 seconds or less) of coal in hydrogen atmospheres with both very long (1 minute or more) (13-18), and very short (30 seconds or less) (17-24) solids residence times.

The Bureau's experiments with rapid heating established that significant liquid yields could be obtained with uncatalyzed as well as catalyzed coal by operating at moderate temperatures (700-800°C) and keeping vapor product residence times to 25 seconds or less (11,12,25-29). While those employing flash heating have obtained higher product yields, no significant liquid yields were reported (aside from a few percent heavy tars). In these experiments gas residence times were too long (13,15,17,18,20-22,24) or reaction temperatures too high (14,17-19, 23,24) for production of liquids.

The Bureau's work (with catalyzed coal) also points to the existence of an optimum vapor residence time (28). Too short a residence time does not allow conversion of heavy materials evolved from the coal to light products; too long a time results in a loss of light liquids by cracking and carbonization.

Experimental Reactor

Our reactor (Figure 1) is similar in design to the Bureau's reactor (11,12) but is capable of much higher heating rates (about one second or less to 800°C). This configuration allows for independent selection of the three important time parameters: heating rate, vapor residence time, and solids contact time. About ten milligrams of coal is deposited in the form of a thin ring on the interior surface of a 316 stainless steel tube, 0.25 inches in outside diameter, 0.20 inches in inside diameter and 12 inches long. The deposit is formed by floating ground coal on carbon tetrachloride. As the carbon tetrachloride evaporates, a deposit about 0.5 cm long is left on the tube. A quartz wool plug at the reactor outlet serves to protect the collection system downstream from particles which might be dislodged from the sample. The reactor is clamped between electrical leads and connected to a source of hydrogen on the left, and evacuated collection tanks on the right. A thermocouple is spot welded to the exterior of the reactor tube at the location of the coal sample.

Flow of hydrogen is established at the desired pressure with the reactor and inlet system at room temperature. At time zero electrical power is supplied from transformers, resistively heating the reactor tube. When a preset temperature is reached a controller switches on a holding current to maintain the desired temperature level for the duration of the experiment.

The vapor product residence time in these experiments is the time required for the products evolved from the coal to be carried by the flow of hydrogen to the right hand electrical lead. Because of its large mass, the lead remains at its initial temperature and serves as the quench point. Variations in vapor residence time are achieved by changes in location of the coal ring or in rate of hydrogen flow.

Following hydrogenation the residual char is burned in situ with oxygen at four atmospheres and the oxidation products collected in a separate tank for analysis.

Analyses are performed with a gas chromatograph using a Poropak-Q column for all hydrocarbons and carbon dioxide and a molecular sieve column for carbon monoxide.

Coal Sample

The yields reported here were obtained with a mine-mouth sample of Illinois No. 6 coal. The sample was crushed and ground in air to less than 325 mesh and subsequently stored under nitrogen. The ultimate analysis (weight percent, moisture free) is as follows:

| | |
|---|---|
| carbon | 68.2% |
| hydrogen | 5.1% |
| nitrogen | 1.1% |
| sulfur | 4.2% |
| oxygen (by difference) | 9.3% |
| ash | 12.1% |

Exploratory Runs

The influence of heating rate, solids contact time and vapor product residence time were explored in a series of preliminary experiments to provide a basis for planning the more extensive study. All runs are in hydrogen at 100 atmospheres.

From the preliminary study we tentatively conclude that a heating rate of 650°C per second is sufficiently high and a solids contact time of ten seconds sufficiently long to characterize the products of flash hydrogenation. Increasing the heating rate to 1400°C per second provides the same yields. Heating at 20°C per second with a solids contact time of 65 seconds results in a three-fold decrease in single ring aromatics and a substantial increase in heavier species. Yields at 30 seconds solids contact time are substantially the same as at 10 seconds when the heating rate is 650°C per second. Shortening the solids contact time to two seconds results in slightly reduced yield of all light species.

Tests at different vapor product residence times show that there is an optimum value for this parameter for yield of light aromatics. For example, in the vicinity of 800°C the BTX (benzene + toluene + xylene) yields are lower both at 0.18 seconds and 23 seconds than at 0.6 seconds.

Yield Structure

On the basis of the preliminary runs, reaction temperature and vapor residence time were selected as variables for more detailed study. Heating rate was fixed at 650°C per second and solids contact time at 10 seconds. The influence of reaction temperature was explored from 620 to 980°C with a vapor product residence time of 0.6 seconds (Figures 2-5). The influence of vapor product residence time was explored from 0.6 to 5 seconds at a temperature of 700°C (Figures 6-8).

Carbon Balance

The principal products observed are methane, ethane, propane, benzene, toluene and xylenes. Other species, such as butanes, ethylene and propylene are found only in trace amounts (less than 1 percent). Tests of the collection system were made by injecting known quantities of components ahead of the reactor. Xylene and lighter species are recovered quantitatively.

A carbon balance is made by summing the carbon content of the observed hydrogenation and combustion products (the latter is $CO_2$ with minor amounts of CO). The difference between the carbon recovered and the carbon content of the weighed coal sample is reported as carbon deficit in Figures 2 and 6.

These figures suggest that the light hydrocarbons directly measured substantially account for the products of flash hydrogenation at temperatures beyond 850°C at 0.6 seconds residence time (Figure 2) and at residence times beyond 3 seconds at 700°C (Figure 6). The scatter in carbon deficit is low. For the 19 runs reported, the precision (95% confidence level) is ±3%.

The carbon deficit at lower temperatures in Figure 2 and shorter residence times in Figure 6 is attributed to species heavier than xylene.

Effect of Reaction Temperature

Carbon conversion to methane (Figure 3) increased from 5% at 620°C to 38% at 980°C. In contrast, carbon conversion to propane (Figure 4) falls quickly from 2% at 620°C to nearly zero at 780°C. Ethane (Figure 4) shows a peak yield near 760°C of 6.8%. By 940°C the ethane drops to an insignificant level.

Little BTX (Figure 5) appears below 620°C. The yield peaks at 800°C with a conversion of 11.6% and drops to 3% at 980°C. Benzene is 41% of the BTX mixture at 620°C. The fraction rises steeply with temperature and beyond 790°C the mixture is nearly pure benzene.

Effect of Vapor Product Residence Time

The effect of increasing vapor product residence time at 700°C is shown in Figures 6-8. At this temperature and 0.6 seconds, 12% of the carbon in the coal is converted to material heavier than xylene. With increasing residence time the yield of this material decreases, vanishing at 3 seconds (Figure 6).

These heavy species are converted to methane, ethane, BTX, and coke. At 3 seconds methane has increased by 5.5%, ethane by 2% and BTX by 5%. Beyond 3 seconds ethane remains nearly constant while methane and BTX decline. This is accompanied by an increase in char deposited on the reactor walls downstream of the coal sample.

Implications

The principal result of the studies reported here is to demonstrate that heavy species evolved from coal by flash heating in hydrogen at

elevated pressure are of such character as to be quickly converted to BTX and light alkanes in the vapor phase. It is significant that little if any tars are produced. Going to higher temperatures results in the formation of even lighter species with temperatures 700 to 800°C being optimum for production of BTX.

References


1. N.Y. Kirov and J.N. Stephens, Physical Aspects of Coal Carbonization, Dept. Fuel Technology, Univ. of New South Wales, Sydney, Australia (1967).
2. F.J. Dent, W.H. Blackburn, H.C. Millett, Inst. Gas Engrs. (London) Publ. 167/56 (November 1937) [Gas J. 220, 470, 473 (1937)]; ibid., Publ. 190/73 (November 1938) [Gas J. 224, 442 (1938)].
3. F.J. Dent, Gas Research Board (London), Publ. GRB 13 (1944) [Gas J. 244, 502 (1944)]; ibid., Publ. GRB 13/3 (1950).
4. F.J. Dent, Proc. Internat. Conf. Complete Gasification of Mined Coal, Liege, Belgium, May 1954, p. 113.
5. F.J. Dent, J. Inst. Fuel, 37, 195 (1966).
6. G.T. Austin, Ph.D. Thesis, Purdue Univ., 1943.
7. J.L. Bray and R.E. Howard, Purdue Univ. Eng. Expt. Station, Lafayette, Ind., Research Ser. 90, (September 1943).
8. J.L. Bray and P.W. Morgal, ibid., Research Ser. 93 (July 1944).
9. C.H. Stockman and J.L. Bray, ibid., Research Ser. 111 (November 1950).
10. K.C. Channabasappa and H.R. Linden, Ind. Eng. Chem. 48, 900 (1956); 50, 637 (1958).
11. R.W. Hiteshue, R.B. Anderson, M.D. Schlesinger, Ind. Eng. Chem. 49, 2008 (1957).
12. R.W. Hiteshue, S. Friedman, R. Madden, U.S. Bur. Mines Rep. Invest. 6027 (1962).
13. E.J. Pyrcioch and H.R. Linden, Ind. Eng. Chem. 52, 591 (1960).
14. H.F. Feldkirchner and H.R. Linden, Ind. Eng. Chem. Proc. Design Dev. 2, 153 (1963).
15. E.J. Pyrcioch, et al., IGT Res. Bull. 39 (1972).
16. T.J. Birch, K.R. Hall, R.W. Urie, J. Inst. Fuel 33, 422 (1960).
17. Bituminous Coal Research, Inc., OCR R&D Rept. No. 20, Final Rept. (1971).
18. R.A. Glenn, E.E. Donath, R.J. Crace, Adv. Chem. Ser. 69, 81 (1967).

19. R.L. Zahradnik and R.J. Crace, Adv. Chem. Ser. 131, 128 (1974).

20. P.S. Lewis, S. Friedman, R.W. Hiteshue, Adv. Chem. Ser. 69, 50 (1967).

21. H.F. Feldmann, W.H. Simons, J.A. Mima, R.W. Hiteshue, Am. Chem. Soc. Div. Fuel Chem. Prepr. 14 (No. 4), 1 (September 1970).

22. H.F. Feldmann, J.A. Mima, P.M. Yavorsky, Adv. Chem. Ser. 131, 108 (1974).

23. F. Moseley and D. Paterson, J. Inst. Fuel 38, 13, 378 (1965).

24. F. Moseley and D. Paterson J. Inst. Fuel 40, 523 (1967).

25. R.W. Hiteshue, R.B. Anderson, and S. Friedman, Ind. Eng. Chem. 52, 577 (1960).

26. R.W. Hiteshue, S. Friedman, R. Madden, U.S. Bur. Mines Rep. Invest. 6125 (1962).

27. R.W. Hiteshue, S. Friedman, R. Madden, U.S. Bur. Mines Rep. Invest. 6376 (1964).

28. S. Friedman, R.W. Hiteshue, M.D. Schlesinger, U.S. Bur. Mines Rep. Invest. 6470 (1964).

29. W.C. Schroeder, U.S. Pat. 3,030,297, April 17, 1962.

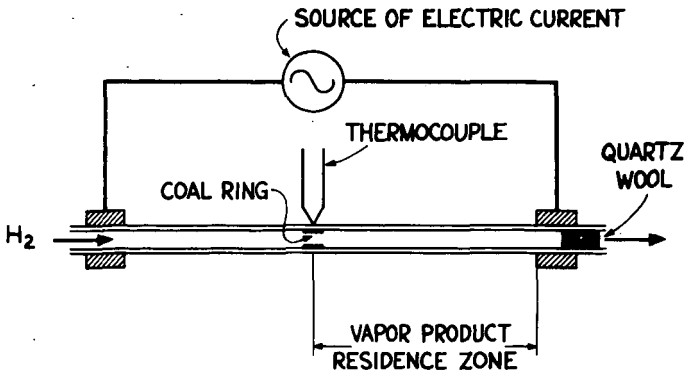


Figure 1. Reactor for flash heating of coal. Location of coal deposit and hydrogen flow rate are selected to give the desired vapor product residence time.

---

Figures 2-5. Yields versus temperature at 100 atm. $H_2$, heating rate 650 °C/sec, 0.6 sec. vapor residence time, 10 sec. solids contact time.

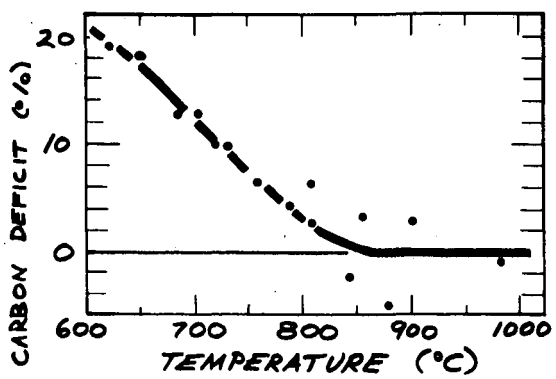


Figure 2. Carbon deficit.

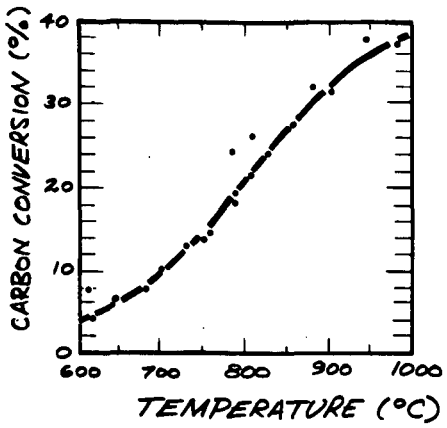


Figure 3. Methane Yield

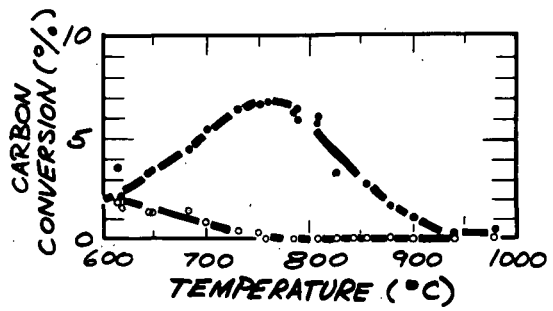


Figure 4. Yield of ethane (closed circles) and propane (open circles).

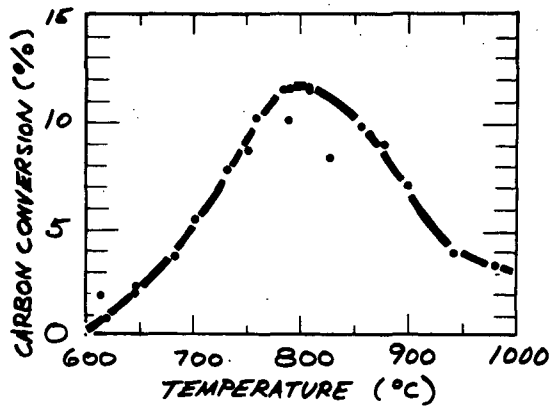


Figure 5. BTX (benzene + toluene + xylenes) yield.

---

Figures 6-8. Yields versus vapor residence time at 700°C, 100 atm. hydrogen, heating rate 650°C/sec., 10 sec. solids contact time. (Closed circles from Figures 2-5.

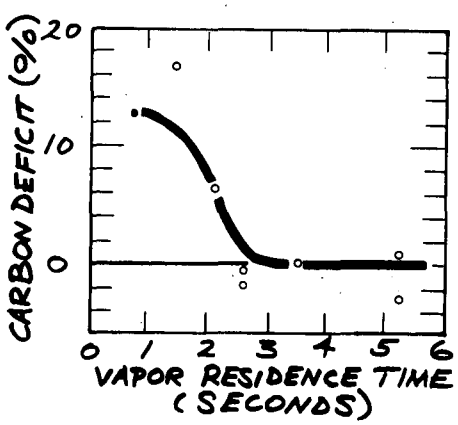


Figure 6. Carbon deficit.

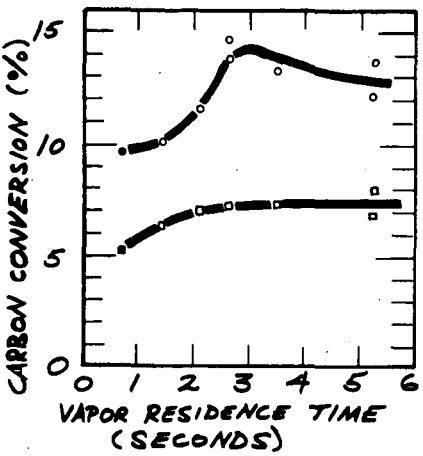


Figure 7. Yields of methane (circles) and ethane + propane (squares)

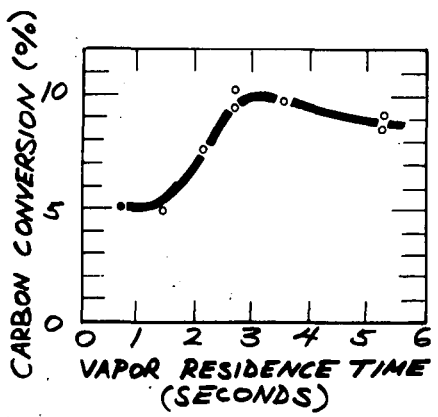


Figure 8. Benzene yield.

"ENTRAINED PRETREATMENT OF COAL" by Glenn E. Johnson, David A. Green, Albert J. Forney, William P. Haynes and Harry B. Neilson, U.S. Energy Research and Development Administration, 4800 Forbes Avenue, Pittsburgh, PA 15213.

A method for destroying the caking properties of coal during transport is under study at the Pittsburgh Energy Research Center of the U. S. Energy Research and Development Administration. Caking coal ground to 20 x 0 mesh is pretreated under pressure in a 75-ft. length of 1/2" pipe while entrained in a heated stream of oxygen and nitrogen. Pittsburgh seam, a highly caking coal, was pretreated at 100 psig with a transport gas linear velocity of 10 ft/sec, an oxygen to coal ratio of 1.5 SCF/lb and a nominal temperature of 375° C. Data from tests with Pittsburgh seam coal was analyzed using a computerized multiple linear regression analysis. An equation was developed which relates the free swelling index (FSI) to the oxygen concentration, temperature, gas velocity, coal feed rate, and operating pressure. Illinois #6, a moderately caking coal, was pretreated during entrainment at less severe conditions (320° C and $0_2$ to coal ratio of 0.7 scf/lb.) than required for Pittsburgh seam coal.

# Development of a Fluidized Bench-Scale Reactor for Kinetic Studies



Louis D. Friedman

COGAS Development Company
P.O. Box 8, Princeton, New Jersey

The COGAS Development Company (CDC) is a consortium made up of Consolidated Natural Gas Service Company, FMC Corporation, Panhandle Eastern Pipe Line Company, and Tennessee Gas Pipeline Company. COGAS Development Company is developing a process for the conversion of coal to gas and oil. The gas can either be pipeline gas (SNG) or an industrial medium-Btu fuel gas. The oil can either be a synthetic crude oil or a low-sulfur fuel oil. The COGAS process combines the fluidized-bed pyrolysis of coal with gasification of the char. Gasification is achieved by steam, producing a syngas -- CO and $H_2$ -- without the need for bulk oxygen. This process has been described previously [1][2].

Fluidized-bed pyrolysis was developed by FMC Corporation under the COED project, which was sponsored by the Office of Coal Research, U.S. Department of the Interior. Results of this project were published [3]. A number of chars produced in the COED pilot plant were utilized in these studies.

Because of the divergent interests in different coals of the several partners, work was initiated to develop a bench-scale unit which could yield the data needed for evaluating potential coals for a COGAS plant.

The requirements for this unit were that it be capable of both estimating the yields of oil that might be expected from fluidized-bed pyrolysis, and of determining the reactivity of the char that would result from this pyrolysis. The design of this Coal Evaluation Unit (CEU) was such that one operator could obtain both coal pyrolysis yields and char reactivity data in one day.

Thermogravimetric analysis (TGA) is widely used for these determinations. However, thermal analysis of coal presents problems inherent in coal's nature [4]. TGA measurements show total loss of weight on pyrolysis, but give no information as to the relative amounts of tar or gas that are or might be obtained in fluidized-bed pyrolysis. Our experience with the TGA also showed that gasification rates obtained with steam and $CO_2$ were as much as one order of magnitude greater than those obtained in large-scale pilot plants. In addition, TGA experiments are expensive and time consuming, and since the TGA uses such small samples, analysis of the residual decomposition products is seldom meaningful. Attempts to develop wet oxidation procedures for determining carbon reactivity give only semi-quantitative data [5].

To overcome these deficiencies the subject investigation was undertaken.

## DESCRIPTION OF THE COAL EVALUATION UNIT

A flow diagram of the coal evaluation unit (CEU) is shown in Figure 1. The reactor is a capped Alonized 310 stainless steel tube 24 inches long and 2 inches ID. The reactor is heated electrically by two hemi-cylindrical 900 kW Lindberg heaters 18 inches long. Two 1/4-inch tubes are welded in the top cap of the reactor. Feed is charged through one

of these tubes, and pyrolysis and gasification products are removed through the other. A stainless steel thermowell which extends to within 4 inches of the top of the reactor is welded in the center of the bottom cap. A perforated stainless steel plate,which supports the solids inside the reactor,is welded on the thermowell about 6 inches above the bottom of the reactor. The bottom cap also contains a section of 1/4-inch tubing through which fluidization gas enters the reactor.

Gases flowing to the reactor are heated to about 1000°F in a closely wound, 310 stainless steel coil 12 inches long and 1 inch in diameter. This gas heater is heated by two Lindberg heaters. Char is fed to the reactor from a 1-1/2-inch ID glass tube which serves as a feed reservoir. This tube is mounted on a Syntron vibrator which charges 70 to 100 g of char over a 15-to 30-minute period. Steam is used as the fluidizing gas in both the pyrolysis and gasification operations. Coal is usually pyrolyzed at 900 to 1100°F. At these temperatures the reaction of steam with coal is negligible.

The condensing system consists of two glass air-and water-cooled condensers, a glass-wool trap, and a quinoline scrubber in series. The glass-wool trap and quinoline scrubber remove tar fog from the gas. Gases leaving the quinoline scrubber are sampled, analyzed by gas chromatography, measured, and vented to a hood. The chromatograph used is a Carle Basic Gas Chromatograph equipped with automatic sampling and switching devices. This instrument analyzes for CO, $CO_2$, $CH_4$, $O_2$, $N_2$ and $H_2O$ every 7-1/2 minutes. Hydrogen is obtained by difference.

## OPERATING PROCEDURE

Ten grams of 1/8 x 25-mesh sand are charged to the reactor to improve transfer of heat to the fluidizing gas, and to prevent fine coal particles from plugging the perforated bed support plate. A 25- x 60-mesh fraction of feed is used. The steam velocity through the reactor is maintained at about 0.5 ft/s. Velocities over 0.8 ft/s carry char fines and low-density gasified char out of the reactor, and velocities below 0.3 ft/s do not fluidize the bed.

### A. Non-Coking Coals

Non-coking coals may be introduced into the reactor at any temperature from room temperature up to the pyrolysis temperature. The feed is added over a 30-minute period. Pyrolysis is usually conducted at a maximum temperature of about 1100°F. The char is held at the maximum temperature for 30 to 60 minutes, at which time oil production has ceased and gas make is negligible.

If the char that remains after pyrolysis is to be gasified, the temperature of the reactor is raised to the desired gasification temperature, and steam is then charged into the reactor at a velocity of approximately 1/2 ft/s. Gasification is normally continued for three hours. Gases produced during pyrolysis and gasification are analyzed continually by gas chromatography.

To determine oil yields, the condensed water is decanted through a filter paper to recover carryover char fines. The filter paper, condensers, fines, and the water-tar receiver are washed with acetone to dissolve the collected oil, and the acetone solution is filtered to remove char that was mixed with the oil The acetonefiltrate is evaporated in a tared flask to determine the weight of oil recovered. The glass-wool trap is dried at 220°F and its gain in weight is considered to be oil.

The small amount of oil that is collected in the quinoline trap is not included in the oil recovery, as quinoline also collects water.

The weight of gas formed during pyrolysis, the amount of carbon gasified, and the gasification rate of char are all calculated from the volume and the analysis of the gases formed during pyrolysis and gasification, respectively. Char recovery is the sum of the weights of char carried overhead and that recovered from the reactor at the end of the run.

B. Coking Coals

Unlike non-coking coals which may be charged to a reactor at any temperature for pyrolysis, coking coals must be charged to the reactor below the incipient coking or softening temperature. This is usually about 650°F. To prevent a buildup of coke in the reactor, coking coals are diluted in a 1:2 weight ratio with an ash fraction that has the same 25-x 60-mesh size as the coal feed. After the coal-ash mixture has been charged, the temperature of the reactor is raised to 1100°F over a 1 to 1-1/2 h period. The reactor is kept at 1100°F for an additional hour to complete removal of the tarry oil fractions from the reactor.

After pyrolysis is complete, gasification and oil recovery is conducted as described above.

C. Char Reactivity

If reactivity data only are desired on chars which are known to evolve no oil on heating, the reactor is heated directly to the gasification temperature. The char may be added either before the reactor is heated or when the reactor has reached the gasification temperature. Experiments with COED chars prepared from Illinois coal showed that both procedures gave the same gasification rates. Char reactivity is calculated from the volume of gas produced and the amount of carbon reacted as described above.

## ANALYSIS OF FEEDSTREAMS

The analyses of coals and chars used in these studies are presented in Tables 1 and 2.

## PYROLYTIC STUDIES

Data obtained in pyrolyzing lignite and Utah coals are shown in Table 3. The lignite yields much less oil and more gas than the Utah coal. The CEU cannot determine liquor yields because steam is the carrier gas. With many coals liquor yields obtained by fluidized-bed pyrolysis are approximately 0.45 times the oxygen content of the coal [6]. This correction is probably high for lignite, but gave a reasonable material balance with the Utah coal. Table 3 also compares the oil and gas yields obtained in the CEU with those obtained by COED in their 4-stage pyrolysis system, using a maximum temperature of 1450°F.

Hot-stage microscope studies showed that shock heating increased the yield of volatiles obtained from coal [7]. A similar effect was noted in the CEU, as shown in Table 4. Although the range of oil yields is narrow, yields increased steadily as the temperature at which the lignite was introduced into the CEU reactor was increased. Thus, the lowest yield of oil was obtained from the run in which the lignite was added to the

reactor at room temperature, even though this char was ultimately heated to the highest temperature shown.

Pyrolysis data for two high-volatile A bituminous coals are presented in Table 5. In all runs, coal was charged to the CEU reactor at 600 to 680°F, and all chars were heated to 1100 to 1180°F. Both coals coked when processed under the same conditions used with the lower-rank coals. When these coals were diluted with two parts of ash, the Sewickley-seam coal gave 21 to 22 wt percent oil, and the Pittsburgh-seam coal, 27.2 wt percent oil. Runs 62, 63 and 64 show how oil yields were reduced drastically when these coals were air-oxidized to inhibit their coking. The sums of the yields of oil, gas, and char for all ash-diluted runs range from 92.4 to 99.5 weight percent, indicating good closures in all runs.

## GASIFICATION OF CHARS

Earlier in the COGAS program, the reactivities of chars were determined in a 3.75-inch ID fluidized-bed char reactivity unit (CRU) that has been described in an earlier publication [8]. Several COED chars were evaluated in both units to determine the correlation of results obtained in the two units. The results are summarized in Table 6. All CRU runs were made with steam velocities of either 0.4 or 0.6 ft/s. As noted above, the CEU was operated at about 0.5 ft/s.

The gasification results obtained in the CEU agree fairly well with those obtained in the larger CRU. Similar results were obtained with Illinois char in the COGAS pilot gasifier [2]. Lignite chars prepared in the CEU in Runs 5 and 6 had reactivities at 1430 and 1500°F that were in line with lignitic chars prepared in the COED reactor system. The lignitic chars were by far the most reactive evaluated.

The CEU studies corroborated unexplained trends found in the CRU. Thus, the third-stage COED Illinois No. 6 char was more reactive than the fourth-stage char (Runs 71 and 22), but this was not the case with the Utah or Western Kentucky chars. In the COED pilot plant, the third stage usually operated at 1000°F; the fourth stage, at 1450-1550°F. Note that a char prepared from Western Kentucky coal in the CEU had the same activity as third-and fourth-stage chars prepared from this coal in the COED reactors. (Compare Run 68 vs. Runs 78 and 79.)

Oxidation reduces the yield of tars derived from pyrolysis. CEU studies demonstrated that oxidation also reduces the gasification rates of the resultant chars markedly. For example, Western Kentucky char produced in the COED pilot plant with mild oxidation in Stage 1 had only half the reactivity of chars made from this coal without oxidation. (Compare Runs 49 and 50 with Runs 78 and 79.) Similarly, chars made from oxidized Pittsburgh-and Sewickley-seam coals were less reactive than those prepared from unoxidized coals. (Compare Runs 64 and 63 with 61.) A sample of coke that was prepared from Sewickley coal in the CEU also had a low char reactivity (Run 55).

The CEU has also been useful for other studies, e.g., determining $CO_2$ reactivities up to 1900°F, conducting fluidization studies, etc. It has proven to be a versatile and useful tool that met all the requirements outlined for it. The CEU has now been used for more than 1000 hours and shows no evidence of corrosion. This is attributed to the aluminizing treatment that was administered to the reactor. An earlier non-aluminized reactor handling the same gases showed corrosion after

less than 150 hours on stream.

ACKNOWLEDGEMENT

The author gratefully acknowledges the encouragement and advice given during the conduct of these studies by Dr. R. T. Eddinger, and thanks Dr. H. L. Malakoff and the members of the COGAS Consortium for permission to present this paper.

BIBLIOGRAPHY

1. Bloom, R.,Jr. and Eddinger, R. T., Paper presented before the Sixth American Gas Association Synthetic Pipeline Gas Symposium, Chicago, Ill., Oct. 28, 1974.

2. Sacks, M. E. and Eddinger, R. T., Paper presented at AIChE Meeting, Houston, Texas, Mar. 18, 1975.

3. Scotti, L. J., Jones, J. F., Ford, L. and McMunn, B. D., Chem. Eng. Progress 71 (4) 61-2 (April, 1975).

4. Smith, J. W. and Johnson, D. R., Proc. Second Toronto Symp. Thermal Analysis, Toronto Sec., Chem. Inst. of Canada, Feb. 27, 1966, pp 95-116.

5. Moore, G. E. and Bahn, S. P., Report No. 105. West Virginia School of Mines, April,1974.

6. Private communication, L. H. Dierdorff, COGAS staff.

7. Rau, E. and Robertson, J. A., Fuel 45, 73-80, Jan., 1966.

8. Seglin, L., Friedman, L. D. and Sacks, M. E., Vol. 19, No. 4, preprints of papers presented before the Division of Fuel Chemistry, 168th National Meeting, Atlantic City, N. J., Sept., 1974.

TABLE 1

Analysis of Coals

| Coal Rank | hvAb | hvAb | hvBv | hvCb | hvBb | Lignite |
|---|---|---|---|---|---|---|
| Seam | Sewickley | Pittsburgh | Hiawatha | Illinois No. 6 | No.9 and 14 | - |
| Source | Consolidated Natural Gas Co. | Consolidated Natural Gas Co. | Utah King Mine | Peabody No. 10 Mine | Paradise Mine, W. Kentucky | Glen Harold Mine, No.Dakota |
| **Proximate Analysis, wt%** | | | | | | |
| Volatile matter | 31.6 | 34.5 | 42.6 | 37.9 | 35.2 | 48.9 |
| Fixed Carbon | 54.8 | 58.7 | 50.7 | 50.0 | 55.1 | 44.6 |
| Ash | 13.6 | 6.8 | 6.7 | 12.1 | 9.7 | 6.5 |
| **Ultimate Analysis, wt%** | | | | | | |
| Carbon | 73.5 | 78.0 | 73.9 | 66.5 | 69.0 | 60.6 |
| Hydrogen | 5.1 | 5.3 | 5.9 | 4.8 | 5.1 | 4.6 |
| Nitrogen | 1.6 | 1.4 | 1.3 | 1.3 | 1.5 | 1.1 |
| Sulfur | 1.3 | 2.7 | 0.6 | 4.0 | 3.3 | 0.9 |
| Oxygen (diff) | 4.9 | 5.8 | 11.6 | 11.3 | 11.4 | 26.3 |
| Ash | 13.6 | 6.8 | 6.7 | 12.1 | 9.7 | 6.5 |

TABLE 2

Analyses of Chars

| | W. Kentucky | | Utah King | | Illinois No. 6 | |
|---|---|---|---|---|---|---|
| | 3rd Stage | 4th Stage | 3rd Stage | 4th Stage | 3rd Stage | 4th Stage |
| **Proximate Analysis, wt%** | | | | | | |
| Volatile Matter | 5.8 | 3.5 | 5.2 | 2.4 | 5.3 | 3.1 |
| Fixed Carbon | 78.9 | 83.5 | 80.1 | 83.2 | 77.2 | 73.4 |
| Ash | 15.3 | 13.0 | 14.7 | 15.1 | 17.5 | 23.5 |
| **Ultimate Analysis, wt%** | | | | | | |
| Carbon | 77.4 | 75.1 | 82.5 | 79.6 | 77.3 | 74.1 |
| Hydrogen | 1.6 | 2.2 | 1.3 | 1.2 | 1.5 | 0.8 |
| Nitrogen | 1.4 | 1.3 | 1.2 | 1.2 | 1.1 | 0.9 |
| Sulfur | 3.1 | 2.9 | 0.6 | 0.6 | 2.9 | 4.0 |
| Oxygen (diff) | 1.2 | 5.5 | - | 2.3 | - | - |
| Ash | 15.3 | 13.0 | 14.7 | 15.1 | 17.5 | 20.2 |

TABLE 3

Pyrolysis of Lignite and Utah Coals

| Run No. | Pyrolysis Temp, °F Initial | Final | Product Yields, wt Percent Oil | Gas | Char | Liquor (Calc) | Total |
|---|---|---|---|---|---|---|---|
| | | | LIGNITE | | | | |
| 10 | 700 | 900 | 5.0 | 32.0 | 56.7 | 11.8 | 105.5 |
| 6 | 900 | 900 | 6.8 | 25.6 | 57.6 | 11.8 | 101.8 |
| | | | UTAH COAL | | | | |
| 30 | 800 | 800 | 17.9 | 17.2 | 59.1 | 4.0 | 98.2 |
| 31 | 900 | 900 | 18.5 | 11.6 | 59.0 | 5.1 | 94.2 |
| COED [3] | | 1450 | 21.5 | 18.3 | - | - | - |

TABLE 4

Effect of Charge Temperatures on Lignite Oil Yields

| Run No. | Pyrolysis Temp., °F Initial | Final | Oil Yield, wt Percent |
|---|---|---|---|
| 13 | 70 | 1400 | 4.7 |
| 10 | 700 | 900 | 5.0 |
| 5 | 800 | 900 | 6.5 |
| 6 | 900 | 900 | 6.8 |
| 14 | 1400 | 1400 | 7.3 |

TABLE 5

Pyrolysis of High Volatile A Coals

| Run No. | Coal Seam | Coal:Ash Ratio | Yields, wt Percent Oil | Gas | Char |
|---|---|---|---|---|---|
| 53 | Sewickley | 1:0 | 11.6 | 11.0 | 57.5[a] |
| 62[b] | " | 1:0 | 9.2 | 12.5 | 77.3 |
| 59 | " | 1:2 | 22.1 | 25.4 | 52.0 |
| 60 | " | 1:2 | 21.4 | 18.8 | 52.2 |
| 63[c] | Pittsburgh | 1:0 | 0.2 | 10.4 | 72.5 |
| 64[b] | " | 1:0 | 15.4 | 10.0 | 69.4 |
| 61 | " | 1:2 | 27.2 | 19.2 | 49.3 |

[a] Sample coked

[b] Coal air-oxidized at 350 to 400°F for 30 minutes

[c] Coal air-oxidized at 350 to 400°F for 60 minutes

TABLE 6

Gasification of Chars

| Run No. | Derivative Coal | Char Source | Gasification Temp., °F | Gasification CEU | Rate[1] CRU |
|---|---|---|---|---|---|
| 5 | Lignite | CEU | 1430 | 0.61 | |
| 6 | " | CEU | 1500 | 0.90 | |
| - | " | COED-4th Stage | 1430 | | 0.60 |
| - | " | COED-4th Stage | 1600 | | >1.0 |
| 71 | Illinois | COED-4th Stage | 1600 | 0.11 | 0.14 |
| 22 | " | COED-3rd Stage | 1600 | 0.30 | 0.24 |
| 23 | " | COED-4th Stage | 1700 | 0.26,0.23 | 0.23 |
| 48 | Utah | COED-3rd Stage | 1600 | 0.15 | 0.18 |
| 46 | " | COED-4th Stage | 1600 | 0.22 | 0.21 |
| 78 | W. Kentucky | COED-3rd Stage | 1600 | 0.29 | 0.24 |
| 79 | " | COED-4th Stage | 1600 | 0.28 | 0.23 |
| 68 | " | CEU | 1600 | 0.27 | - |
| 49 | " (oxidized) | COED-3rd Stage | 1600 | 0.14 | - |
| 50 | " " | COED-4th Stage | 1600 | 0.14 | - |
| 64 | Pittsburgh " | CEU - Oxidized | 1600 | 0.12 | - |
| 63 | " " | CEU - Oxidized | 1600 | 0.15 | - |
| 61 | " | CEU | 1600 | 0.38 | - |
| 55 | Sewickley | CEU - Coked | 1600 | 0.18 | - |
| 59 | " | CEU | 1600 | 0.40 | - |
| 60 | " | CEU | 1600 | 0.48 | - |

[1]g C gasified/(h)(g C in bed)

Figure 1

## COAL EVALUATION UNIT (CEU)

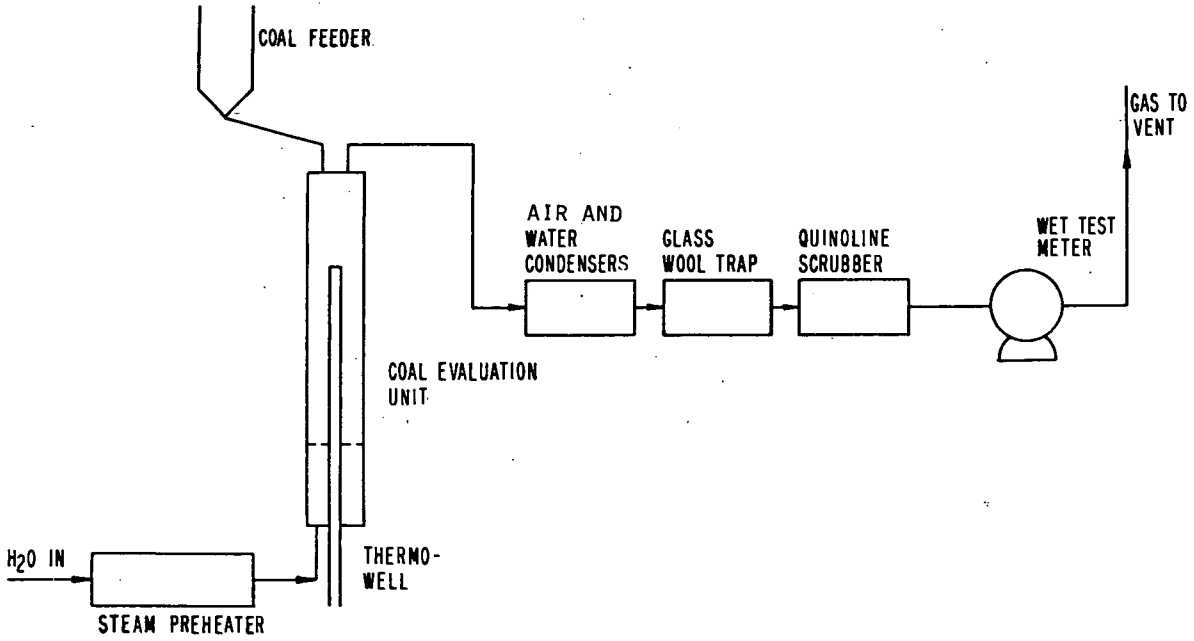

# FACTORS AFFECTING REACTIVITY OF COAL CHARS

Philip L. Walker, Jr. and Edwin J. Hippo

Pennsylvania State University
Department of Material Sciences
University Park, Pennsylvania 16802

## INTRODUCTION

It is helpful when attempting to understand reactivity of coal chars to draw on what is known about gas-solid interaction from voluminous studies on both the gasification of more crystalline carbons and heterogeneous catalysis. Rates of gasification of porous carbons are primarily affected by three parameters: active site concentration; accessibility of the reactant gas into the internal area of the char and, hence, to active sites; and presence of catalysts which are active for the dissociation of molecular species into reactive oxygen atoms or hydrogen atoms (1,2). Following a discussion of these parameters, reactivities to air and $CO_2$ of sixteen chars produced from coals of varying rank will be considered.

## THEORETICAL CONSIDERATIONS

It is well to review briefly the structure and thermal behavior of coals insofar as they will determine whether a char is produced from coal and what physical characteristics the char will possess. Extensive x-ray, infrared, and NMR studies have been conducted on coal; and even though there is not today complete agreement on the "building blocks" which make up coal, we will take a position. Our position is based primarily on the detailed x-ray studies of Cartz and Hirsch (3).

Coals are composed of aromatic and hydroaromatic layers, terminated at their edges by various functional groups and crosslinked by various functional groups. The average size of the layers and the number aligned closely parallel increase with increasing rank of coal. More or less poor alignment between packets of layers produces internal porosity and results in coal being a microporous material. Upon heat treatment all coals lose volatile matter, primarily from the periphery of the layers. Further, some coals soften extensively, form an anisotropic mesophase, which coalesces into a coke (4). Other coals, upon heat treatment, do not soften (they behave as thermosetting materials) and are converted to a char. The extent of softening is thought to be primarily determined by the concentration and thermal stability of the crosslinking groups. The micropore structure which was in the precursor coal is essentially preserved in the char if it has not been taken to too high a temperature. Indeed the microporosity can become more accessible to reactant gases because of loss of volatile matter. However, if the processing temperature is taken too high, microporosity in the char is rapidly lost. This is a result of the thermal breakage of crosslinks between planar regions in the char, allowing improved alignment of these regions with loss of porosity between regions. The structure of chars is envisioned as being composed of small trigonally bonded planar regions, terminated by markedly fewer hetero-atom functional groups than in the original coal, and still containing substantial (but somewhat less) crosslinking than the original coal. The exact structure of a char produced from a given precursor coal can be changed by altering such variables as: possible coal pretreatment (to introduce more crosslinks), coal particle size, rate of heating, maximum temperature and time at maximum temperature, atmosphere and total pressure present during heating. It is with this background that the reactivity of coal chars can be considered.

Active sites To understand the kinetics of the gasification of a carbonaceous solid, a correct term for the concentration of sites which can potentially take part in the reaction is needed. Given the ability to measure total surface areas of solids by physical adsorption of gases in 1938, efforts were made to correlate gasification rates

of carbonaceous solids with their total area. These efforts were not successful. Finally, in 1963 Walker and co-workers (5) showed for the $C-O_2$ reaction that the appropriate concentration term was that given by dissociative oxygen chemisorption onto sites -- this was a measure of active sites. Later Walker and co-workers (6), Hennig (7), and Thomas and Roscoe (8), showed clearly that the active sites involved in the gasification of carbon in a trigonally bonded solid are those located at the periphery of layer planes and at vacancies and non-basal dislocations within layer planes. In this light, it can be said that if one wishes to maximize the reactivity of coal chars, the average crystallite size should be kept to a minimum and the defect concentration in the layer plane kept to a maximum.

Mass transport limitations Thiele (9), Zeldowitsch (10), and Wheeler (11), pioneered the concept that for a gas interacting with a porous solid the active sites within the solid, under some circumstances, may be exposed to the reactant gas at a concentration significantly lower than its concentration at the surface of the solid. This can result in the "utilization efficiency" of the active sites for gasification becoming $<<1$. The phenomenon occurs at higher gasification rates when a large concentration gradient of reactant between the surface of the solid and its center is needed to supply the gas within the solid for reaction. The situation has been considered in detail by Walker and co-workers (1) for the gasification of carbon. Figure 1 presents an idealized Arrhenius plot depicting the situation, when one considers a half cylinder of porous carbon. In Zone I, the reactant concentration gradient is negligible within the solid; the utilization efficiency, $\eta$, of active sites is $\approx 1$. With increasing temperature and gasification rate, $\eta$ eventually $\rightarrow 0$. In a char gasification process, it is important to locate the zone in which reaction is occurring in order that the kinetics may be understood.

Mass transport limitations are expected to vary significantly as chars produced from coals of different rank are gasified. That is, coals and coal chars have a trimodal pore distribution, with most of the active sites located within the micropores which are defined as being less than 12A in diameter (12). Walker and co-workers (13) have shown that the rate of gaseous diffusion within the micropore system is slow and, indeed, an activated process for pores (apertures) less than about 5A. Thus it is certain that if the sites located in the micropores are to be well utilized for reaction (that is $\eta \rightarrow 1$), the interior of the solid must have an adequate number of larger, feeder pores off which the micropores connect. Diffusion through the feeder pores to the mouths of the micropores will be reasonably rapid; and, therefore, reactant concentration at the mouths of the micropores can closely approach the value of reactant concentration at the exterior particle surface.

Walker and co-workers (12) show that low rank coals tend to have a greater percentage of their total pore volume in larger pores than do the higher rank coals. Thus, it is expected that chars derived from the lower rank coals will have a larger feeder pore system and be less mass transport limited during their gasification.

Catalysis Almost every metal in a reduced and/or oxidized state is a catalyst for carbon gasification (2). Catalyst activity varies between impurities and with their concentration and extent of dispersion (ratio of atoms in the surface to total atoms). Specific catalyst activity, that is activity per unit catalyst weight, usually decreases as the amount of catalyst present and its particle size increase (2). Therefore, even though most of the inorganic impuritiy content in most coals is located in the mineral matter, the possible catalytic activity of trace and minor elements (present as organo-metallics) cannot be ignored. That is, many of the trace elements are very highly dispersed within the coal matrix compared to the extent of mineral matter dispersion.

In this regard the situation with lignitic chars is most interesting. Lignites have high concentrations of carboxyl groups at the edges of their layers. Ion exchange has occurred in nature with cations like calcium replacing a significant amount of hydrogen on the carboxyl groups. Upon the thermal conversion of lignites to chars, the

carboxyl groups decompose depositing large amounts of highly dispersed calcium (and other metals) onto the char surface. Probably, as a result, the reactivity of chars to air has been found to correlate reasonably well with the amount of calcium present (14).

## EXPERIMENTAL

The coals used were the same as those used in a previous reactivity study (14). Table 1 presents analyses of the coals. Methods of char preparation and procedures for measuring char reactivity have been described previously by Jenkins et al on their studies in air (14). A small quantity of coal (5-10 mg) was placed on a Cahn Model RG Electrobalance of a Fisher TGA apparatus and heated at a rate of 10°C per min to 1000°C in a $N_2$ atmosphere. Samples were held at 1000°C until no further weight loss was detectable.

Selected coals were treated with warm 10% HCl for 48 hr, followed by their being washed with water, dried, and charred. Demineralized samples were prepared by taking acid washed coals and treating them with warm HF, followed by extensive washing and drying prior to charring.

Samples of PSOC 127, a relatively unreactive low volatile coal char, and PSOC 87, a highly reactive lignite char, were chosen for an investigation of the effect of particle size on reactivity. Both chars derived from the parent coals and demineralized coals were studied. Approximately 40 g of each coal of 40x100 mesh particle size were further ground using a pestle and mortar. The ground coals were then hand sifted for 20 min to obtain four cuts: +100, 100x150, 200x325, and -325 mesh. Chars were prepared and reactivities measured for all cuts.

In this study reactivity of chars to $CO_2$ has been measured, with the objective of comparing reactivities with those measured previously in air (14). Since the carbon-carbon dioxide reaction is a much slower reaction than the carbon-air reaction (1), it must be carried out at a much higher temperature to obtain the same rate as for the air reaction. A temperature was selected at which the rate of reaction of the more reactive lignites in $CO_2$ corresponded closely to their reactivities in the air at 500°C. Such a temperature was 900°C for the 40x100 mesh coal-derived chars. The use of less than 5 mg of char ensured that the reactivity per unit weight of char was independent of char weight (or bed depth).

Following preparation of a char at 1000°C, it was cooled in dry $N_2$ to 900°C prior to reaction. Dry $CO_2$ was admitted at a flow rate of 300cc (NTP) per minute, and weight of the char was continuously recorded. As with the air reaction, burn-off curves usually go through three regions of reactivity: purge and activation, linear burn-off rate, and decreasing burn-off rate. During the linear region the char loses weight but increases in specific surface area because of activation. This region continues until the specific surface area no longer increases; the gasification rate begins decreasing and the third region is entered. The linear region for each coal varies in duration, but in each case the rate in the linear period is measurable. The linear region represents the maximum rate at which chars gasify.

Reactivities of the chars were calculated as follows:

$$R = \frac{1}{W}\frac{dW}{dt}$$

R = reactivity of the char (mg $hr^{-1}$ $mg^{-1}$)
W = weight of initial char on ash free basis (mg)
dW/dt = change in char weight with time (mg $hr^{-1}$)

## RESULTS AND DISCUSSION

Figure 2 plots reactivity of the chars versus carbon content of the parent coals for both the $CO_2$ and air reactions. As with the air reaction, the lignites are the most reactive chars and have the widest spread of reactivity values. Reactivities in $CO_2$ and air at 900°C and 500°C, respectively, are closely similar for all chars. The lowest reactivity for both reactions was recorded for a char from LV bituminous coal PSOC 127. For the $CO_2$ reaction this coal was over 150 times less reactive than was a highly reactive Montana lignite, PSOC 91. This low reactivity of PSOC 127 char is attributed to a relative absence of large (feeder) pores in coal of this rank and, hence, poor utilization of the surface area in the micropores for reaction. The high reactivity of the lignites is attributed, at least in part, to a large percentage of pore volume in macro and transitional pores and, hence, better utilization of the micropore surface area for reaction.

Ash in the coals was studied by Jenkins et al (14). The ash was analyzed for K plus Na, Ca, Mg, and Fe. A reasonably good linear correlation between increasing Ca content (up to about 7% CaO in the coal) and increasing reactivity of the chars in air or $CO_2$ was found. A similar correlation for Mg was found up to about 1% MgO. No correlations were found for Fe or for Na plus K.

Reactivity measurements were made in $CO_2$ on four particle sizes of chars from original and demineralized samples of PSOC 127 and 87. Results are listed in Table 2. For all samples, a decrease in particle size results in an increase in reactivity which is an indication that reactivities are in part controlled by diffusional resistance of $CO_2$ into the interior of the particles. Whereas reduction in particle size of PSOC 87 from 40x100 to 200x325 mesh results in a reactivity increase of only 2.7 fold, a similar particle size reduction of PSOC 127 results in a reactivity increase of 35 fold. The fact that particle size reduction of PSOC 127 has a very marked effect on increasing reactivity is as expected since this char, produced from a low volatile coal, presents a high resistance to the internal diffusion of reactant gases.

For each particle size studied demineralization of PSOC 87 results in a decrease in reactivity, whereas demineralization of PSOC 127 leads to an increase in reactivity. These results show the important roles and balance which catalysis and mass transport resistance play in affecting reactivity of coal chars. For PSOC 87, mass transport resistance is at a minimum since lignites and their chars possess significant macro and transitional (feeder) porosity. Introduction of additional feeder porosity by mineral matter removal results in decreasing mass transport resistance relatively little compared to the effect of mineral matter removal on decreasing catalytic activity for gasification. By contrast, since PSOC 127 has little macro and transitional porosity, removal of mineral matter results in a dramatic increase in this porosity and, hence, a substantial decrease in mass transport control of gasification. In this case the decrease in mass transport resistance more than offsets the loss of catalytic activity due to mineral matter removal.

Thus reactivity of chars which differ by more than 100 times can be brought increasingly closer together by reduction in their particle size and/or acid treatment of the parent coal. Undoubtedly other approaches are available to modify reactivities of chars. Some of these are being studied at present.

## ACKNOWLEDGMENTS

This research was supported by the U.S. Energy Research and Development Administration on Contract No. 14-01-0001-390. Professor W. Spackman supplied the coals studied.

REFERENCES

1. Walker, P. L., Jr., Austin, L. G. and Rusinko, F., Jr., Advances in Catalysis, Vol. 11, Academic Press, New York, 1959, pp. 133-221.

2. Walker, P. L., Jr., Shelef, M., and Anderson, R. A., Chemistry and Physics of Carbon, Vol. 4, Marcel Dekker, New York, 1968, pp. 287-383.

3. Cartz, L. and Hirsch, P. G., Trans. Royal Soc. (London), A252, 557 (1960).

4. Brooks, J. D. and Taylor, G. H., Chemistry and Physics of Carbon, Vol. 4, Marcel Dekker, New York, 1968, pp. 243-286.

5. Laine, N. R., Vastola, F. J., and Walker, P. L., Jr., J. Phys. Chem., 67, 2030 (1963).

6. Walker, P. L., Jr., Austin, L. G., and Tietjen, J. J., Chemistry and Physics of Carbon, Vol. 1, Marcel Dekker, New York, 1966, pp. 327-365.

7. Hennig, G. R., ibid, Vol. 2, 1966, pp. 1-49.

8. Thomas, J. M. and Roscoe, C., ibid, Vol. 3, 1968, pp. 1-44.

9. Thiele, E. W., Ind. Eng. Chem., 31, 916 (1939).

10. Zeldowitsch, J. B., Acta Physicochim. USSR, 10, 583 (1939).

11. Wheeler, Ahlborn, Advances in Catalysis, Vol. 3, Academic Press, New York, 1951, pp. 249-327.

12. Gan, H., Nandi, S. P. and Walker, P. L., Jr., Fuel, 51, 272 (1972).

13. Walker, P. L., Jr., Austin, L. G., and Nandi, S. P., Chemistry and Physics of Carbon, Vol. 2, Marcel Dekker, New York, 1960, pp. 257-371.

14. Jenkins, R. G., Nandi, S. P., and Walker, P. L., Jr., Fuel, 52, 288 (1973).

TABLE 1

ANALYSES OF COALS

| PSOC Sample No. | ASTM Rank | State | Ash Content (Dry Basis) % | Ultimate Analysis (wt % daf) C | H | N | S | O (by diff) | Vitrinite Content Volume % (mmf) |
|---|---|---|---|---|---|---|---|---|---|
| 89 | Lignite | N. Dakota | 11.4 | 63.3 | 4.7 | 0.47 | 1.60 | 29.9 | 70.3 |
| 91 | Lignite | Montana | 7.9 | 70.7 | 4.9 | 0.81 | 0.41 | 23.2 | 66.4 |
| 87 | Lignite | N. Dakota | 7.0 | 71.2 | 5.3 | 0.56 | 0.70 | 22.2 | 64.7 |
| 138 | Lignite | Texas | 8.5 | 74.3 | 5.0 | 0.37 | 0.75 | 19.6 | 75.1 |
| 98 | Sbb. A | Wyoming | 6.6 | 74.3 | 5.8 | 1.20 | 1.30 | 17.4 | 84.6 |
| 101 | Sbb.C | Wyoming | 6.2 | 74.8 | 5.1 | 0.89 | 0.50 | 18.7 | 70.8 |
| 26 | HVB | Illinois | 9.6 | 77.3 | 5.6 | 1.10 | 7.50 | 8.5 | 89.2 |
| 22 | HVC | Illinois | 14.4 | 78.8 | 5.8 | 1.50 | 2.90 | 11.0 | 88.2 |
| 24 | HVB | Illinois | 11.6 | 80.1 | 5.5 | 1.10 | 4.50 | 8.8 | 88.1 |
| 105A | HVC | Indiana | 7.5 | 81.3 | 5.8 | 1.10 | 1.80 | 10.0 | 62.5 |
| 171 | HVA | W. Va. | 7.2 | 82.3 | 5.7 | 1.40 | 3.40 | 7.2 | 71.1 |
| 4 | HVA | Kentucky | 1.7 | 83.8 | 5.8 | 1.60 | 0.88 | 7.9 | 67.4 |
| 114 | LV | Pa. | 10.5 | 88.2 | 4.8 | 1.20 | 0.68 | 5.1 | 89.6 |
| 127 | LV | Pa. | 5.0 | 89.6 | 5.0 | 1.00 | 0.83 | 3.6 | 77.7 |
| 81 | Anthracite | Pa. | 9.7 | 91.9 | 2.6 | 0.79 | 0.54 | 4.2 | 96.3 |
| 177 | Anthracite | Pa. | 4.0 | 93.5 | 2.7 | 0.25 | 0.70 | 2.9 | 86.5 |

TABLE 2

EFFECT OF PARTICLE SIZE ON REACTIVITY IN CARBON DIOXIDE

| Mesh Size | Reactivity ($mg\ hr^{-1}\ mg^{-1}$) PSOC 87 | PSOC 87 Dem. | PSOC 127 | PSOC 127 Dem. |
|---|---|---|---|---|
| 40x100 | 2.7 | 0.23 | 0.02 | 0.23 |
| 100x150 | 4.8 | 0.65 | 0.29 | 0.70 |
| 200x325 | 7.4 | 1.1 | 0.69 | 0.92 |
| -325 | * | - | 1.2 | - |

*Rate too rapid to measure.

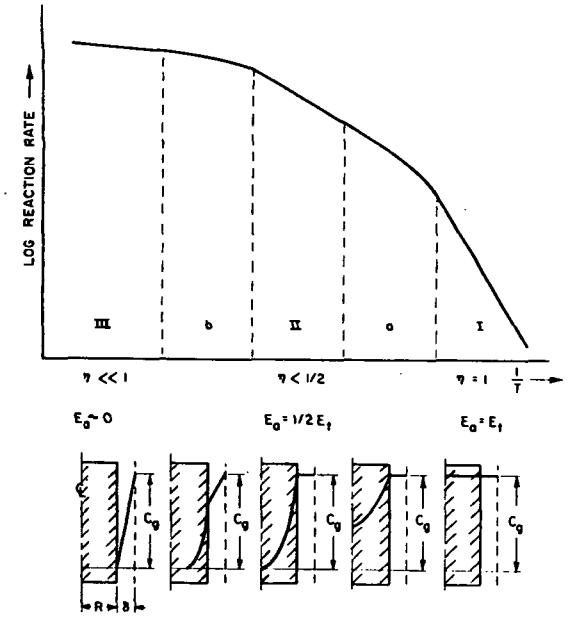


Figure 1 Ideally, the three zones representing the change of reaction rate of a porous carbon with temperature.

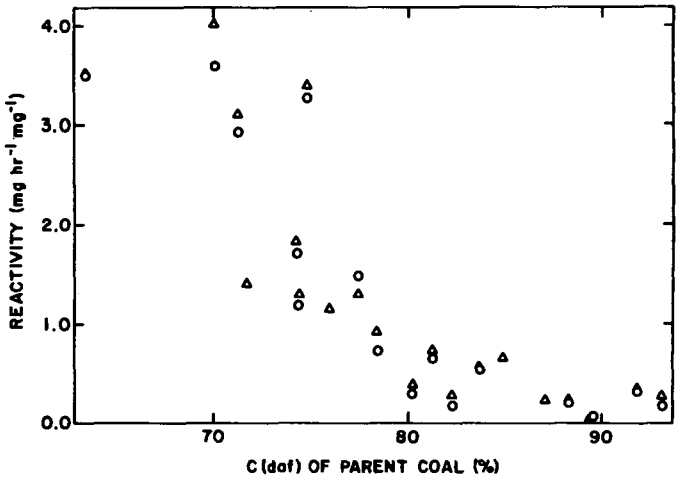


Figure 2 Variation of reactivity of 1000°C chars produced from coals of different rank. (O) $CO_2$ at 900°C, (Δ) air at 500°C.

# CATALYZED GASIFICATION OF COALS AND COAL CHARS

by

K.A. Wilks, N.C. Gardner, J.C. Angus
Department of Chemical Engineering
Case Western Reserve University
Cleveland, Ohio 44106

## INTRODUCTION

The alkali metal or alkaline earth oxides, hydroxides, and carbonates have long been known as excellent promotors of the steam and hydrogen gasification reactions, although the catalytic mechanism is not understood. (Reference 1 contains a good review of gasification technology up to 1963.)

Recent work on catalysis is focusing on substantiation and understanding of much of this past work. Some of the most recent findings are:

1. Alkali metal compounds are the most active in promoting increased gasification rates [2,3,4,5,6,7]. A few metals, e.g., Ca, may be as catalytically active as the alkali metals [2,3].
2. Catalyst contacting by impregnation appears to be the most effective [1,7,8,9]. Very little is known about dual catalyst systems [10,11].
3. Studies of catalysis of various carbon systems by Walker et al [12] have pointed out that: a) the chemical state of the catalyst is critically important, b) for pure carbon, substantial catalytic effects are observed with catalyst concentrations in the parts per million range, c) anions play an important role, d) even for pure carbons the mechanism of action of the catalysts is not understood.
4. A kinetic model has been proposed based on the carbon structure becoming more graphitic with increasing extent of reaction [3,4]. Others have noted changes in the carbon structure and activation energy upon gasification [7,9,13,14].

The present work looks at the effect on reactivity of dual catalyst systems, varying catalyst concentrations, catalyst annealing, and catalyst preparation.

## EXPERIMENTAL

The char, obtained from FMC Corporation, was derived from an Illinois No. 6 coal pyrolyzed at 1550°F (for complete analysis see Reference 3). The coals, obtained from Pennsylvania State University, were PSOC 4, a high volatile A bituminous coal from the Elkhorn #3 seam in Deane, Kentucky, and PSOC 106, a high volatile B bituminous coal from the Indiana #1 Block Jefferson Twp.,

Indiana (for complete analysis, see Reference 15). All catalysts were deposited by impregnation from water solutions [4] except where noted, and all catalyst percentages are expressed as weight of the metal.

All experiments were carried out in the high temperature, high pressure thermobalance described earlier [3,4]. Procedures were identical to those in the earlier work.

## RESULTS

Gasification of the FMC char in steam showed that potassium and sodium bicarbonates exhibited the greatest catalytic activity. Similar earlier experiments with this char in hydrogen gave the same results [3]. (The effectiveness of the catalysts can be judged by comparing the time to 90% conversion, $X_A = .90$, given in Table 1.) Other work with this char also showed that potassium concentrations on the order of 1 wt. % had little or no effect. This might be expected considering the quantity of metal already present in the char as ash. Increasing the catalyst concentration to 5 wt. % and 10 wt. % gave significantly greater rates of carbon gasification [16].

Gasification rates with caking high volatile bituminous coals at 850°C and 500 psi steam varied approximately with the apparent geometric surface area of the sample. All experiments carried out with these coals were performed under identical conditions so that the comparison of relative catalyst effectiveness would be valid. Dual catalyst experiments with the PSOC coals showed that 5 wt. % $K_2CO_3$ was more active than mixtures of 5 wt. % potassium plus 5 wt. % of other metals (see Table 1). Potassium carbonate by itself produced methane yields close to the best potassium-cracking catalyst combination $K_2CO_3$-[$(Al_2O_3)(SiO_2)_3$] and potassium-methanation catalyst combination, $K_2CO_3$-$CoCO_3$-$MoO_3$.

Annealing these coals in helium at the reaction temperature for 400 seconds with catalyst present gave increased rates. The non-catalyzed PSOC 4 which has a very low ash content, showed no change upon annealing. The non-catalyzed PSOC 106, which has a very high ash content, exhibited significant rate increases upon annealing. Also, annealing the $K_2CO_3$-ZnO dual catalyst on PSOC 4 particularly enhanced the rate. Moderate to substantial yields in methane were observed for annealed samples.

In general, impregnation of the catalyst from water solution on the sample was more effective than dry mixing. An exception was tungsten disulfide which

mixed and adhered exceptionally well with the coal in the dry state. This catalyst gave better activity mixed dry than it did upon impregnation. Dry catalyst experiments with sodium sulfide also showed a greater ability to adhere to the coal than sodium sulfate, sulfite, phosphate, and carbonates. The addition of 30 % CO to the inlet $H_2O$ decreased the catalytic activity for the three dual catalysts tested.

Reactivity of the catalyzed and non-catalyzed PSOC coals was also measured at 650°C and similar catalytic activities were noted for the potassium combinations. Lowering the temperature decreased the volatile yield as expected. Addition of catalysts had little or no effect on volatile yield at 650°C or 850°C. The effect of annealing was also decreased at 650°C. The reactivity with a catalyst present increased modestly with annealing; however, the total methane yield dropped, instead of increasing, as at 850°C. In general, the catalysts reduced total methane production compared to the non-catalyzed coal at 650°C. However, total methane yields from the catalysts at 650°C were the same or greater than the non-catalyzed coal at 850°C.

## DISCUSSION

Two simple semi-empirical models were used here to fit the data. The first model is that discussed earlier by two of the present authors [4], and the second is a generalized form of a model proposed by Johnson [17].

Model 1: $\frac{dx}{dt} = K_1 e^{-bx}(1-x)$ where x = fractional conversion of coal, and

Model 2: $\frac{dx}{dt} = K_2 (1-x)^n$ n, b, $K_1$, $K_2$ = constant

Each model will fit the data with equal accuracy and there is little evidence to indicate one is more valid than the other. However, some interesting results have been observed. For the non-catalyzed FMC char at 950°C and the non-catalyzed PSOC coals at 650°C, the reaction order appears to be 1st order (n=1) with respect to the mass of carbon present. This is most easily explained by the reaction taking place throughout the entire mass of the sample and has been reported by other investigators for various gas-carbon reactions [13,14,18]. Gasification rates of the non-catalyzed PSOC coals at 850°C varied with apparent sample geometric area. These coals showed very negative b values by model 1, and a shift of n to approximately 2/3 in model 2. Negative values of b indicate that the activation enthalpy is decreasing as conversion proceeds and that the char is becoming easier to gasify. The results

may indicate a surface reaction or catalyst diffusion controlling model. Surface reaction control has been observed by others for steam and oxygen gasification of carbon [14,17,19].

Increasingly more negative values of b were observed in model 1 as the gasification rate of the catalyzed FMC char increased. There was no obvious trend in the values of b in model 1 for the catalyzed PSOC coals. Model 2 showed decreases in the value of n to around n=2/3 for the catalyzed FMC char. Values of n in model 2 for the catalyzed PSOC coals were very low, possibly indicating a shift to film diffusion control in the Stokes Regime where n = 1/3 [20].

Activation enthalpies calculated for the coals from the 650°C and 950°C data were rather low, again indicating that the gasification reaction was not taking place under pure chemical reaction rate control (for PSOC 4, $\Delta H_1$ = 16.4 kcal/gmole and $\Delta H_2$ = 11.3 kcal/gmole; for PSOC 106, $\Delta H_1$ = 19.3 kcal/gmole and $\Delta H_2$ = 16.6 kcal/gmole.

The PSOC coals were examined by scanning electron microscopy and electron microprobe analysis for such features as particle structure, catalyst distribution, and structural changes at the catalyst sites as a result of gasification.

The particles of the PSOC 4 coal expanded considerably upon initial gasification. PSOC 106 changed but to a much lesser degree. This metamorphosis produced a highly porous structure in the PSOC 4 coal and a lesser evolved interior in the PSOC 106. Addition of catalysts had no macroscopic effect on this process and remained on the surface of the coal particle.

The use of catalysts to enhance gasification rates could be a significant contribution to present technology. However, economic viability is of paramount importance. Savings from decreases in endothermic heat requirements hopefully could offset catalyst costs. Equilibrium calculations of a 1 to 1 steam to carbon ratio at 500 psi show that the heat of reaction to form the equilibrium composition is reduced from approximately 22.0 kcal/gmole at 900°C to 7.0 kcal/gmole at 650°C. If all of the heat for this reaction were supplied by a 13,000 BTU/lb coal at $20/ton for a 12,000 ton/day or 250 MM SCF/day gasification plant, that would amount to operational savings of approximately $33,000/day. To break even, the cost of a catalyst containing 50 wt. % potassium deposited at 10 wt. % potassium on the coal would have to be approximately $15/ton, assuming no catalyst recovery. Much more

research will be necessary to support catalyst utility. Substantial methane yields from catalysts at 650°C will be necessary. Steam to carbon ratios in our present apparatus are too high (10:1) to be specific about methane production at practical process conditions.

## SUMMARY

Potassium salts were found to be catalytically more active when used singly than in combination with cracking or methanation catalysts. The gasification rates of the PSOC coals at 850°C were not solely controlled by chemical reaction rates. Increase in rates upon annealing indicate that catalyst diffusion and reaction with the coal (and char) may be limiting the rates in some cases.

TABLE I

Steam Gasification of the FMC Char and PSOC 4 and PSOC 106 coal at 500 psi

| Run No | Coal | Catalyst | Temp (°C) | Time to 90% Conversion (Seconds) | b | $K_1 \times 10^3$ (1/sec) | n | $K_2 \times 10^3$ (1/sec) | $CH_4$ produced as mole % of original sample |
|---|---|---|---|---|---|---|---|---|---|
| 20222 | FMC Char | 5% $KHCO_3$ | 950 | 215 | -1.50 | 3.32 | .54 | 5.22 | 10.0 |
| 10225[a] | " | 5% $NaHCO_3$ | 940 | 295 | -1.29 | 2.59 | .60 | 3.77 | 11.1 |
| 30225 | " | 5% $ZnCl_2$ | 950 | 370 | -1.17 | 2.51 | .63 | 3.49 | 17.6 |
| 20301 | " | 5% Ag(Acet) | 940 | 400 | -1.13 | 2.57 | .62 | 3.44 | 9.6 |
| 20225 | " | 5% $UO_2(NO_3)_2$ | 950 | 535 | -0.41 | 3.17 | .79 | 3.22 | 18.5 |
| 70225 | " | 5% $CoCl_2$ | 940 | 740 | -0.25 | 2.45 | .91 | 2.59 | 24.7 |
| 40220 | " | No Cat. | 950 | 890 | -0.00 | 2.43 | 1.01 | 2.45 | - |
| 20226 | " | 5% $Pb(NO_3)_2$ | 950 | 1000 | +0.25 | 2.43 | 1.10 | 2.33 | - |
| 20205 | PSOC 4 | 5% $K_2CO_3$ | 850 | 350 | -2.20 | 1.08 | .19 | 1.81 | 16.1 |
| 50717[a] | " | (5% $K_2CO_3$, 2.5% $Co^2CO_3$, 2.5% Ni $CO_3$) | 850 | 430 | -1.40 | 1.46 | .64 | 2.44 | 14.7 |
| 40710 | " | (5% $K_2CO_3$, 5% Zn O) | 850 | 435 | -1.56 | 1.32 | .59 | 2.29 | 10.8 |
| 10203 | " | (5% $K_2CO_3$, 5% Zn O)[b] | 850 | 530 | -2.20 | 0.78 | .19 | 1.30 | 15.0 |
| 20805-A[c] | " | (5% $K_2CO_3$, 5% Zn O) | 850 | 240 | -3.00 | 0.66 | .31 | 2.24 | 11.3 |
| 10205 | " | (5% $K_2CO_3$, 5% $W^2S_2$) | 850 | 440 | -2.08 | 1.11 | .24 | 1.81 | 13.8 |
| 20131 | " | (5% $K_2CO_3$, 5% $W^2S_2$)[b] | 850 | 560 | -2.20 | 0.77 | .32 | 1.45 | 13.3 |
| 20717[a] | " | (5% $K_2CO_3$, 2.5% $Co^2CO_3$, 4.0% Mo $O_3$) | 850 | 555 | -1.86 | 0.95 | .39 | 1.54 | 16.1 |

TABLE I
continued

| Run No | Coal | Catalyst | Temp (°C) | Time to 90% Conversion (seconds) | b | $K_1 \times 10^3$ (1/sec) | n | $K_2 \times 10^3$ (1/sec) | $CH_4$ produced as mole % of original sample |
|---|---|---|---|---|---|---|---|---|---|
| 20218 | " | (5% $K_2CO_3$, 5% $[(Al_2O_3)(SiO_2)_3]$)[b] | 852 | 540 | -1.96 | 0.90 | .34 | 1.54 | 20.4 |
| 40129 | " | 10% $[(Al_2O_3)(SiO_2)_3]$[b] | 850 | 1220 | -2.04 | 0.28 | .34 | 0.52 | 16.0 |
| 40203 | " | 10% $WS_2$ | 855 | 1820 | -1.64 | 0.35 | .40 | 0.52 | 18.6 |
| 60129 | " | 10% $WS_2$[b] | 855 | 1260 | -2.36 | 0.29 | .19 | 0.53 | 15.2 |
| 20708 | " | No Cat. | 850 | 1800 | -1.56 | 0.30 | .49 | 0.48 | 12.5 |
| 40802-A[c] | " | " | 850 | 1900 | -1.80 | 0.24 | .29 | 0.35 | 11.0 |
| 20710 | PSOC 106 | " | 850 | 2360 | -0.44 | 0.55 | .89 | 0.65 | 8.2 |
| 40805-A[c] | " | " | 850 | 1360 | -1.19 | 0.51 | .59 | 0.70 | 17.0 |
| 11017 | PSOC 106 | No Cat. | 650 | 8100 est. | -1.40 | 0.70 | .99 | 0.13 | 10.7 |
| 31016 | PSOC 4 | " | 650 | 7800 est. | -1.40 | 0.08 | 1.09 | 0.16 | 14.8 |
| 11024 | " | (5% $K_2CO_3$, 5% Zn O3) | 650 | 805 | -1.93 | 0.63 | .34 | 1.04 | 11.2 |
| 31024 | " | (5% $K_2CO_3$, 2.5% $Co^3CO_3$, 4.0% Mo $O_3$) | 650 | 1190 | -2.20 | 0.36 | .34 | 0.69 | 12.8 |
| 31015 | " | (5% $K_2CO_3$, 2.5% $Co^3CO_3$, 2.5% Ni $CO_3$) | 650 | 1010 | -1.72 | 0.55 | .51 | 0.96 | 11.9 |
| 31025-A[c] | " | (5% $K_2CO_3$, 2.5% $Co^3CO_3$, 2.5% Ni $CO_3$) | 650 | 910 | -1.88 | 0.53 | .42 | 0.93 | 8.9 |

a) estimated final weight

b) dry catalyst preparation

c) annealed in helium at the reaction temperature for 400 seconds.

REFERENCES


1. Chemistry of Coal Utilization, Supplementary Volume, Lowry, H.H., Ed., Wiley and Sons, Inc., 1963.

2. W.P. Haynes, S.J. Gasior and A.J. Forney, ACS Div. Fuel Chem. Proc. 18, No. 2, 1-28 (1973).

3. K. Wilks, M.S. Thesis, "The Gasification of Coal Chars", Case Western Reserve University, Cleveland, Ohio, January 1974.

4. N.C. Gardner, W.E. Samuels and K. Wilks, "Coal Gasification" L. Massey ed., ACS Advances in Chemistry Series, Vol. 131, p. 213-276 (1974).

5. C.L. Aldridge and D. Buben, U.S. Patent 3,689,240 (1972).

6. Gas Generator Research and Development Phase II Process and Equipment Development. Prepared for the Office of Coal Research, Contract #14-01-0001-324 (1970).

7. Wood, R.D., and Hill, G.R., ACS Division of Fuel Chemistry, Vol. 17, No. 1, Aug. 1972.

8. Weller, S. and Pelipetz, M.C., Ind. and Eng. Chem., 43, 1243 (1951).

9. Dent, F.J., Blackburn, W.H., and Millett, H.C., Trans. Inst. Gas Engrs. 88, 150 (1938).

10. M. Hering, S. Keraudy, F.M. Lang and S. May. Proceedings of the Fourth Conference on Carbon, Buffalo, 1959, Pergamon Press, N.Y., 1960, p. 115-122.

11. W.G. Wilson, L.J. Sealock, F.C. Hoodmaker, R.W. Hoffman, J.L. Cox, and D.L. Stinson, ACS Div. Fuel Chem. Proc. 18, No. 2, 29 (1973).

12. P.L. Walker, M. Shelef, and R.A. Anderson, "Catalysis of Carbon Gasification", Chemistry and Physics of Carbon 4, 287 (1968).

13. Satterfield, C.N., Mass Transfer in Heterogeneous Catalysis, pp. 224-227, M.I.T. Press, 1970.

14. P.L. Walker, F. Rusinko, Jr., L.C. Austin, "Gas Reactions of Carbon", Cat. Rev., IX, (1959).

15. Mineral Matter and Trace Elements in U.S. Coals Research and Development Report No. 61, Interim Report No. 2, July 15, 1972, Contract No. 14-01-0001-390 by Coal Research Section, Pennsylvania State Univ., for Office of Coal Research.

16. unpublished work, N.C. Gardner, K.A. Wilks

17. J.L. Johnson, ACS Div. Fuel Chem. Proc. 18, No. 1, 228-68 (1973).

18. Will, H.A., Ph.D. Thesis, "Growth of Diamond Seed Crystals by Vapor Deposition", Case Western Reserve Univ., Cleveland, Ohio 44106, June, 1968.

19. Field, M.A., Gill, D.W., Morgan, B.B., Hawksley, P.G.W., Combustion of Pulverized Coal, The British Coal Utilization Research Association, Leatherhead, Surrey, England (1967).

20. Levenspiel, O., Chemical Reaction Engineering, 2nd Ed., Ch. 12, John W. Wiley and Sons, Inc. N.Y., N.Y., (1972).

# GASIFICATION OF MONTANA LIGNITE IN HYDROGEN AND IN HELIUM DURING INITIAL REACTION STAGES

James L. Johnson

Institute of Gas Technology
3424 South State Street
Chicago, Illinois

## INTRODUCTION

Light hydrocarbon yields obtained during the initial stages of coal gasification are of particular importance in affecting overall performances and thermal efficiencies of processes directed toward conversion of coal to pipeline gas. It is during this gasification stage that coals undergo devolatilization reactions leading to the formation of carbon oxides, water, oils and tars, and, most importantly, significant quantities of light hydrocarbons, particularly methane, in the presence of hydrogen at elevated pressures. Since, however, the exceptionally high reactivity most coals exhibit for methane formation during initial reaction stages is transient, existing only for a period of seconds at higher temperatures, rational design of commercial systems to optimize methane yields requires as detailed a kinetic characterization of pertinent processes occurring as is possible. Because of its importance, this reaction has been studied in a variety of experimental investigations, using fixed beds (1, 5, 6, 7, 10), fluidized beds (2, 7, 10), and dilute solid-phase systems (3, 4, 8, 9, 11, 12). In spite of the extensive amount of information obtained from these studies, however, primary emphasis in the development of kinetic correlations has been placed on description of total methane yields obtained after relative deactivation of coal solids has occurred, rather than on the more detailed behavior occurring during the transient period of "rapid-rate" methane formation. Although this existing information is of significant value at one level of process design, it is primarily limited to application to large-scale systems in which reaction conditions closely parallel the laboratory conditions employed in obtaining the information.

This current investigation has, therefore, been stimulated by the need for additional information that quantitatively characterizes intermediate reaction processes occurring prior to completion of the "rapid-rate" methane formation reaction. In this study, a continuous dilute-phase transport reactor has been employed having the particularly unique feature of variable temperature control along the length of the reactor, which permits the establishment of various desired gas-solid, time-temperature histories.

This paper discusses some initial results obtained with this experimental system for gasification of Montana lignite in hydrogen, helium, and hydrogen-helium mixtures, under the more conventional conditions of isothermal operation, and under conditions of constant gas-solid heat-up rate (~50°F/s). Results are reported for tests conducted at temperatures from 900°F to 1550°F and pressures from 18 to 52 atmospheres.

## EXPERIMENTAL

### Apparatus and Procedures

The composition of the Montana lignite used in this study is given in Table 1, and a schematic diagram of the experimental apparatus is shown in Figure 1. The main component of the experimental system is a helical-coiled

Table 1. FEED COMPOSITION
(Montana Lignite, Dry Basis)

| | | Mass, % |
|---|---|---|
| Ultimate Analysis | | |
| Carbon | | 65.13 |
| Hydrogen | | 4.13 |
| Oxygen | | 24.20 |
| Nitrogen | | 0.89 |
| Sulfur | | 0.57 |
| Ash | | 5.08 |
| | Total | 100.00 |
| Proximate Analysis | | |
| Fixed Carbon | | 51.30 |
| Volatile Matter | | 43.62 |
| Ash | | 5.08 |
| | Total | 100.00 |

transport reactor formed from a 1/16-inch-ID tube. General information describing the reactor coil is given in Table 2. The diameter of the coil is

Table 2. REACTOR-COIL DATA

| | |
|---|---|
| Total Tube Length | 200 ft |
| Tube ID | 1/16 in. |
| Tube OD | 1/8 in. |
| Tube Material | 316 stainless steel, seamless |
| No. of Individually Controlled Heating Zones | 9 |
| Tube Length Per Zone | 22.2 ft |
| Helix Dimensions | 1-ft diameter X 2-1/2 ft high |
| Electrical Resistance per 22.2-ft Tube Section | 1 ohm |
| Transformer Output | |
| Zones 1-6 | 35 volts, 35 A |
| Zones 7-9 | 40 volts, 40 A |
| Maximum Power Requirement for Transformers (total) | 12 kW |
| Maximum Operating Temperature | 1600°F |
| Maximum Design Pressure | 1000 psi |
| Temperature Controller Type | Weathermeasure, TRA-1, Triac-Triggered SCR gate |

about 1 foot, with a total tube length of 200 feet and a vertical reactor height of about 2-1/2 feet. With this design, gas flow rates of 5 to 50 SCF/hr and solids flow rates of 50 to 500 gph are possible. The relative gas-solids flow rates used in individual tests were such that solids/gas volume ratios were less than 0.02. The solids particles used in this system were relatively uniform in size, ranging in diameter from 0.0029 to 0.0035 inch. Such small particles flowed essentially at gas velocities, and calculated temperature differences between the gas and solids and between the reactor tube wall and the flowing gas-solids stream were negligible.

The reactor tube itself serves as the heating element, and electrodes are attached directly at various points along the length of the helical coil. Nine independent heating zones are thereby incorporated into the system to provide flexibility in establishing desired temperature profiles.

In a typical experimental test, the following operational procedures were generally used:

Initially, the system is brought to a desired pressure, and a preliminary temperature profile is established in the reactor coil by adjusting the controls for the nine heating zones. When feed-gas flow is established at a desired rate, the flow from the solids feed hopper is initiated. Solids are screwed into a mixing zone, there combining with the feed gas, and the resulting mixture then flows through the reactor coil. The temperature in the mixing zone is maintained equal to the temperature at the entrance of the coil — usually about 600°F. This is sufficiently high to inhibit steam condensation at the highest pressures used in this study, but low enough to inhibit any significant reaction of coal solid.

When both gas and solids flows are begun, the final desired temperature profile is established in the reactor tube. In the various tests conducted, the temperature either increased along the coil in the direction of gas-solids flow or was maintained at a constant value. For increasing temperatures, the temperature-versus-distance characteristic along the coil corresponded to a linear relationship between the temperature and the gas-solids residence time in the coil of about 50°F/s. In isothermal tests, gas-solids residence times ranging from 5 to 14 seconds were employed.

The hot gas-solids mixture exiting from the bottom of the reactor coil passes through an initial quench system that rapidly reduces its temperature to approximately 600°F to inhibit further reaction. At this point in the system, a lower temperature is avoided in order to prevent steam from condensing on the solids. The partially cooled mixture then proceeds through one of three solids filters, which retains the solids but permits gas flow. The gas continues through a condensor that removes water and oils and then passes through a gas-sampling panel, which is used intermittently to obtain gas samples for mass spectrographic analysis. In some of the tests conducted, the product gas was also continuously monitored with a Beckman Model 400 hydrocarbon analyzer to measure the total concentration of carbon in hydrocarbon species.

The data of primary interest in a given test corresponded to steady-state operation. Since a certain amount of time is required to achieve such operation, certain facilities are incorporated into the system to permit the collection of solid residues corresponding to steady-state operation but not contaminated with residues resulting from unsteady-state operation. To accomplish this, the product solids could be collected in any of the three solids filters, depending on the position of a multiple-exit hot valve (valve V2 in Figure 1). During unsteady-state operation, when the desired gas and solids flows and the temperature profile in the reactor coil were being established, the product gas and solids flows were directed through solids filter A. When steady-state conditions were established, the product gas and solids were directed through solids filter B, which then accumulated a solids residue for analysis. Before the end of some tests, a direct determination of the solids inventory in the reactor coil was made to estimate the average solids residence times. This was accomplished by simultaneously closing valve V1 at the top of the coil, stopping the screw feeder, and diverting the product gas and solids flow through solids filter C. Valve V1 is a hot valve fitted with a solids filter that stops solids flow but permits gas flow when in a closed position. After these simultaneous operations, the solids inventory in the reactor coil is accumulated in solids filter C. Average solids residence times computed from chemical analyses and weight measurements of these solids generally corresponded very closely to calculated gas residence times, indicating negligible gas-solids slippage in the reactor coil.

Data Analysis

The experimental system employed in this study is an integral system in the sense that the gas, liquid, and solids conversion determined by analyses of the reactor-coil exit streams are the result of chemical interactions occurring along the length of the coil under systematically varying environmental conditions. With this type of system, the information required for proper kinetic characterization includes definitions of the conversions and local environmental conditions along the entire length of the coil, not only at the exit. Although this information could not be obtained in a single experimental test, a good approximation was achieved by series of properly designed tests. The basis for design of such test series depended on the fact that the gas and solids were essentially in plug flow through the coil, and slippage of the solids relative to the gas flow was negligible, since, under these conditions, both gas and solids conversions could be expressed solely as a function of pressure, initial gas/solids feed ratio, temperature, and temperature-time history.

Individual tests in isothermal test series were conducted at the same temperature, pressure, feed gas/solid ratio, and feed gas composition, varying only total feed gas and solids flow rates to obtain results as a function of residence time. Individual tests in test series conducted at constant heat-up rate conditions were designed to obtain results as a function of final temperature at the same pressure, feed gas/solids ratio, feed gas composition, initial temperature, and heat-up rate. This was accomplished by varying the feed-gas flow rate and temperature profile in individual tests according to the following expressions:

$$G_o = \frac{\pi d^2 P L \alpha}{2R(T_f^2 - T_o^2)} \qquad 1)$$

and

$$T = [T_o^2 + (T_f^2 - T_o^2)\, z/L]^{1/2} \qquad 2)$$

where

| | | |
|---|---|---|
| $z$ | = | length at intermediate point along the reactor coil |
| $L$ | = | total length of reactor coil |
| $T_o$ | = | temperature at entrance of reactor coil |
| $T_f$ | = | temperature at reactor-coil exit (final temperature) |
| $T$ | = | temperature at intermediate point z along the reactor coil |
| $G_o$ | = | feed-gas flow rate (mol/time) |
| $R$ | = | gas constant |
| $d$ | = | reactor-tube diameter |
| $\alpha$ | = | gas-solids heat-up rate |
| $P$ | = | pressure |

With this approach, and in the absence of catalytic reactor wall effects, yields obtained in individual tests conducted at a constant heat-up rate at various final temperatures could be interpreted as approximating yields occurring along the length of the reactor coil in a single test conducted at the maximum final temperature employed.

The question of reactor-wall-catalyzed reactions was investigated in a series of preliminary tests with simulated feed gases in the absence of coal solids. The results of these tests indicated that the only reaction of significance that occurred in the presence of typical concentrations of the major gas species was the water-gas shift reaction, which was initiated at approximately 1200°F.

## RESULTS

Feed-gas compositions used in individual test series are given in Table 3 along with a definition of notation to distinguish primary results obtained in these test series, as illustrated in Figures 2 to 12. This notation is also applicable to Figures 13, 14, 15, and 17. In the presentation of experimental results, various species and species groups that evolved during gasification have been catagorized as follows:

- Carbon monoxide, carbon dioxide, hydrogen, methane, ethane, and benzene: Determined by mass-spectrographic analysis of dry product gases.
- Water: Computed as the difference between total oxygen gasified and oxygen present in carbon monoxide and carbon dioxide in the product gas.
- Unknown gaseous hydrocarbon: Computed as the difference between total carbon in gaseous hydrocarbon species, as determined by a hydrocarbon analyzer, and carbon present in methane, ethane, and benzene in the product gas.
- "Heavy hydrocarbon": Computed as the difference between total carbon gasified and carbon present in carbon monoxide, methane, and ethane.

The basis for this classification of species and species groups is related to the accuracies of analytical measurements in this study. Such measurements were limited by the fact that, in all tests conducted, the concentrations of reaction products in the dry product gas were less than 5% by volume (CO or $CO_2$, 0% to 1.5%; $CH_4$, 0% to 3%; $C_2H_6$, 0% to 0.8%; $C_6H_6$ 0% to 0.3%). These conditions were employed so that, in individual tests, the partial pressures of feed gas components were essentially constant throughout the length of the reactor coil, which facilitates quantitative kinetic analyses.

Table 3. FEED-GAS COMPOSITIONS

| Notation in Figs. 2-15, 17 | Feed Gas Pressure, atm | | | Temperature Profile | |
|---|---|---|---|---|---|
| | $H_2$ | He | Total | Isothermal | Constant Heat-up Rate |
| ● | 0 | 35 | 35 | | X |
| △ | 18 | 0 | 18 | | X |
| ▲ | 18 | 17 | 35 | | X |
| □ | 35 | 0 | 35 | | X |
| ▽ | 52 | 0 | 52 | | X |
| ◐ | 0 | 35 | 35 | X | |
| ◭ | 18 | 0 | 18 | X | |
| ◮ | 18 | 17 | 35 | X | |
| ◪ | 35 | 0 | 35 | X | |

The direct measurement of water yield in condensed liquid products was not usually accurate because of the relatively small amounts obtained and the uncertainty of the quantity of this species that was not condensed in the knockout pot. Computed values for the yield of this species are likely to be somewhat greater than actual yields because of the likelihood that some oxygen could be combined in oils and tars. This error, however, is probably small.

The measurement of concentrations of gaseous hydrocarbon species, other than methane and ethane, and to a lesser degree benzene, by mass-spectrographic analysis was difficult for the test conditions used because of the small molecular concentrations of individual species. Although measurements of benzene concentrations in the gas were sufficiently accurate to be meaningful,

the interpretation of this concentration in terms of total benzene yields is questionable because some of the benzene formed in the reactor coil may have condensed in the knockout pot, but later may have vaporized when the liquid products warmed to ambient temperatures prior to containment.

The unknown-gaseous-hydrocarbon group probably consists primarily of lighter aliphatic species such as ethylene, propane, propylene, butane, and butylene. The heavy-hydrocarbon group consists of the potentially condensible tars and oils, including benzene, and the unknown-gaseous-hydrocarbon species. In a few of the tests conducted, sufficient condensed hydrocarbon liquids were recovered to make direct experimental evaluations of total carbon balances. The fact that these balances showed better than 98% recovery suggests that, in the majority of tests in which insufficient liquids were recovered for quantitative analysis, the computed difference between the carbon in the heavy-hydrocarbon group and the carbon in the unknown-gaseous-hydrocarbon group probably is quite representative of the carbon in the actual condensed hydrocarbons, when benzene yields are negligible.

The results given in Figures 1 to 12 exhibit the following major trends:

Evolution of Major Coal Components: Carbon, Oxygen, and Hydrogen (Figures 2, 3, and 4)

The evolution of total carbon from the coal solids generally increases with increasing temperature and hydrogen partial pressure, with conversions obtained for isothermal operation being greater than for operation at constant heat-up rate. Total oxygen evolution from coal solids also increases with increasing temperature, and although conversions obtained in hydrogen are greater than in helium, no significant effect of hydrogen partial pressure on conversion is apparent in the range from 18 to 52 atmospheres. As with total carbon conversion, total oxygen evolution is also greater under isothermal operation. Total evolution of hydrogen from the coal solids increases with increasing temperature and is greater in isothermal tests, but is not a significant function of hydrogen partial pressure. This is a particularly important result, indicating that hydrogen evolution is primarily a thermally activated phenomenon dependent only on time-temperature history.

It is also of significance that the results shown in Figures 2, 3, and 4 for operation with a hydrogen-helium mixture (hydrogen partial pressure = 18 atmospheres) are essentially identical to results obtained with pure hydrogen at a total pressure of 18 atmospheres. This similarity is also apparent in yields of gasified products and suggests that hydrogen partial pressure and not total pressure is the main parameter affecting kinetic behavior during the initial gasification stages of Montana lignite. A somewhat different effect has been observed in an investigation with bituminous coal by Anthony (1), where it was found that initial gasification yields tended to increase with increasing hydrogen partial pressure, but to decrease with increasing total pressure. This effect was explained as being due to increased diffusion resistance within the coal structure. This was not observed in this previous study with lignite, which does not become plastic during devolatilization.

Oxygen-Containing Product Species (Figures 5 and 6)

For tests conducted at a constant heat-up rate, total carbon dioxide evolution is completed below 1000°F (Figure 5). The amount evolved (about 0.029 g-mol/g-atom feed carbon) is essentially the same in hydrogen and in helium and is independent of hydrogen partial pressure. This amount is probably reflective of the concentration of carboxyl functional groups in the raw lignite. As temperature increases above 1000°F, the carbon dioxide yield remains substantially constant up to about 1200°F, then decreases with further increases in temperature for tests conducted in hydrogen, but increases with further increases in temperature for tests conducted in helium. These variations above 1200°F are probably due to the water-gas shift reaction, as suggested by results of tests conducted in the absence of coal solids. The dashed line shown in Figure 5B represents the assumed carbon dioxide yield for the case in which no water-gas shift occurs and was used as a basis for adjusting the total oxygen distribution in directly evolved species, as illustrated in Figure 6.

Hydrocarbon Product Species (Figures 7 to 12)

Methane-plus-ethane yields are highly dependent on hydrogen partial pressure (Figure 7). For tests conducted at a constant heat-up rate in hydrogen, methane-plus-ethane formation is slight below 1000°F (about 0.01 g-atom carbon/g-atom feed carbon). With further increases in temperature, yields in helium increase slightly, leveling off at a value of about 0.03 g-atom carbon/g-atom feed carbon above about 1300°F; in hydrogen, dramatic increases in methane-plus-ethane yields occur with increasing temperature. From about 1000° to 1200°F, this increase is about the same for hydrogen partial pressures from 18 to 52 atmospheres; above 1200°F, methane-plus-ethane yields increase with increasing hydrogen partial pressure, and yields at all pressures tend to suggest leveling off at higher temperatures. Reasonable extrapolation of the curves shown would indicate little increases in yields above about 1700°F for the reaction times employed.

Methane-plus-ethane yields obtained in isothermal tests are essentially independent of gas-solids residence times ranging from 5 to 14 seconds and are the same as yields obtained in constant heat-up rate tests at 1000° and 1400°F. This is true for tests conducted in hydrogen and in helium. At 1200°F, yields obtained in isothermal tests are somewhat greater than those obtained in constant heat-up rate tests.

The sum of methane plus ethane has been referred to in the above discussion instead of the yields of each species individually because of an apparent stoichiometric relationship between the formation rates of each species. One such indication is illustrated in Figure 8, which shows that ethane yields are approximately directly proportional to methane yields up to values of methane yields of about 0.06 g-atom carbon/g-atom feed carbon. At higher methane yields, ethane yields tend to approach a maximum and then decrease with further increases in methane yields, with the maximum increasing with increasing hydrogen pressure. This behavior can be explained by assuming that, at all temperature levels, ethane is formed in direct proportion to methane, but that, at sufficiently high temperatures (above about 1300° to 1400°F), ethane converts to methane in the presence of hydrogen.

The increasing maximum ethane yields with increasing hydrogen pressure can be explained by noting that these maxima occur at about the same temperature. This is demonstrated in Figure 9, which shows that the ratio of ethane-to-methane yield is apparently a function only of temperature and not pressure. This evidence suggests that hydrogen attack on lignite does not result in formation only of methane at any level of temperature, but rather results in a formation of both ethane and methane in a fixed ratio. Examination of data available in the literature (5, 6) suggests that this ratio tends to decrease with increasing coal rank.

The heavy-hydrocarbon yields shown in Figure 10 are substantially constant above 1000°F for tests conducted at constant heat-up rates, and yields obtained in hydrogen and in helium are generally similar. This species group, consisting of oils, tars, and light aliphatic gaseous species, apparently is formed below 1000°F, and although variations in the distribution of individual species within this group are likely at higher temperatures, there is apparently only limited transformation of species in this group to methane, ethane, or char, at least up to 1560°F. Heavy-hydrocarbon yields obtained in isothermal tests are significantly greater than those obtained in constant heat-up rate tests, particularly at 1400°F. This may primarily occur because, for isothermal operation, feed-coal solids heat up very rapidly to reactor temperature in the first few feet of the reactor coil. Assuming that most heavy-hydrocarbon formation occurs below 1000°F, increased heat-up rates through this range of temperature would tend to favor evolution of tars and oils, in competition with repolymerization in the solid phase. With this explanation, it is pertinent that increased isothermal temperature levels correspond to increased heat-up rates through the oil-tar formation range, being of the order of several thousand degrees per second at an isothermal temperature of 1400°F.

Figure 11 indicates that, in hydrogen, the unknown-gaseous-hydrocarbon yield decreases above about 1200°F. Although this decrease is not reasonably detectable in a corresponding decrease in the heavy-hydrocarbon yield, possibly because of data scatter, above 1200°F, light aliphatic species can reasonably be expected to begin to convert to ethane and methane in the presence of hydrogen. In helium, this conversion does not occur.

Semiquantitative indications of benzene yields (Figure 12) suggest that the heavier components in the oil-tar fraction begin to convert to benzene at about 1300°F, with substantial conversions being achieved by 1450°F. No benzene was detected in gas analyses for any test conducted below 1270°F with hydrogen, nor at any temperature for tests conducted in helium, suggesting that benzene is not a significant fraction of the oils and tars that initially evolve below 1000°F.

Relationship Between Equivalent Methane-Plus-Ethane Yield and Hydrogen Gasified

Figure 13 shows that, at any hydrogen pressure, "equivalent" methane-plus-ethane yields are directly proportional to the amount of hydrogen gasified. Equivalent methane-plus-ethane yields represent the difference between actual methane and ethane yields and an adjustment term obtained

from Figure 11 at a corresponding temperature. The correction term is the difference between values of the unknown-gaseous-hydrocarbon yield indicated by the dashed line and the solid line. The basis for this correction is the assumption that the unknown-gaseous-hydrocarbon group consists of relatively low-molecular-weight aliphatic species (other than methane and ethane), which hydrogenate to form ethane and methane at increased temperatures in the presence of gaseous hydrogen. Because a relationship is sought to characterize methane and ethane formation only as derived directly from the coal or coal char, the estimated amount of methane and ethane formed from gaseous interactions was subtracted from total methane-plus-ethane yields.

The relationship shown in Figure 13 is a very important one. It indicates that, at any hydrogen partial pressure, methane and ethane evolve directly in proportion to the total amount of hydrogen evolved from the coal, although the proportionality increases significantly with increasing pressure. It should be recalled that results given in Figure 4 show that total hydrogen evolution is not a function of hydrogen partial pressure and is essentially identical in hydrogen and in helium. This combined evidence suggests then that the formation of active sites that catalyze methane and ethane formation in the presence of hydrogen is directly related to the process in which coal hydrogen is released, this latter process being independent of gaseous atmosphere and dependent only on time-temperature history. A model for quantitatively correlating equivalent methane and ethane formation rates from coal solids, based on the evidence discussed, is presented in the final section of this paper.

## CORRELATION OF "RAPID-RATE" METHANE AND ETHANE FORMATION

In consideration of the data obtained in this study with Montana lignite, the following model is proposed to describe the kinetics of methane and ethane formation during initial stages of gasification.

During heat-up of raw lignite (Structure A), interactions within the coal initially occur below 1000°F and result primarily in the evolution of a) carbon dioxide, probably resulting from gasification of all carboxyl functional groups; b) some water and carbon monoxide; c) some relatively low molecular weight aliphatics; and d) oils and tars. These reactions are essentially pyrolysis reactions that occur because of the breaking of certain of the weaker side-chain bonds as well as bonds connecting relatively large polyatomic molecules in the carbon matrix. This latter process results in the intermediate formation of large fragments, possibly free radicals, which then either a) become stabilized because of hydrogen disproportionation or interaction with gaseous molecular hydrogen and evolve as oils and tars, or b) polymerize to form an intermediate type of solid (Structure B). The total amounts of materials other than oils and tars that gasify below 1000°F are essentially independent of gas atmosphere or heat-up rate, suggesting a stoichiometric relationship between the individual species formed and the functional groups present in the raw lignite. Total oil and tar formation is similar in hydrogen and in helium, and increases with increasing heat-up rate, which is apparently a result of the competition between stabilization and polymerization of intermediate free-radical fragments.

Between 1000° and 1300°F, most of the remaining oxygen in the coal is evolved as carbon monoxide and water, with water formation being slightly greater in hydrogen than in helium. The gasification of hydrogen from the coal solids is relatively small between 1000° and 1200°F, being due to the formation of water and some methane and ethane in the presence of gaseous hydrogen and both water and hydrogen in the presence of helium. Above 1200°F, evolution of coal hydrogen begins to increase rapidly with increasing temperature, accompanied by a rapid increase in the formation of methane and ethane in the presence of gaseous hydrogen.

The removal of oxygen between 1000° and 1300°F can be considered to correspond to the transition of the main carbon matrix from Structure B to a second intermediate main structure (Structure C). Structure C is considered to be comprised primarily of carbon and hydrogen and, with increases in temperature above about 1200°F, converts to a relatively stable "char" structure (Structure E) through the evolution of hydrogen. During this transition, however, Structure C initially converts to an active intermediate structure. Structure D, as hydrogen is evolved, and Structure D then can either convert to the stable char structure, Structure E, or interact with molecular hydrogen to form methane and ethane.

The following quantitiative representation of the steps leading to methane and ethane formation assumes for simplicity that all oxygen is gasified prior to the formation of methane and ethane as a result of interactions of gaseous hydrogen with Structure B. Although the experimental data indicate some overlap between the final stages of oxygen gasification and the initial stages of methane and ethane formation between 1200° and 1300°F, this assumption does not appreciably alter the quantitative evaluation of the parameters derived based on the model proposed.

The processes that lead to "rapid-rate" methane and ethane formation are assumed to occur according to the following overall reactions:

$$CH_x^0(s) \xrightarrow{k_0} CH_y^* (s) + (x-y)\, H(g) \qquad \text{I)}$$

$$H_2(g) + CH_y^*(s) \xrightarrow{k_1} (1-m)CH_y^0(s)$$

$$H_2(g) + CH_y^*(s) \xrightarrow{k_2} \left(\frac{m}{1+B}\right) CH_4(g) + \left[\frac{mB}{2(1+B)}\right] C_2H_6(g) + ymH(g) \qquad \text{II)}$$

where

| | | |
|---|---|---|
| $CH_x^0$ | = | solid component resulting from interactions occurring during primary pyrolysis (Structure C) |
| $CH_y^*$ | = | intermediate solid active species (Structure D) |
| H | = | hydrogen evolved from solids in Reactions I and II |
| $CH_y^0$ | = | product coal char (Structure E) |

$H_2$ = gaseous molecular hydrogen

x = atomic ratio of hydrogen to carbon in $CH_x^0$

y = atomic ratio of hydrogen to carbon in $CH_y^0$ and $CH_y^*$

B = carbon ratio of ethane to methane formed in Reaction II

m = fraction of carbon in $CH_y^*$ converted to methane and ethane in Reaction II

$k_0$, $k_1$, $k_2$ = first-order rate constants

s = solid

g = gas.

Let —

$\lambda$ = fraction of feed carbon as $CH_x^0$ when conversion to Structure C is complete, g-atom carbon/g-atom feed carbon

$n_C^*$ = equivalent methane and ethane formed from coal at any time during gasification, g-atom carbon/g-atom feed carbon

$n_C^0$ = equivalent methane and ethane formed by pyrolysis reactions prior to the onset of Reaction I, g-atom carbon/g-atom feed carbon

f = fraction of $CH_x^0$ converted via Reaction I at any time during gasification

$n_H^*$ = total coal hydrogen gasified at any time, g-atom hydrogen/g-atom feed carbon

$n_H^0$ = hydrogen gasified via pyrolysis reactions prior to the onset of Reaction I, g-atom hydrogen/g-atom feed carbon

Based on the definitions given above, it is possible to determine certain of the unknown stoichiometric parameters which characterize the model assumed, prior to consideration of the kinetics of Reaction I. In these evaluations, it it assumed that the ratio $k_2/k_1$ is independent of temperature.

According to the above definitions —

$$f = (n_C^* - n_C^0)/m\lambda \qquad 3)$$

and

$$f = (n_H^* - n_H^0)/(x - y + ym)\lambda \qquad 4)$$

Combining Equations 3 and 4 and rearranging leads to —

$$n_C^* = mn_H^*/(x - y + ym) + \{n_C^0 - n_H^0[m/(x - y + ym)]\} \qquad 5)$$

Letting $S = m/(x - y + ym)$ and $I = [n_C^0 - n_H^0 m/(x - y + ym)]$, Equation 5 can be represented as —

$$n_C^* = Sn_H^* + I \qquad 6)$$

Thus, where m is constant, a plot of $n_C^*$ versus $n_H^*$, both experimental parameters, should yield a straight line with a slope equal to S and intercept at $n_H^* = 0$ of I. Figure 13 shows such a plot for data obtained in constant heat-up rate tests in helium and in hydrogen. Values of S increase with increasing pressure because of increasing values of m with increasing pressure. The common point of intersection of the lines drawn corresponds to values of $n_C^0 = 0.01$ g-atom carbon/g-atom feed carbon, and $n_H^0 = 0.272$ g-atom hydrogen/g-atom feed carbon. Table 4 tabulates the values of S obtained from Figure 13 as a function of hydrogen partial pressure, $P_{H_2}$.

Table 4. VARIATION IN S WITH $P_{H_2}$

| $P_{H_2}$, atm | S, g-atom carbon/ g-atom hydrogen |
|---|---|
| 0 | 0.084 |
| 18 | 0.352 |
| 35 | 0.514 |
| 52 | 0.649 |

Now, let —

$Y_C$ = total carbon in partially gasified lignite, g-atom carbon/ g-atom feed carbon

$Y_H$ = total hydrogen in partially gasified lignite, g-atom hydrogen/ g-atom feed carbon

$Z = Y_H/Y_C$ = hydrogen/carbon ratio in partially gasified lignite, g-atom hydrogen/g-atom carbon.

From the stoichiometry defined in Reactions I and II, Z is given by the expression —

$$Z = \frac{x - f(x - y + ym)}{1 - fm} \qquad 7)$$

Solving for f in Equation 7 results in —

$$f = (x - Z)/(x - y + ym - mZ) \qquad 8)$$

Equating the expression for f in Equation 8 to the expression for f in Equation 3 leads to —

$$(n_C^* - n_C^0)/\lambda m = [(x - Z)/m]/[(x - y + ym)/m - Z] \qquad 9)$$

Rearranging Equation 9 and substituting S for the expression defined results in —

$$(n_C^* - n_C^0)\ (1/S - Z) = \lambda\ (x - Z) \qquad 10)$$

Thus, a plot of the term on the left-hand side of Equation 10 versus Z should result in a straight line with a slope equal to $-\lambda$ and an intercept at Z = 0 of $\lambda x$. Figure 14 shows such a plot for constant heat-up rate tests conducted in hydrogen. Data obtained with helium were not included in this plot because of the scatter that results from small values of S, which magnify variations in the term $(n_C^* - n_C^0)$. In accordance with the model assumed, data obtained at hydrogen partial pressures of 18, 35, and 52 atmospheres are reasonably correlated with a single straight line corresponding to a value of $\lambda = 0.83$ g-atom carbon/g-atom feed carbon, and a value of $x = 0.578$ g-atom hydrogen/g-atom carbon. The value of $\lambda$ was not determined by a least-squares fit of the data, but was "forced" so that the amount of carbon initially present in the component $CH_x^0$ is equal to the total amount of carbon initially present in the raw lignite, less the total carbon evolved during pyrolysis due to formation of carbon monoxide, carbon dioxide, and the heavy-hydrocarbon species. Note that if the component $CH_x^0$ consisted of polycondensed aromatic units of hexagonally arranged carbon, with hydrogen present on lattice edges, then the value of $x = 0.578$ corresponds to an average ring number of 5.

The value of y is assumed to be 0.25 g-atom hydrogen/g-atom carbon, based on measurements made of hydrogen contents of Montana lignite chars gasified at elevated temperatures for extended times. With this assumption, values of m can be computed for corresponding values of S obtained from Figure 13, according to the expression —

$$m = S(x - y)/(1 - Sy) \qquad 11)$$

In addition, values of $r = k_2/k_1 = m/(1 - m)$ can also be computed. Values of m and r are given in Table 5 as a function of hydrogen pressure for constant heat-up rate tests.

Table 5. VARIATION OF m AND r WITH $P_{H_2}$

| $P_{H_2}$, atm | m | r |
|---|---|---|
| 0 | 0.028 | 0.029 |
| 18 | 0.127 | 0.145 |
| 35 | 0.194 | 0.240 |
| 52 | 0.254 | 0.341 |

The values of r given above increase with increasing hydrogen partial pressure. Figure 15 shows, in fact, a linear relationship between r and $P_{H_2}$, which is represented by the expression —

$$r = 0.03 + 0.00605\ P_{H_2} \qquad 12)$$

Thus, all the parameters necessary to quantitatively characterize the model assumed have been determined, except for parameters indicative of the kinetics of Reaction I. After complete conversion of the reaction intermediate, $CH_x^*$, however, the maximum methane-plus-ethane yield is independent of the kinetics of Reaction I and can be expressed as a function of the hydrogen partial pressure by the following expression:

$$\text{Maximum methane-plus-ethane yield, g-atom carbon/g-atom feed carbon} = \frac{0.83(0.029 + 0.00587P_{H_2})}{1 + 0.00587P_{H_2}}$$

It is of interest that the empirical form of the above expression is essentially the same as an expression proposed by Zahradnik et al. (12) to relate total methane yield as a function of hydrogen partial pressure during the initial hydrogenation of coals.

The following assumptions were made, consistent with results obtained in both constant heat-up rate and isothermal tests, to describe the kinetics of Reaction I:

1. $CH_x^0$ reacts according to Reaction I by a first-order process, but where there is a distribution of activation energies for the first-order rate constant, $k_0$.
2. The distribution function of activation energies is a constant; i.e., f(E)dE = fraction of total carbon in which the activation energy E in the rate constant,

$$k_0 = k_0^0 \exp(-E/RT)$$

is between E and E + dE

where —

$f(E) = 0$ for $E < E_0$

$f(E) = C$ (constant) for $E_0 \leq E \leq E_1$

$f(E) = 0$ for $E > E_1$

$k_0^0$ = preexponential factor

Note that because —

$$\int_{E_0}^{E_1} C \, dE = 1$$

then —

$$C = 1/(E_1 - E_0)$$

From these assumptions, the average conversion fraction of $CH_x^0$ can be expressed by the following relationship for any time-temperature history:

$$1 - f = \frac{1}{E_1 - E_0} \int_{E_0}^{E_1} \left\{ \exp \left[ -k_0^0 \int_0^{\theta} \exp(-E/RT) d\theta \right] \right\} dE \qquad 14)$$

where —

| | | |
|---|---|---|
| $\theta$ | = | time |
| T | = | absolute temperature |
| R | = | gas constant. |

For the specific case of constant heat-up rate, where $\alpha = dT/d\theta$, then Equation 14 can be expressed as the following:

$$1 - f = \frac{1}{E_1 - E_0} \int_{E_0}^{E_1} \left\{ \exp \left[ -\frac{k_0^0}{\alpha} \int_{T_0}^{T} \exp(-E/RT) dT \right] \right\} dE \qquad 15)$$

For isothermal conditions, Equation 14 has the form —

$$1 - f = \frac{1}{E_1 - E_0} \int_{E_0}^{E_1} \left\{ \exp \left[ -k_0^0 \, \theta \exp(-E/RT) \right] \right\} dE \qquad 16)$$

The best fit of our experimental data was obtained with the following values of $E_0$, $E_1$, and $k_0^0$:

| | | |
|---|---|---|
| $E_0$ | = | 79,500 cal/g-mol |
| $E_1$ | = | 118,100 cal/g-mol |
| $k_0^0$ | = | $7 \times 10^{20}$ $s^{-1}$ |

Experimental and calculated equivalent methane-plus-ethane yields are compared in Figure 16, where calculated yields were determined based on the parameters given above, using the appropriate correlation form for isothermal or constant-heat-up rate operation.

In summary, the correlations described in this paper provide a basis for predicting methane and ethane yields as a function of temperature, hydrogen partial pressure, and time-temperature history during the gasification of Montana lignite. Although these correlations were developed based on data obtained in hydrogen, helium, and hydrogen-helium mixtures, the results of a previous thermogravimetric study conducted at the Institute of Gas Technology (7, 10) showed that "rapid-rate" methane formation kinetics with air-pretreated bituminous coal are a function of hydrogen partial pressure even in gas mixtures containing other synthesis gas species, which may also be the case for the Montana lignite used in this current study. The generality of the parameters evaluated is, of course, not known because experimental results obtained only with Montana lignite were used in the development of the model. Although future studies are anticipated using other coals to evaluate this aspect, there is some evidence currently available from studies conducted at the U. S. Bureau of Mines, reported by Feldmann et al. (4), in which results obtained for hydrogasification of raw bituminous coals in a 3-inch-ID transport reactor show a strong similarity to corresponding results obtained in this study with Montana lignite. Figure 17, for example, compares methane and ethane yields obtained under isothermal temperature operation as a function of temperature for the two studies considered, at approximately corresponding average hydrogen partial pressures.*

The results shown indicate that relatively minor adjustments in one or two of the parameters defined in the model proposed in this paper would be required to fit the data obtained with the bituminous coals and the North Dakota lignite.

Another data comparison is shown in Figure 18, which plots total methane and ethane yields versus total coal hydrogen evolution for these same coals. Although the model proposed predicts linearity in these relationships only when referring to "equivalent" methane-plus-ethane yields and only when total oil/tar yields do not vary, the results shown are nevertheless suggestive that equivalent methane-plus-ethane yields obtained with the bituminous coals are essentially proportional to coal hydrogen evolution, as was indicated in this study with Montana lignite.

## ACKNOWLEDGMENT

This paper is based on work conducted at the Institute of Gas Technology with support from the American Gas Association.

---

* The study at the U. S. Bureau of Mines was conducted under integral conditions, and the results presented correspond to operation with hydrogen-methane feed-gas mixtures. The average hydrogen partial pressure indicated in Figure 17 is the linear average of the feed and product gases.

REFERENCES CITED

1. Anthony, D. G., "Rapid Devolatilization and Hydrogasification of Pulverized Coal," Sc. D. thesis, Massachusetts Institute of Technology, Cambridge, Mass., 1974.

2. Blackwood, J. D. and McCarthy, D. J., "The Mechanism of Hydrogenation of Coal to Methane," Aust. J. Chem. 19, 797-813 (1966) May.

3. Feldmann, H. F. et al., "Reaction Model for Bituminous Coal Hydrogenation in a Dilute Phase." Paper presented at the 160th National Meeting of the American Chemical Society, Division of Petroleum Chemistry, Chicago, September 13-18, 1970.

4. Feldmann, H. F., Mima, J. A., and Yavorsky, P. M., "Pressurized Hydrogasification of Raw Coal in a Dilute-Phase Reactor," Coal Gasification, in Adv. Chem. Ser. No. 131 (1974).

5. Hiteshue, R. W., Friedman, S. and Madden, R., "Hydrogasification of Bituminous Coals, Lignite, Anthracite, and Char," U.S. Bur. Mines Rep. Invest. No. 6125 (1962).

6. Hiteshue, R. W., Friedman, S. and Madden R., "Hydrogasification of a High-Volatile A Bituminous Coal," U.S. Bur. Mines Rep. Invest. No. 6376 (1964).

7. Johnson, J. L., "Kinetics of Bituminous Coal Char Gasification With Gases Containing Steam and Hydrogen," Coal Gasification, in Adv. Chem. Ser. No. 131 (1974).

8. Mosely, F. and Patterson, D., "The Rapid High-Temperature Hydrogenation of Coal Chars. Part 2: Hydrogen Pressures up to 1000 Atmospheres," J. Inst. Fuel 38, 378-91 (1965) September.

9. Mosely, F. and Patterson, D., "The Rapid High-Temperature High-Pressure Hydrogenation of Bituminous Coal," J. Inst. Fuel 40, 523-30 (1967) November.

10. Pyrcioch, E. J., Feldkirchner, H. L., Tsaros, C. L., Johnson, J. L., Bais, W. G., Lee, B. S., Schora, F. C., Huebler, J. and Linden, H.R., "Production of Pipeline Gas by Hydrogasification of Coal," IGT Res. Bull. No. 39. Chicago, November 1972.

11. Zahradnik, R. L. and Glenn, R. A., "Direct Methanation of Coal," Fuel 50, 77-90 (1971) January.

12. Zahradnik, R. L. and Grace R. J., "Chemistry and Physics of Entrained Coal Gasification," Coal Gasification, in Adv. Chem. Ser. No. 131 (1974).

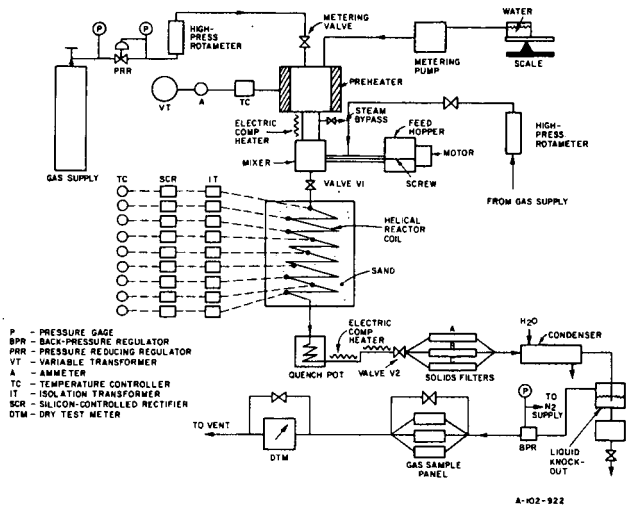


Figure 1. DIAGRAM OF THE EXPERIMENTAL SYSTEM

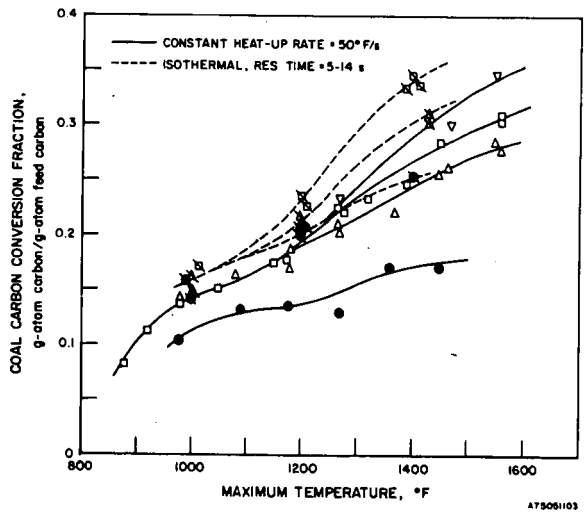


Figure 2. COAL CARBON CONVERSION

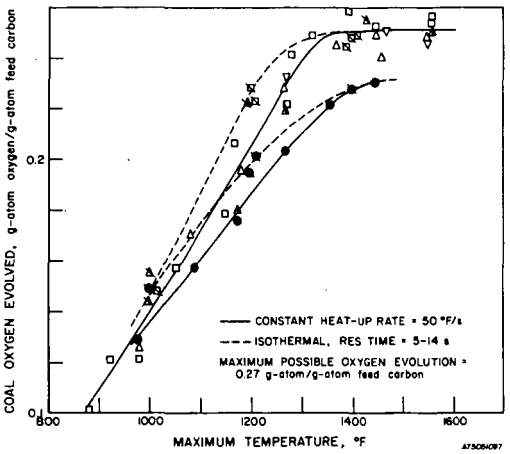


Figure 3. COAL OXYGEN CONVERSION

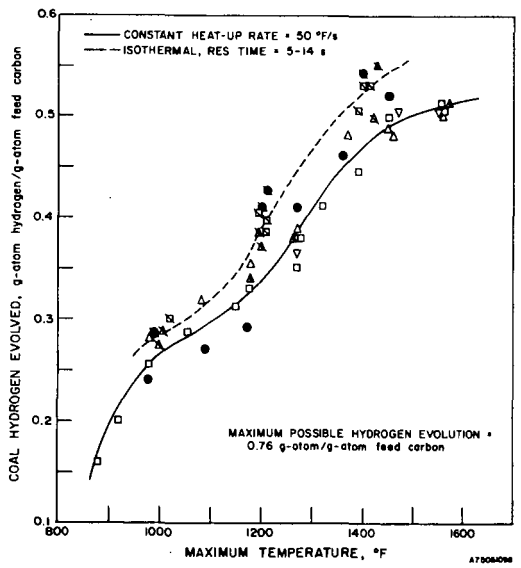


Figure 4. COAL HYDROGEN CONVERSION

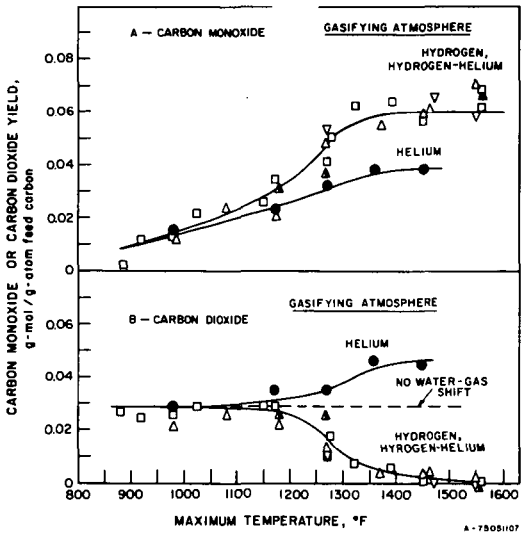


Figure 5. CARBON MONOXIDE AND CARBON DIOXIDE YIELDS

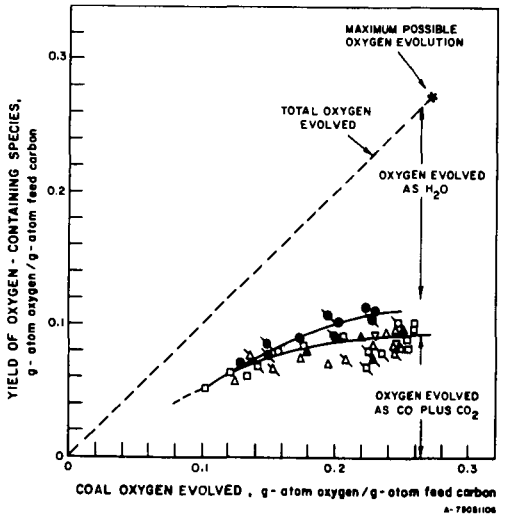


Figure 6. ADJUSTED EVOLVED OXYGEN DISTRIBUTION

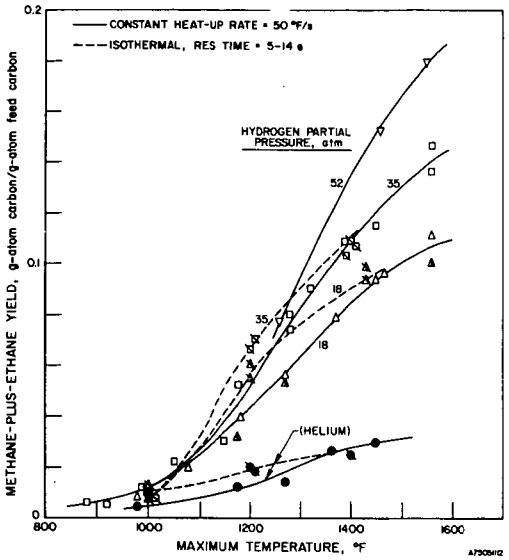


Figure 7. METHANE-PLUS-ETHANE YIELDS

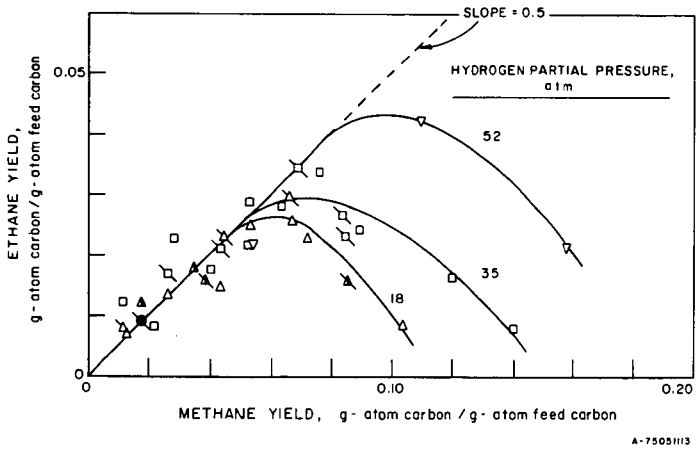


Figure 8. RELATIONSHIP BETWEEN METHANE AND ETHANE YIELDS

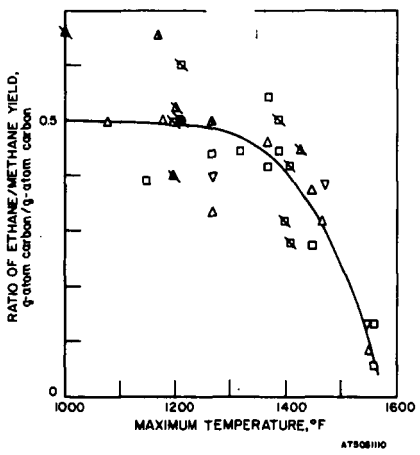


Figure 9. EFFECT OF TEMPERATURE ON ETHANE/METHANE RATIO

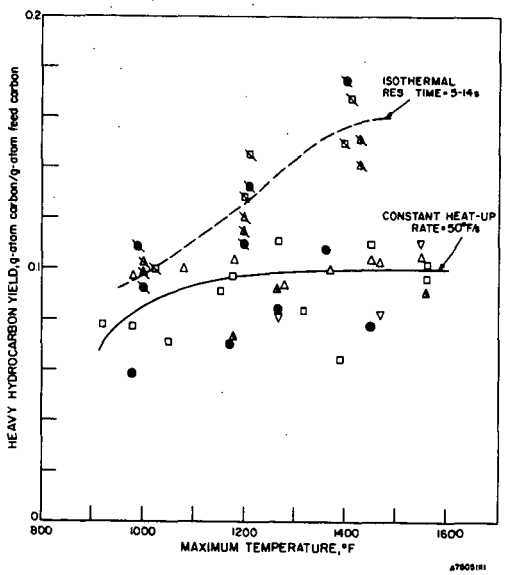


Figure 10. HEAVY-HYDROCARBON YIELDS

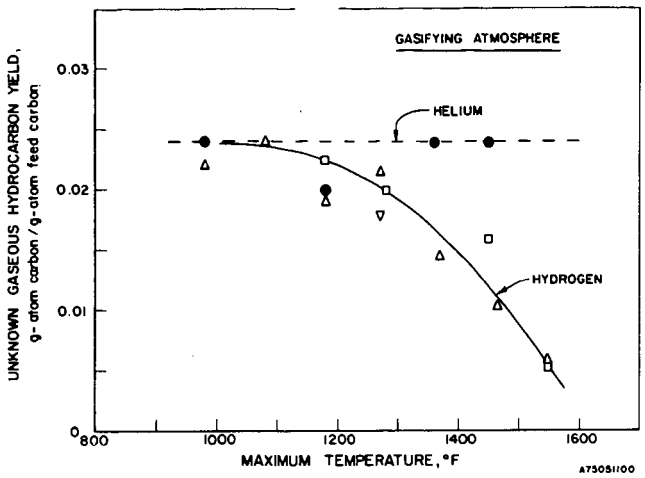


Figure 11. UNKNOWN-HYDROCARBON YIELDS

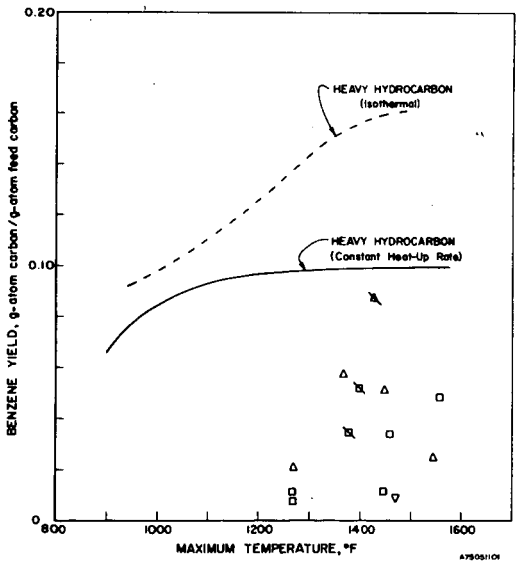


Figure 12. BENZENE YIELDS

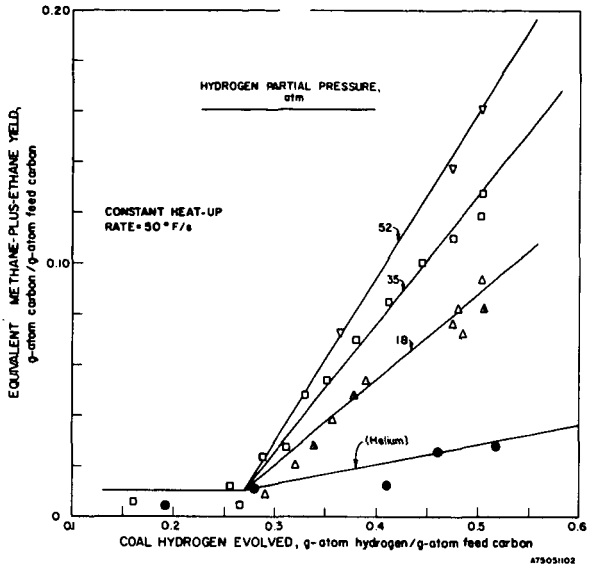


Figure 13. STOICHIOMETRIC RELATIONSHIP BETWEEN EQUIVALENT METHANE-PLUS-ETHANE YIELD AND COAL HYDROGEN CONVERSION

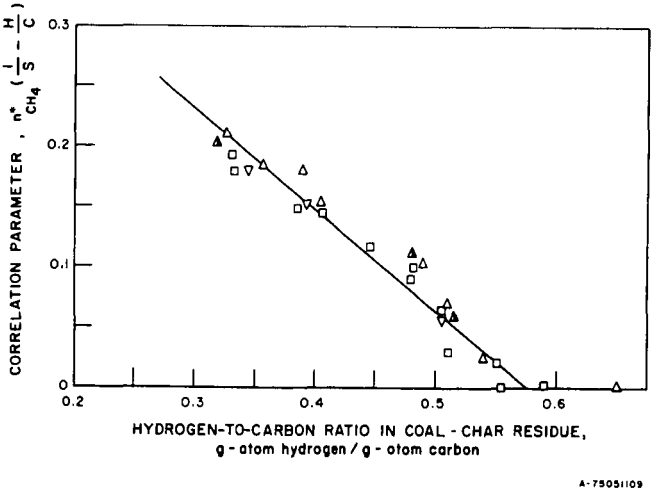


Figure 14. RELATIONSHIP BETWEEN STOICHIOMETRIC CORRELATION PARAMETER AND COAL HYDROGEN-TO-CARBON RATIO

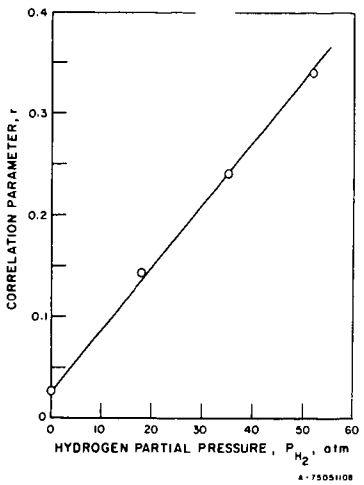


Figure 15. EFFECT OF HYDROGEN PARTIAL PRESSURE ON KINETIC PARAMETER, r

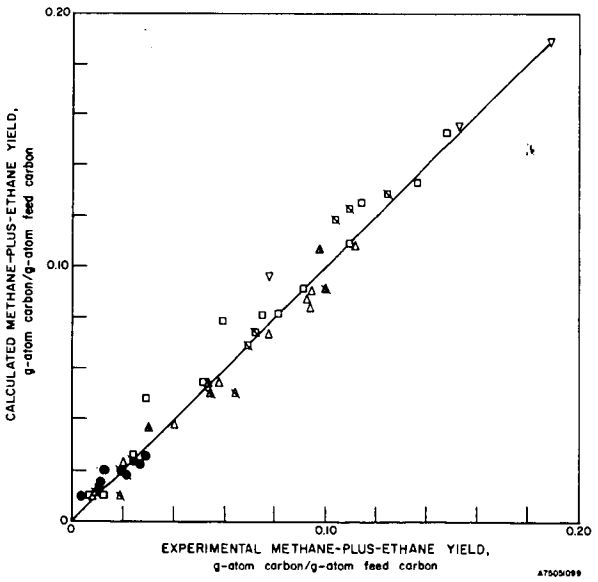


Figure 16. COMPARISON OF CALCULATED AND EXPERIMENTAL METHANE-PLUS-ETHANE YIELDS

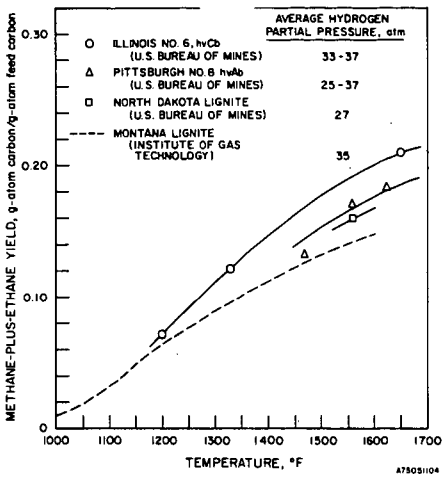


Figure 17. COMPARISON OF METHANE-PLUS-ETHANE YIELDS WITH DIFFERENT COALS

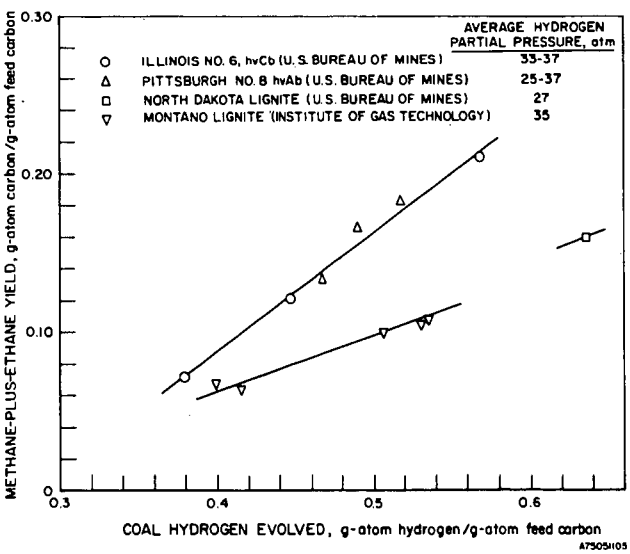


Figure 18. COMPARISON OF METHANE-PLUS-ETHANE YIELDS VERSUS COAL HYDROGEN CONVERSION CHARACTERISTICS FOR DIFFERENT COALS

# Rate of Reaction of Oxygen and Steam with Char/Coke*

Satyendra P. Nandi, Robert Lo and Jack Fischer
Chemical Engineering Division, Argonne National Laboratory
Argonne, Illinois 60439

In most coal gasification processes, raw coal is initially subjected to heat treatment. Even in the presence of reactive gases the initial rapid weight loss of the coal can be ascribed primarily to devolatilization. The resultant char is then converted to desired products in subsequent steps. It is believed that the gasification of the char is the slow step in the overall conversion reactions. The overall char gasification process consists of a number of reactions, amongst them the steam-carbon and oxygen-carbon reactions are the most important. The steam-carbon reaction

$$C + H_2O \rightarrow CO + H_2 \qquad 1)$$

is endothermic and its rate does not become significant below about 750°C. The heat required by reaction 1) can be supplied by the highly exothermic carbon-oxygen reaction

$$C + O_2 \rightarrow CO_2 \text{ and } CO \qquad 2)$$

The $CO/CO_2$ ratio is a function of temperature and carbon monoxide is favored at higher temperatures. Depending on the nature of carbon, the rate of this reaction may become significant at a temperature as low as 350°C. In the overall gasification scheme, judicious combinations of reactions 1) and 2) are used. It is therefore necessary to obtain a measure of the rates of these two reactions using various chars made from coals which are practical for use in gasifiers.

Various workers (1) have studied the carbon-steam and carbon-oxygen reactions using graphites. Because of the pronounced difference in inherent reactivity of the two gases, it is rather difficult to obtain values of the reactivity of a char for the two reactants at the same temperature. Similar data for graphite are scanty. Jenkins et al. (2) determined the reactivity parameter, defined later in this report, for a series of coal chars in air at 500°C. All the chars in Jenkins' work were prepared by heating various types of coal in nitrogen at a heating rate of 10°C/min to a maximum heat-treatment temperature of 1000°C. The results showed that the reactivity of the char was a function of the rank of the parent coal; the low-rank coals produced chars of much higher reactivity. It was also shown that the value of the reactivity parameter was the same, whether the chars were produced in a thermobalance (static bed) in milligram quantities or in a fluid bed in gram quantities.

In our work the approach taken was to measure the rates of char-steam and char-oxygen reactions over a range of temperature, determine the temperature coefficient of rates (apparent activation energy) of the separate reactions, and estimate the value of the relative rates at a common temperature. The magnitude of the apparent activation energy when compared with the values reported for pure carbon may indirectly provide some insight into the mechanisms of both the reactions.

*Based on work performed under the auspices of the United States Energy Research and Development Administration.

## EXPERIMENTAL

The porous nature, particle size, and maximum heat-treatment temperature of the char, the rank of the parent coal, and the inorganic matter present in the char are the variables which may affect the rate of the char-oxygen or char-steam reaction. The rate of heating used in preparation of the char is expected to affect the porous nature and is not considered as a separate variable. In this work the particle size, heating rate, and the maximum heat-treatment temperature are kept invariant.

### Samples

Four samples of coal were selected for this work. Three coals are of low rank (subbituminous or lower) and the fourth is of MVB rank. There are vast resources of subbituminous coals in Western U.S., and their gasification behavior is of interest. The MVB sample was included for comparative purposes.

The analyses of the samples are shown in Table 1.

### Experimental Procedure

The coal samples were pyrolysed in a tube furnace in a flow of nitrogen with a heating rate of 8°C/min to a maximum temperature of 900°C and held at that temperature for two hours. The coal samples were sieved and the fraction (35 x 80) mesh Tyler was used. The particle size of the char is expected to be somewhat smaller. On pyrolysis, sample 274 produced a coke mass, this was crushed, and a sieved fraction of (35 x 80) mesh was used for the reactivity determination.

The reactions were carried out using a thermobalance. A char sample was spread uniformly in a shallow platinum thermobalance pan. The amount of sample used, ∿10 mg, was such that the bed was about one particle diameter high. The samples were initially brought to the reaction temperature in nitrogen and after steady weight was attained, the reactive gas was introduced. Dry air was used for oxygen reactivity measurements. Pure nitrogen was passed through a series of bubblers containing distilled water to obtain a partial pressure of 2.3 volumn per cent of water vapor in the stream. This mixture was used to determine the rate of the steam-char reaction. The reaction was followed isothermally by means of a thermobalance and the rate was calculated from the weight loss. The flow rate of the reactive gas was kept constant and was such that the supply of the reactive gas was two orders of magnitude greater than could be consumed when the rate of carbon loss was at the maximum. The temperature range for the oxygen-char reaction was from 350 to 575°C and for the steam-char reaction, from 750 to 900°C.

### (a) Char-Oxygen Reaction

The percent weight loss based on the weight of original sample of char on a dry ash-free basis as a function of time for 274 coke is shown in Fig. 1. The low rate observed during the initial period is partially due to the time required for the air to replace the nitrogen from the vicinity of the carbon. This period is longer at lower temperature, which indicates that there is an induction period (the gas flow rate being the same in all cases). The induction period in carbon-oxygen reaction had been explained (3) by assuming that initially oxygen becomes chemisorbed on the surface. This is followed by subsequent desorption of the bound oxygen as oxides of carbon. With the removal of carbon from the surface, the char remaining increases in porosity, i.e., its specific surface area increases. From similar arguments, the middle linear portion of Fig. 1 can be regarded as a region where the opposing effects of carbon removal and generation of extra surface area are in balance. When the

carbon loss is high, the absolute value of the total reactive area is decreased, and consequetnly, the rate falls off. In this work, the middle linear portions of the experimental curves are used to calculate the characteristic rates.

The reactivity parameter was calculated by the following equation

$$R_{max} = \frac{1}{w_o} \frac{dw}{dt}$$

where $R_{max}$ = maximum reactivity at the experimental temperature expressed as mg of char reacted per minute per mg of initial sample; $w_o$ = initial mass of the char on dry ash-free basis and $\frac{dw}{dt}$ = maximum rectilinear weight loss rate (mg. $min^{-1}$). The approach taken to obtain $R_{max}$ is the same as that of Jenkins et al. (2)

The weight loss data for the air-char reaction for the other samples are shown in Figs. 2 to 4. The calculated values of $R_{max}$ are shown in an Arrhenius plot in Fig. 5. The reactivity of the coke sample (sample 274) was much lower compared with those for the char samples. It is also observed that the plots for char/coke from 274, 248 and 247 are straight lines in the temperature interval. The values of the apparent activation energy are nearly the same ($\sim$21 kcal/mole) for these three samples.

Values of the activation energy for the carbon-oxygen reaction (1) using pure carbon (graphite) have been reported to be in the range of 37 to 58 kcal/mole. The value, 36.7 kcal/mole, was obtained by Gulbersen and Andrew, (4) who reacted thin spectroscopic graphite plates between 425 and 575°C under 0.1 atmosphere of oxygen. The much smaller values of the apparent activation energy obtained in this work indicate that (i) catalysis by inorganic matter in the char occurred and/or (ii) the reaction occurred inside small pores whose length are much greater than their diameter. In the latter case Wheeler (5) had shown that the apparent activation energy will be equal in magnitude to half the value of the true activation energy of reaction. The nature of the minerals present in the chars was not determined. However, the possibility appears unlikely that the minerals were similar in nature or that they catalyzed the reaction in such a way as to produce the same apparent activation energy for the three materials. This strongly suggests that the reaction is being controlled by pore diffusion. The Arrhenius plot for the LLL char is not linear. Initial reactivity of this sample is very high and the curvature in the plot indicates that the reaction at high temperature, for this sample, is being partially controlled by bulk diffusion.

(b) Steam-char reaction

The experimental data for this reaction are presented in Figs. 6 to 9. The initial period of low reaction rate is of much lesser duration than in the oxygen-char reaction. It has been reported (1) that the steam-carbon reaction also proceeds through a chemisorbed oxygen intermediate, which may be of a different nature than that in the carbon-oxygen reaction. The much higher temperature used for the carbon-steam reaction may contribute to a rapid build-up of a steady-state concentration of chemisorbed species on the surface, resulting in a shorter induction period. A linear rate of weight loss over an extended reaction range is then obtained in all cases. This linearity results from the same opposing factors identified earlier for the char-oxygen reaction.

The shape of the curves shown in Figs. 7 to 9 are similar and show a qualitative resemblence to the curves obtained in char-air reaction. The data for the

coke shown in Fig. 6 are quite different. Two distinct linear regions are observed. A possible way of explaining the data is to assume a small fraction of disorganized carbon is mixed in with the relatively well-ordered carbon of the coke. After the fast reaction of the disorganized carbon has been completed, the rate falls to a value that is characteristic of the well-organized carbon.

The $R_{max}$ values for the steam-carbon reaction have been calculated from the data in Figs. 6 to 9 in a way similar to that used for the air-carbon reaction calculations. These data are shown graphically in Fig. 10. The values of the apparent activation energy for the 274 coke are based on limited data; the slope obtained at the low rate is about half of that at the high rate. The value of the apparent activation energy calculated from the low rate is ∿82 kcal/mole, which is in the neighborhood of the value (80 kcal/mole) reported for the graphite-steam system. (1)

The carbon contents of coals 247 and LLL are not very different. The apparent activation energy values obtained for the chars of these two coals are nearly the same (23 and 27 kcal/mole). The value for sample 248 was somewhat higher, ∿42 kcal/mole. This sample belongs to SubbC rank of coal. The ash content of this sample was lower than that of 247 and LLL samples.

This low value of the apparent activation energy indicates that the reaction studied in this work probably proceeded by a different mechanism than that for graphite-steam reaction. Wheeler's explanation for the difference in the magnitude of the activation energy for the same reaction taking place inside long narrow capillary, and on a plain surface has been mentioned earlier. It appears that for the three char samples, the major part of the reaction could be occurring inside narrow pores. In addition, the reaction may be influenced by catalytic impurities in some cases.

(c) Relative reactivity in oxygen and steam

Walker et al., (1) in their review of the gas-carbon reaction reported that the rate of carbon-oxygen reaction was $3 \times 10^4$ times as rapid as that of the carbon-steam reaction under equivalent conditions (temperature = 800°C, pressure of gas = 0.1 atm). The experimental results used in the above estimation were obtained primarily with graphite. From the experimental data obtained in this work for 247 char, the relative rates of oxygen to steam reaction were calculated using the computational method of Walker et al. For this sample the ratio of the rates of oxygen to steam reactions was found to be only ∿24 · (T = 800°C and P = 0.1 atm). The reactivity ratio for the LLL char would be even lower because the slope of the Arrhenius plot (char-air) for this sample decreased at higher temperature. It is concluded that the reactivity ratio of oxygen to steam reactions with coal chars will be much lower than that expected for pure forms of carbon.

ACKNOLEDGEMENT

The authors wish to thank Professor W. Spackman of Pennsylvania State University for providing three of the coal samples and their elemental analyses, and Lawrence Livermore Laboratory for supplying the fourth coal sample (LLL) and its elemental analyses.

Table 1

Analyses of Coal

| Sample No. | ASTM Rank | Percent as received | | | Percent dry ash basis | | | | |
|---|---|---|---|---|---|---|---|---|---|
| | | Moist. | Ash. | Wt. loss to 900°C | C | H | N | S | O (by diff) |
| 274 | MVB | 1.42 | 1.75 | 27.2 | 86.30 | 4.32 | - | 1.2 | - |
| 248 | SbbC | 16.67 | 2.48 | 51.4 | 75.16 | 5.15 | 1.73 | 0.66 | 17.26 |
| 247 | L | 14.10 | 6.52 | 50.2 | 74.43 | 4.91 | 1.49 | 0.53 | 18.62 |
| LLL | L | 29.60 | 6.50 | 59.1 | 74.34 | 5.52 | 1.18 | 0.45 | 18.51 |

## REFERENCES

1. P. L. Walker, Jr., F. Rusinko, Jr., and L. G. Austin, Adv. Catal., Vol. 11, Academic Press, New York, 1959, pp. 134-217.

2. R. G. Jenkins, S. P. Nandi, and P. L. Walker, Jr., Fuel 52, 288 (1973).

3. B. G. Tucker and M. F. R. Mulcahy, Trans. Faraday Soc., 65, 274 (1969).

4. E. A. Gulbersen and K. F. Andrew, Ind. Eng. Chem. 44, 1034 (1954).

5. A. Wheeler, Adv. Catal., Vol. 3, Academic Press, New York, 1951, pp. 250-326.

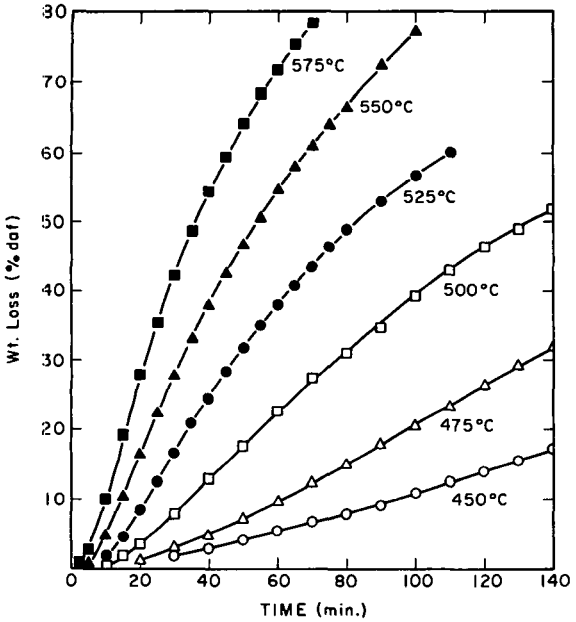


Figure 1. Rate of reaction between AIR and 274 COKE

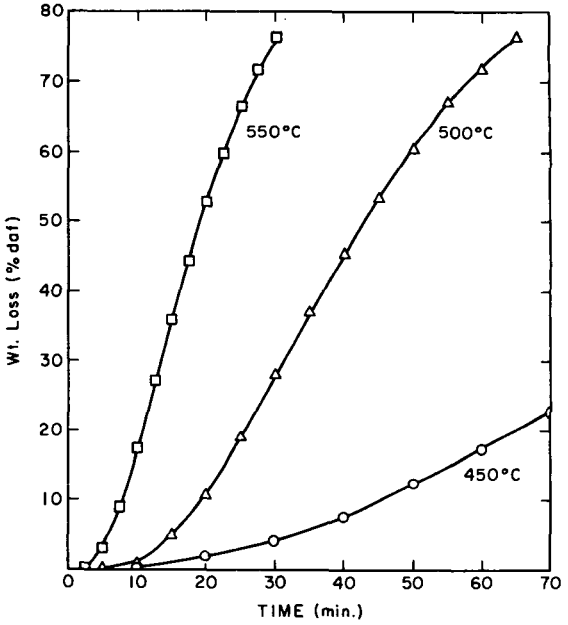


Figure 2. Rate of reaction between AIR and 248 CHAR

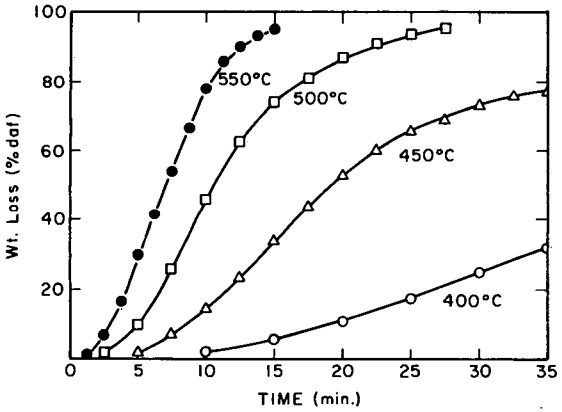


Figure 3. Rate of reaction between AIR and LLL CHAR

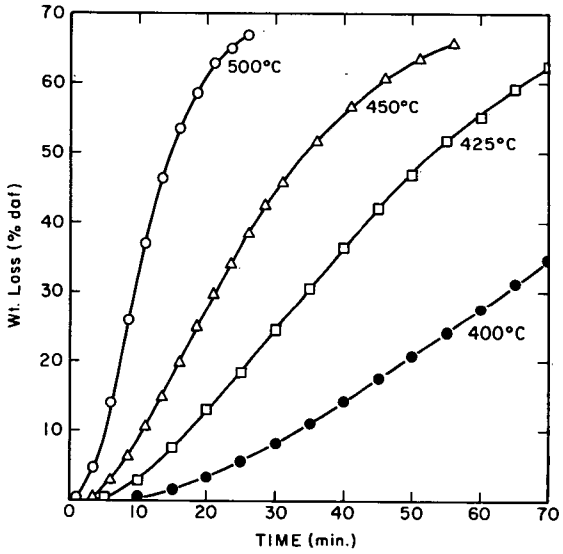


Figure 4. Rate of reaction between AIR and 247 CHAR

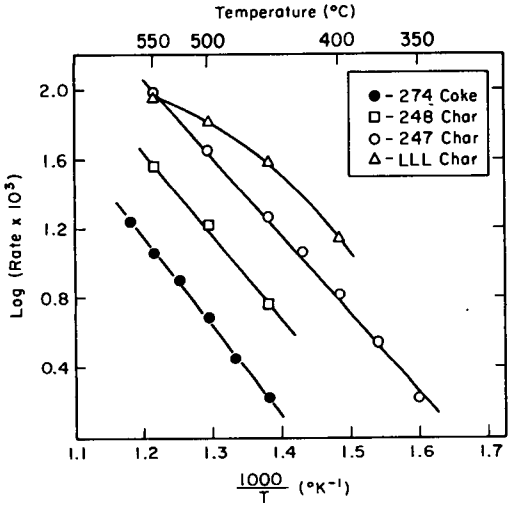


Figure 5. Arrhenius Plot - Maximum reaction rate in AIR - CHAR/COKE system

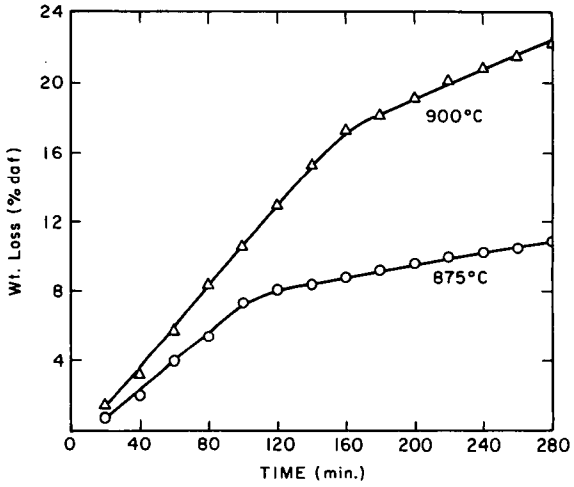


Figure 6. Rate of reaction between 2.3% STEAM and 274 COKE

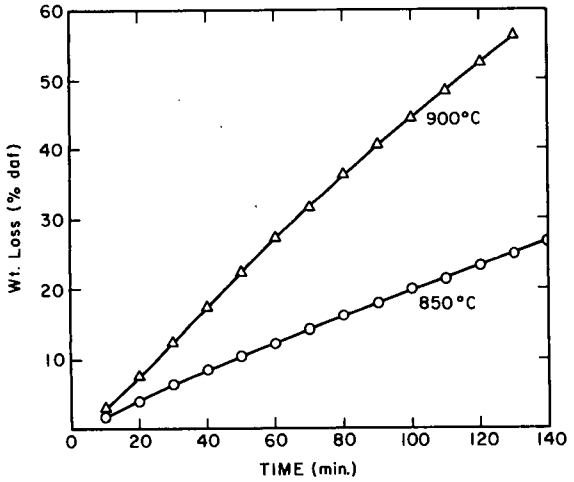


Figure 7. Rate of reaction between 2.3% STEAM and 248 CHAR

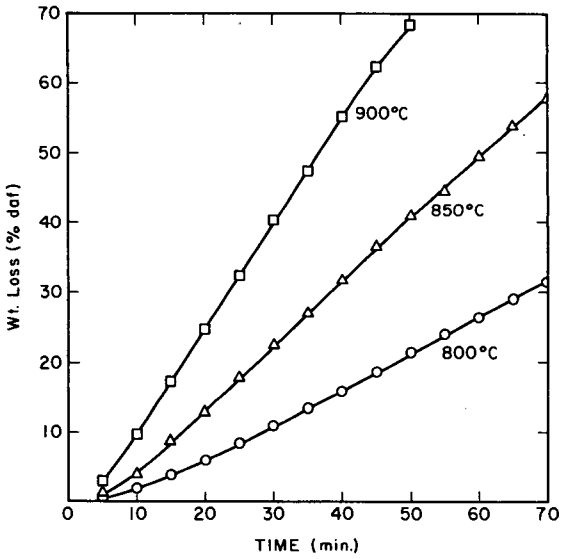


Figure 8. Rate of reaction between 2.3% STEAM and LLL CHAR

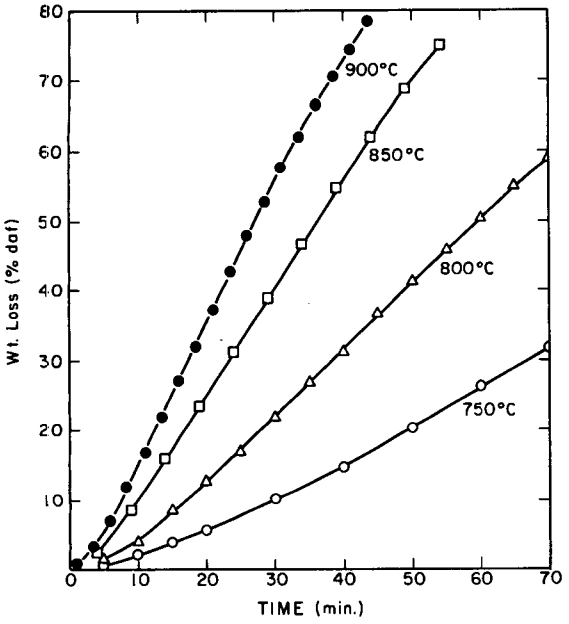


Figure 9. Rate of reaction between 2.3% STEAM and 247 CHAR

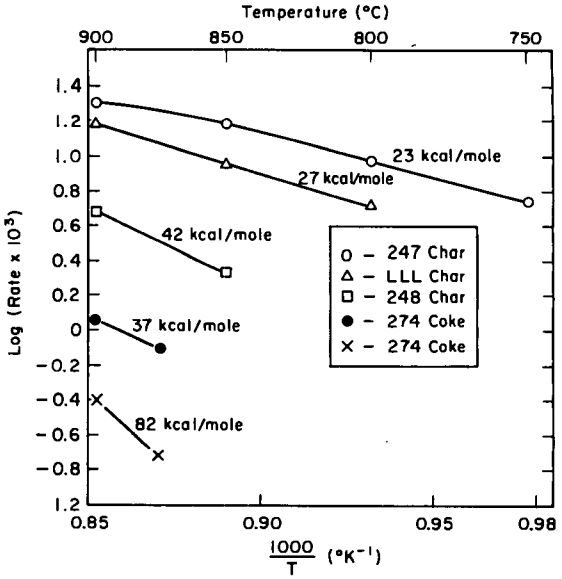


Figure 10. Arrhenius Plot - Reaction rate in STEAM - CHAR/COKE system

# REACTIVITIES OF HEAT-TREATED COALS IN HYDROGEN

A. Tomita, O. P. Mahajan, and P. L. Walker, Jr.

The Pennsylvania State University
Department of Material Sciences
University Park, Pennsylvania 16802

## INTRODUCTION

In previous papers, we reported reactivities of various American coal chars in air (1) and in carbon dioxide (2). It was found that reactivities of chars are predominantly determined by the rank of the parent coal and mineral matter composition. The main aim of this paper is to compare the reactivities in hydrogen with those obtained earlier.

The reaction of coal chars with hydrogen is an important part of the over-all process for the production of substitute natural gas; consequently it has received considerable attention (3-8). The reaction of low temperature chars with hydrogen proceeds in two stages: a very rapid first stage reaction and a slow second stage reaction, involving the gasification of a remaining char which has a graphitic-like (trigonally-bonded) structure. Most workers have studied the reactivity of the chars which have been pretreated at some fixed maximum temperature. Because the maximum temperature was usually reasonably low, the chars had, however, a certain amount of volatile matter remaining. In order to study the slow, second stage hydrogasification reaction, it would be better to work with a char prepared at a higher temperature. Throughout this study chars prepared at 1000°C are used. The variables chosen for investigation were the rank of parent coals, mineral matter content, particle size, reaction temperature and pressure.

## EXPERIMENTAL

Char Preparation Eighteen U.S. coals, of widely varying rank, were carbonized in nitrogen at 1000°C for 2 hr. This procedure was sufficient to devolatilize these coals. The preparative method of 'acid-washed' char, demineralized char, and chars with different particle sizes were essentially the same as described earlier (2).

Procedure A high-pressure, electronic balance was used to record continuously small weight changes during hydrogasification. The balance assembly, a DuPont 951 TGA, was mounted in an autoclave. Generally, char powders of 40x100 U.S. mesh were charged to a sample holder in 10 mg quantities. The autoclave was evacuated and then pressurized with nitrogen to 400 psi. Helium was introduced into the quartz tube reactor, which was attached to the balance housing and also was surrounded by a tube furnace. The furnace was activated to raise the reactor temperature to 980°C. The pressure was kept constant by bleeding off excess gas. Helium was kept flowing at reaction temperature for 15 min to ensure thermal stability; and then a stream of hydrogen was admitted to the reactor at a flow rate of 1200 cc/min (STP). The weight of the sample was then continuously recorded.

Reactivity Measurement The conversion vs time curve usually had a slow induction period, followed by a rate increase as was reported for the reaction with air (1), carbon dioxide (2), hydrogen (7), and steam (7). Jenkins et al (1), found that the rectilinear portion, after an induction period, extended over a range in which about 40% of the char was gasified. They calculated the reactivity parameter by the following equation:

$$R_o = \frac{1}{W_o} \frac{dw}{dt}$$

where $W_o$ is the initial weight of char on a dry ash free basis (mg) and dw/dt is the maximum rectilinear weight loss rate (mg $hr^{-1}$). In the present study, the rectilinear region was considerably shorter than reported previously (1,2). On the other hand, the rate calculated on the basis of unreacted char remained constant for a longer period. This reactivity parameter R is expressed as

$$R = \frac{1}{W} \frac{dw}{dt}$$

where W is the weight of char at time t. Two parameters $R_i$ and $R_c$ were determined by this equation. $R_i$ represents the initial rate at t = 0, and $R_c$ represents the constant rate in the region where kinetics follows a first order rate expression with respect to unreacted char.

## RESULTS AND DISCUSSION

Reactivity versus rank of parent coal Table 1 summarizes the analyses of coals and chars together with the reactivity parameters. It can be seen that there is some relation between $R_i$ values and the rank of the parent coal. The lower rank coal chars have larger $R_i$ values. However, $R_c$ values have no definite correlation with rank. For example, the reactivity of the Pennsylvania anthracite char (PSOC 81) is larger than most chars of lower rank. This fact is in marked contrast with those reported for the reactivity of the same series of chars with air and carbon dioxide. In these cases, a plot of reactivity $R_o$ vs carbon content shows a fairly well defined band. Even if the parameter $R_o$ is used for the hydrogasification reactivity, no correlation with rank of parent coal is found. Feldkirchner et al (4) found a similarity in hydrogasification rates of the residual portion of three coal chars with greatly different initial properties.

Mineral matter removal Jenkins et al (1) found that the reactivity of lignite and anthracite chars in air decreased upon demineralization, whereas reactivity of a LV bituminous char increased. The same effect of demineralization was observed in this study for PSOC 138, 101, 127 and 81. However, the removal of mineral matter from lignite char PSOC 87 resulted in a remarkable increase of $R_c$ value, although the $R_i$ value decreased considerably.

Bed weight and particle size In order to determine the possible effect of diffusional resistance, reactivity measurements were made for PSOC 91, 87, 87 Dem, 127 and 127 Dem at different bed weights and particle sizes. For starting weights below 10 mg, reactivity is constant for most chars. There is some effect of particle size, but the rate increase due to the reduction of size is rather small compared with that reported for the reactivity study in $CO_2$ (2). Reduction in particle size of PSOC 127 char from 40x100 to 200x325 mesh results in a reactivity increase of only 1.6-fold in hydrogen, whereas a similar particle size reduction of the same char resulted in a reactivity increase of 35-fold towards carbon dioxide (2). This fact can be attributed to the smaller kinetic diameter of hydrogen (2.9A) compared to carbon dioxide (3.3A).

Pressure The dependence of rate on hydrogen pressure in the range between 100 and 400 psi was determined for PSOC 91 char. The rate was proportional to hydrogen pressure as reported in the literature (4-7).

Temperature Zielke et al (3) reported that the pseudo-activation energy changed from 17 to 49 kcal/mole as a function of conversion. Gardner et al (8) also found an increase of activation enthalpy with conversion of char to methane. Although the chars used in this study had a different thermal treatment than those used by

Gardner et al (8), we also observed a similar trend. The pseudo-activation energy for PSOC 91, 87 Dem, and 127 Dem chars were 31, 29, and 14 kcal/mole at the initial slow stage, while at a steady state rate they were 48, 44, and 44 kcal/mole, respectively. This fact suggests that the reaction during the induction period is diffusion-controlled, and further that the later stage is a chemically-controlled step. During the induction period, the char undergoes activation, and thus the diffusion rate of hydrogen or methane into the interior of the char particles becomes more rapid.

PSOC 217 char has an unusually low reactivity among all chars. The pseudo-activation energy was determined for this char up to a conversion of 20%, and it was found to be nearly constant at 16 kcal/mole. This low activation energy (and, thus extensive diffusion control of the gasification rate) is expected because of the small percentage of feeder pores in the parent LV bituminous coal (9).

ACKNOWLEDGEMENTS

This research was supported by the U.S. Energy Research and Development Administration on Contract No. 14-01-0001-390. Professor W. Spackman supplied the coals studied.

REFERENCES

1. Jenkins, R. G., Nandi, S. P., and Walker, P. L., Jr., Fuel, 52, 288 (1973).

2. Walker, P. L., Jr. and Hippo, E. J., Preprints of Papers Presented at 170th National Meeting ACS, Division of Fuel Chemistry, 1975.

3. Zielke, C. W. and Gorin, E., Ind. Eng. Chem., 47, 820 (1955).

4. Feldkirchner, H. L. and Linden, H. R., Ind. Eng. Chem. Proc. Res. Devel., 2, 153 (1963).

5. Moseley, F. and Paterson, D., J. Inst. Fuel, 38, 13 (1965).

6. Blackwood, J. D., Cullis, B. D. and McCarthy, D. J., Aust. J. Chem., 20, 1561 (1967).

7. Johnson, J. L., Advan. Chem. Ser., 131, 145 (1974).

8. Gardner, N., Samuels, E. and Wilks, K., ibid, 131, 217 (1974).

9. Gan, H., Nandi, S. P. and Walker, P. L. Jr., Fuel, 51, 272 (1972).

TABLE 1

CHAR REACTIVITY IN HYDROGEN

| PSOC | Parent Coal | | | Char | Reactivity, mg $hr^{-1}$ $mg^{-1}$ | |
|---|---|---|---|---|---|---|
| Sample No. | ASTM Rank | State | C(daf), % | Ash, % | $R_i$ | $R_c$ |
| 89 | Lignite | N.D. | 63.3 | 22 | 0.73[a] | 1.0 |
| 91 | Lignite | Mont. | 70.7 | 11 | 1.0[a] | 1.2[b] |
| 87 | Lignite | N.D. | 71.2 | 13 | 2.1[a] | 2.1[b] |
| 140 | Lignite | Tex. | 71.7 | 12 | 0.55 | 1.7 |
| 138 | Lignite | Tex. | 74.3 | 16 | 0.62 | 1.5 |
| 98 | Sbb. A | Wyo. | 74.3 | 12 | 0.34 | 1.0[b] |
| 101 | Sbb. C | Wyo. | 74.8 | 8 | 1.2[a] | 1.2[b] |
| 26 | HVB | Ill. | 77.3 | 20 | 0.37 | 0.99 |
| 22 | HVC | Ill. | 78.8 | 23 | 0.38 | 2.0 |
| 24 | HVB | Ill. | 80.1 | 14 | 0.50 | 2.3 |
| 67 | HVB | Utah | 80.4 | 5 | 0.30 | 1.9 |
| 171 | HVA | W.Va. | 82.3 | 11 | 0.08 | 0.64 |
| 4 | HVA | Ky. | 83.8 | 2 | 0.13 | 1.7 |
| 137 | MV | Ala. | 87.0 | 19 | 0.23 | 0.24[b] |
| 114 | LV | Pa. | 88.2 | 12 | 0.22 | 0.39[b] |
| 127 | LV | Pa. | 89.6 | 7 | 0.05 | 0.09 |
| 81 | Anthracite | Pa. | 91.9 | 6 | 0.13 | 2.0 |
| 177 | Anthracite | Pa. | 93.5 | 5 | 0.06 | 0.73 |

a No or very short induction period.
b Constant rate region is less than 50% of complete burn-off.

# REACTIVITY OF COAL AND CHAR IN $CO_2$ ATMOSPHERE

S. Dutta, C. Y. Wen and R. J. Belt*

Department of Chemical Engineering, West Virginia University, Morgantown, WV 26506

*ERDA, Morgantown Energy Research Center, Collins Ferry Road, Morgantown, WV 26506

Abstract - Reactivities of a few raw coals and chars of these coals obtained from gasifiers operating under different conditions have been measured in $CO_2$ at the temperatures 1550-2000°F. The reactivities have been measured in a thermogravimetric analyzer up to complete conversions of the samples in most cases. Properties like surface area, pore size distribution, porosity and density have been determined for each sample. Actual pore structures of a few samples have been observed at different conversion levels by a scanning electron microscope. In order to compare the reactivities of different samples, the char-gasification process has been divided into two distinct stages: the first stage due to pyrolysis and the second stage due to char-$CO_2$ reaction. Reactivities due to the first stage can be roughly related to volatile matter contents of the solids and the rate of heating. Through an Arrhenius type equation, an activation energy of about 2.5 Kcal/mole is obtained for the first stage. The reactivity of a char in the second stage is found to depend more on its coal seam than on the gasification scheme used in its production. Activation energy for the second stage reaction has been found to be about 59 Kcal/mole. A rate equation has been proposed for the second stage that incorporates the effect of relative available pore surface area changing during reaction. The rate conversion curves calculated from this equation fit well with the experimental data.

## Introduction

A proper understanding of the coal/char gasification kinetics is essential for successful design of a gasifier. Effects of temperature, pressure and gaseous environments on the rate of gasification of coal/char have been extensively studied by various investigators. In addition, the rate depends also on the nature and origin of the coal or char itself. The pore characteristics and hence the reactivity of a char have been found to vary not only with the maceral of its parent coal but also with the history of its genesis, i.e., the temperature, pressure, rate of heating and gaseous environments, etc., prevailed during its formation. The present study is devoted to determination of reactivities of a few coal and char samples which are produced in some pilot plant experiments conducted under different gasification schemes. This investigation will help find the relationship, if any, between the reactivities and the physical characteristics of the samples.

In the present investigation reactivities are measured in a flowing stream of pure $CO_2$ at the atmospheric pressure. The rate of C-$CO_2$ reaction has been studied by various investigators[1,5,7,9,10,12,13]. However, considerable discrepancy has been reported between the values of activation energy of this reaction, ranging from 48 to 86 Kcal/mole .

Pyrolysis of coal or char takes place prior to or concurrent with other reactions in a gasifier. The behavior of pyrolysis is not yet properly established. It is, however, known that the rate of pyrolysis and the amount and composition of volatile products from a given sample of coal or char depends on several factors[3] such as (a) rate of heating, (b) final decomposition temperature attained, (c) vapor residence time and (d) the environment under which the pyrolysis takes place. In the present investigation pyrolysis of coal and char in a $CO_2$ atmosphere can be studied separately from $CO_2$ reaction. This is due to the fact that pyrolysis normally starts at about 350-400°C and is almost complete at about 1000°C[2] within seconds, whereas the C-$CO_2$ reaction is hardly detectable below 800-900°C. Therefore, at a moderate rate of heating, the two stages, the pyrolysis and the char-$CO_2$ reaction, will be separable from each other, the latter starting only after the former stage is essentially

complete. The char-$CO_2$ reaction after the pyrolysis reaction is completed takes place on char surface and is essentially carbon-$CO_2$ reaction.

Gulbransen and Andrew[4] showed that the internal surface area of graphite increases markedly during reaction with both oxygen and $CO_2$. Walker, Foresti and Wright[10] made the detailed study on the possible correlation existing between reaction rates and changes in surface area during reaction. They concluded that the reaction develops new surface by enlarging to some extent the micropores of the solid but principally by opening up pore volume not previously available to reactant gas because the microcapillaries were too small or because existing pores were unconnected. During the reaction surface area increases up to a point when the rate of formation of new area is paralleled by the rate of destruction of old area. Surface area decreases on further conversion. For graphite-$CO_2$ reaction, Petersen, Walker and Wright[6] found that the observed rates were not simple functions of the total available surface area, as determined by the low temperature gas adsorption technique, as might be expected if the reaction was chemical reaction controlled.

Turkdogan, et.al.[8] made a detailed investigation on the pore characteristics of several forms of carbon. Their studies indicate that depending on the type of carbon, about 1/4 to 1/2 of the volume is isolated by micropores and hence is not available for reaction at the beginning. The surface areas of carbon investigated by them covered a large range from 0.1 to 1100 $m^2/g$. In all cases, most of the internal area was attributed to the micropores, 10-50 Å dia.

## Experimental

A Fisher TGA apparatus (model 120P) was used in the present investigation. Two coal samples (one from Pittsburgh seam and the other from Illinois seam) and four char samples derived from these coals under different gasification schemes were investigated.

To start a run 15-30 mg. of coal or char particles of -35+60 mesh were placed in the platinum holder hanging from one arm of the balance of the TGA. After fixing the hangdown tube in position, the system was first evacu ated to about 20 mm Hg and then flushed with $CO_2$ at a flow rate of about 200 ml./min. for about two and a half hours. The outlet gas was analyzed by gas chromatograph to assure that it is air-free. The oven was preheated to the desired temperature. The $CO_2$ gas stream was turned to the desired flow rate (150 ml./min.) and the furnace was quickly raised to a prefixed level, to enclose the hang-down tube. The weight and the time derivative of weight loss of the sample and the sample temperature were recorded continuously throughout the experiment.

The porosity, density, pore volume and pore size distribution of the devolatilized chars and coals have been determined by mercury porosimetry using pressures up to 50,000 psi. The pore surface areas and pore size distribution of the samples have been determined by BET nitrogen adsorption method using NUMEC surface-area-apparatus, model AfA4. Moreover, the actual macropore matrix of a few of these samples have been visually observed, at several stages of their conversions, by a scanning electron microscope up to a magnification of 6,000.

## Experimental Results and Discussions

Figure 1 is the reproduction of two typical chart recordings of the weight loss and the rate of weight loss curves by the TGA apparatus. In this figure the initial peaks in the rate curves are due to the very fast pyrolysis stage. After this stage, the second stage reaction begins which is comparatively slow and is mostly C-$CO_2$ reaction. The analyses of the chars just after the pyrolysis stage show carbon contents of 95-98% on an ash-free basis for all the six samples.

Figure 1 also shows an intermediate region, between the two vertical lines a and b, where not only the pyrolysis but also the second stage char-$CO_2$ reaction is affected by the heating rate of the sample. The sample temperature versus time for these two cases are shown in Figure 2. In these experiments the sample temperature is assumed to be identical with that recorded by an open thermocouple placed about 3 mm. from the surface of the reacting solid sample. The rate of gasification at the first and intermediate stages will obviously depend on the sample heating rate. Once the sample attains equilibrium temperature (approximately within 4 min. in the present case), the rest of the process proceeds essentially under isothermal condition.

## A. The First Stage - Pyrolysis

The rate of gasification and the fraction conversion due to pyrolysis are shown for four samples in Figure 2. The total conversions obtained at this stage have been found to be nearly equal to the volatile matter contents of the chars and coals as determined by the proximate analyses. The conversion (f) in the first stage (pyrolysis) is defined here as that conversion which is attained at the almost-constant weight period (the region between the vertical lines a and b in Figure 2, immediately after the rapid weight loss at the start of the process. Such a constant-weight-period has been observed in almost all cases. Figure 2 also shows that the pyrolysis is almost complete before a temperature of about 1500°F is reached, while the char-$CO_2$ reaction is insignificant up to this temperature, as will be seen later.

The total conversion (f) from the pyrolysis stage increases with the increase in temperature. However, this increase (~1%) is not appreciable, at a particular heating rate, in the studied temperature range 1550~1975°F.

Figure 3 shows the effect of sample heating rate on the rate of pyrolysis of hydrane char #150. It is noted that the peak heights of these rate curves are roughly proportional to the average slopes of the heating rate curves.

A Pyrolysis Model: Pyrolysis cannot be considered as a single-step process involving a simple reaction. It occurs in stages or as "waves" of reactions involving many complex steps, which in turn vary from sample to sample and with the conditions of pyrolysis. No simple model would, therefore, represent this process completely. However, on an overall basis Wen et.al.[11] proposed an Arrhenius type equation as follows:

$$\frac{dx}{dt} = A\, e^{-B/RT}(f-x) \qquad 1)$$

Following this equation, a plot of $(dx/dt)/(f-x)$ versus $1/T$ has been made with the values of dx/dt, f, x and T obtained from Figure 2. f is assumed constant in the studied temperature range. The plot is shown in Figure 4 for three char samples. The figure shows that no single straight line can be drawn through the points with certainty. This is partly due to the fact that the process is so fast that values of x, dx/dt at any instant cannot be read precisely from such rate and conversion curves shown in Figure 2.

Equation 1 has, therefore, been tested indirectly by assigning arbitrary values of A and B (in the ranges predicted by the points in Figure 4) and seeing whether the resulting values of x and dx/dt can match with the experimental ones. Since temperature is changing with time in this region, the values of x have been determined as a function of time from the following equation:

$$x = f\,[1-e^{-A\int_0^t e^{-B/RT}dt}] \qquad 2)$$

The evaluation of the integral in the above equation has been done numerically from known values of temperature (T) as a function of time (t). The rate, dx/dt, is next calculated from Equation 1. With A=2,500 cal/mole and B=20.0 $min^{-1}$, the predicted

conversion and rate curves for three chars have been found to match the experimental curves quite closely, as is shown in Figure 5a. The predicted curves and the experimental values for different heating rates are shown in Figure 5b. Calculations have been done only up to 1.5 min. in order to avoid the possible influence of the second stage process in the subsequent period.

The straight line drawn through the experimental points in Figure 4 are based on the above values of A and B.

Thus if the Arrhenius-type Equation 1 is assumed to approximate the pyrolysis stage, the value of activation energy becomes 2.5 Kcal/mole.

## B. The Second Stage - Char-$CO_2$ Reaction

As has been mentioned earlier, the rate of pyrolysis or the first stage of char/coal gasification is very rapid and can be assumed nearly complete, when an almost-constant-weight period is attained in the weight-loss versus time curve. The remaining fraction of the solid reacts slowly with $CO_2$ which is termed the second stage of gasification. Although a small part of volatile matters may still remains with this fraction, this fraction consists essentially of carbon (95-98%), and ash. The rate, dx/dt, and conversion, x, are based on the reactive portion of char, which is the weight of solid remaining after the first stage less the weight of ash, and is termed as the base carbon.

Before studying the effect of temperature the effects of sample size, sample holder, particle size and gas ($CO_2$) flow rate on char gasification rate were examined.

Three kinds of sample holders of different sizes and shapes were tested using different amounts of samples placed on them. They were (a) a shallow petri-dish type holder of diameter 8.5 mm. and depth 2 mm., holding 3.75 mg. of sample, (b) a cup-shaped holder of mouth diameter 8.5 mm. and depth 7 mm., holding 18.5 mg. of sample and (c) a perforated cylindrical holder of diameter 6 mm. and depth 15 mm., holding 35.02 mg. of sample. No significant difference was found between the observed rates in the three cases at a gasification temperature of 1877°F and a gas flow rate of 150 ml/min. The cup-shaped sample holder was used in the rest of the experiments. Gas flow rates were varied in the range 42-210 ml/min., through the reactor tube of diameter 19 mm. No change in rate was observed at flow rates above 70 ml/min., at the gasification temperature of 1877°F. A flow-rate of 150 ml/min. was chosen for subsequent experiments. Particle size selected was -35+60 mesh, which showed negligible intraparticle diffusion resistance up to a temperature of about 1800°F.

Figures 6-11 show the rate versus conversion curves as a function of temperature for the six different samples studied. These figures also show the base carbon content of the chars at the fraction conversions indicated.

The experiments were conducted up to the complete conversions of the samples, except at lower temperatures where rates were extremely slow.

The Figures 6-11 clearly show that every sample has its own characteristic rate-conversion curve. For Hydrane Char #49, the curves can be considered linear (and passing through the origin) without significant error. However, for the other samples this is not true. Again for Hydrane Char #150, the rates are almost steady up to certain conversion levels, after which they decline. For Pittsburgh coal, rate-conversion curves show maxima at lower temperatures.

It is also noted that for the Pittsburgh coal and for the Hydrane Char #150, the nature of the curves changes also with temperature. This change is shown more clearly in Figure 12, where the rates are normalized with respect to the rates observed at 20% conversion level and plotted against conversion. The rate-conversion curve shows a maximum at lower temperatures only.

The variety of rate-conversion curves is due to the fact that different coal/char samples vary greatly from one another with respect to their pore structures and the change of such pore structures with conversion and temperature. To account for such phenomena, a term "a" is introduced into the rate equation, which represents the relative available pore surface area and is defined as follows:

$$a = \frac{\text{Available pore surface area per unit volume at any stage of conversion}}{\text{Initial available pore surface area per unit volume}}$$

The value of "a" varies with conversion and temperature. Ignoring the effect of temperature, the change of "a" with conversion, x, can be fitted into a function, up to x approaching unity, as follows:

$$a = 1 \pm 100\, x^{\nu\beta}\, e^{-\beta x} \qquad 0 \le \nu \le 1 \qquad 3)$$

In this Equation $\nu$ and $\beta$ are the physical parameters characteristic of a given coal or char. The value of $\nu$ indicates the conversion x at which the relative available surface area reaches the maximum or minimum value. According to this equation the relative available pore surface area of the particles may increase, decrease or may show a maximum or minimum as the reaction proceeds, according to the sign (+ or -) used in Equation 3. Since a drastic change in surface area and pore size would take place at the very end approaching complete conversion, the above Equation should not be applied beyond $x > 0.9$.

Therefore, the rate of disappearance of char due to $CO_2$ reaction, for chemical reaction control, may be expressed as

$$\frac{dx}{dt} = a\, k_v\, C_A(1-x) \qquad 4)$$

Arrhenius-type temperature dependence is assumed for the rate constant, $k_v$, according to the following equation:

$$k_v = k_{v_o}\, e^{-E/RT} \qquad 5)$$

In Figure 13, $(dx/dt)/C_A(1-x)$ at $x = 0.2$ are plotted against $1/T$. The values of $ak_{v_o}$ and the activation energy E are determined from this plot. This Figure shows that the rates (at 20% conversion level) of Illinois seam Coal #6 and the three chars obtained from Illinois seam coal are significantly higher than those of Pittsburgh seam coal and the Hydrane Char #150 obtained from the Pittsburgh seam.

Among the four Illinois coal and chars, Synthane Char #122 appears to be the most reactive, although the difference in reactivity is not large.

The activation energy, E, is found to be 59.26 Kcal/more for all coals and chars.

Equation 4 is applicable only when the chemical reaction rate controls the process. At higher temperature, however, diffusion resistance within the solid particles may become appreciable and therefore, an effectiveness factor must be introduced for such cases. Effectiveness factor, $\eta$, is defined here as follows:

$$\eta = \frac{\left(D_e \cdot \left.\frac{dC_A}{dr}\right|_s\right) 4\pi r_o^2}{(4/3\pi r_o^3)\{ak_v \cdot C_{As} \cdot (1-x)\}} \qquad 6)$$

If the change in effective diffusivity, $D_e$, during reaction is assumed negligible, Equation 6 can be solved by appropriate boundary conditions as follows:

$$\eta = \frac{3}{M}\left(\frac{1}{\tanh M} - \frac{1}{M}\right) \qquad 7)$$

where $M = \phi_{vo}\,[(1-x)a]^{1/2}$

and $\phi_{vo} = r_o\sqrt{\frac{k_v C_{So}}{D_e}}$

For chemical reaction control, $\phi_{vo} = 0$. Thus, the rate of gasification with the influence of intraparticle diffusion is expressed as

$$\frac{dx}{dt} = \eta\, a k_v\, C_A (1-x) \qquad 8)$$

Using the rate expression shown by Equation 8, the conversions are calculated for all the chars and coals tested. The calculated rates are compared with those observed from experimentation in Figures 6-11. The values of $k_{v_o}$, $\nu$, $\beta$ and $\phi_{vo}$ used in these calculations are given in Table I. The calculated rates agree closely with experimental rates except that for Pittsburgh coal at higher temperatures. This may partly be due to the following reason. In contrast to the other coals and chars, the Pittsburgh coal is a highly caking coal having a swelling index of 8.5. These particles (-35+60 mesh) swell up to a considerable volume and agglomerate into a single lump during the pyrolysis stage. The whole sample (~20 mg) is thus glued together and reacts as a single particle of a considerably larger diameter. The change of porosity and hence the effective diffusivity in such a particle, as a function of conversion, may be appreciable deviating from assumptions made in the development of Equation 8.

As is indicated by Table I, the available surface area change with conversion is independent of temperature, in the studied range, for the Illinois seam coal and chars. However, for the Pittsburgh seam coal and char this change is a function of temperature. For the Pittsburgh seam coal and char the increase of available surface area appears to be less at higher temperature, for a particular conversion level.

Figure 14 shows how the relative available pore surface area "a" of the particles changes with conversion for different samples, in the temperature range 1600~1800°F.

Pore Characteristics of the Coal and Char Samples

The pore structures of Synthane Char #122, Hydrane Char #49, Hydrane Char #150 and Pittsburgh HVab coal have been observed through a scanning electron microscope, at several stages of their conversions in the range x = 0 - 1. The photographs taken at several magnifications (up to a maximum of 6,000) show that, as the reaction proceeds, the pores initially of a few microns (2-10 μ) in diameter, grow in size and bigger cavities are formed by the collapse of the solid linkage between the adjoining pore. The dimension of the solid particles have been observed to remain practically unchanged (except for the high swelling Pittsburgh seam coal) up to a conversion of about 80%. The highly porous matrix of the solid disintegrates into smaller fractions as the reaction proceeds further.

Table II shows the net pore volumes, volume-average pore diameters, densities and the porosities of the devolatilized samples as determined by the mercury penetration method on a Micromeritics' Model 905 0 - 50,000 psia Porosimeter. The average

TABLE I PHYSICAL AND RATE PARAMETERS USED IN CALCULATION FOR THE COAL AND CHAR SAMPLES

| Sample | $k_{v_o} \times 10^{-15}$, $cm^3$/mole-min. | Temperature | $\nu$ | $\beta$ | $\phi_{vo}$ |
|---|---|---|---|---|---|
| IGT Char #HT155 (from Illinois Coal #6) | 0.113 | 1657-1922°F | 0.75 | 5.5 | 0 |
| Hydrane Char #49 (from Illinois Coal #6) | 0.123 | 1578-1938°F | 0.75 | 10.0 | 0 |
| Synthane Char #122 (from Illinois Coal #6) | 0.136 | 1565-1972°F | 0.75 | 6.0 | 0 |
| Illinois Coal #6 | 0.120 | 1569-1938°F | 0.75 | 6.0 | 0 |
| Hydrane Char #150 (from Pittsburgh HVab Coal) | 0.0670 | 1623°F | 1.0 | 4.4 | 0 |
| | | 1688°F | 1.0 | 4.4 | 0 |
| | | 1794°F | 1.0 | 4.7 | 0 |
| | | 1875°F | 1.0 | 5.0 | 2.5 |
| | | 1965°F | 1.0 | 5.5 | 4.2 |
| Pittsburgh HVab Coal | 0.0536 | 1682°F | 0.6 | 5.0 | 0 |
| | | 1742°F | 0.6 | 5.0 | 0 |
| | | 1778°F | 0.6 | 5.5 | 0 |
| | | 1888°F | 0.6 | 10.0 | 3.0 |
| | | 1952°F | 0.6 | 10.0 | 4.2 |

TABLE II. PORE CHARACTERISTICS OF COALS AND CHARS

| | Properties Measured By Mercury Porosimetry | | | | Properties Measured by BET Method | |
|---|---|---|---|---|---|---|
| Devolatilized Samples | Net Pore Volume (cc/g) | Volume Average Pore Diameter (μ) | Density (g/cc.) | Porosity | Surface Area ($m^2$/g) | Surface Average Micropore Diameter, $\bar{d}_{ps}$, (Å) |
| IGT Char #155 | 0.9200 | 9.2 | 1.54 | 0.767 | 423.87 | 11.61 |
| Hydrane Char #49 | 1.0344 | 2.3 | 1.43 | 0.765 | 171.69 | 22.34 |
| Synthane Char #122 | 2.1978 | 8.8 | 1.31 | 0.864 | 280.94 | 18.34 |
| Illinois Coal #6 | 2.6522 | 9.2 | 1.71 | 0.809 | 26.05 | -- |
| Hydrane Char #150 | 0.6463 | 2.4 | 1.53 | 0.655 | 18.04 | 106.00 |
| Pittsburgh HVab Coal | -- | -- | 2.11 | -- | 29.97 | -- |

pore diameters determined by this method agrees well with those observed by the scanning electron microscope.

Table II also shows the pore surface areas and the surface-average micro-pore diameters of devolatilized coal and char samples as determined by the BET nitrogen adsorption method. The surface-average micropore diameters ($\bar{d}_{ps}$) have been calculated from the measured micropore size distribution, according to the equation.

$$\bar{d}_{ps} = \frac{\Sigma d_{ps} \Delta A_p}{A_p}$$

where $\Delta A_p$ is the surface area occupied by the micropores of diameter $d_{ps}$ and $A_p$ is the total surface area of the solid.

These measurements show that although the bulk of void volumes of these coals and chars are occupied by comparatively large pores, several microns in diameter, almost all the surface areas determined by BET method are occupied by micropores, below 100-200 Å in diameter.

Reactivity of coal/char can be characterized by its intrinsic rate constant for the second stage reaction, $k_{v_o}$. The values of $k_{v_o}$ (listed in Table I) apparently show no direct relationship with the measured pore surface areas. The pore surface areas and pore size distribution curves, however, show that higher surface areas are caused by the larger number of smaller pores. Calculations show that for the coal and char samples studied, only the fraction of surface area which is occupied by pores having diameter more than about 27.5 Å is available for reaction with $CO_2$. The table below shows the surface areas covered by pores bigger than 27.5 Å, the total surface areas and the values of $k_{v_o}$ for four chars.

| Sample | Surface Area ($m^2/g$) Covered by Pores Bigger Than 27.5 Å in dia. | Total Surface area ($m^2/g$) | $k_{v_o} \times 10^{-15}$ $cm^3$/mole.min. |
|---|---|---|---|
| Hydrane Char #150 | 18.75 | 18.75 | 0.0670 |
| IGT Char #HT155 | 25.43 | 423.87 | 0.113 |
| Hydrane Char #49 | 34.42 | 171.69 | 0.123 |
| Synthane Char #122 | 38.06 | 280.87 | 0.136 |

The reactivities are found to be almost proportional to the surface areas occupied by pores above 27.5 Å in diameter.

## Conclusions

Gasification of coal/char in $CO_2$ atmosphere can be divided into two stages, the first stage due to pyrolysis and the second stage due to char-$CO_2$ reaction. Reactivity in the first stage is mainly a function of the volatile matter content of the char/coal and the rate of heating. The rate of pyrolysis can be approximated by an Arrhenius type expression (Equation 1) with an activation energy of about 2.5 Kcal/mole.

Reactivity of a char in the second stage char-$CO_2$ reaction, is found to depend more on its coal seam than on the gasification scheme used for its production. Each char/coal sample is found to have its own characteristic rate curve. The different rate characteristics of coals and chars are apparently due to the difference in their pore characteristics, which again change with conversion and temperature.

A parameter, that represents the change in available pore surface areas of the particles during reaction, is introduced into the rate equation to account for the rate-conversion curves. The calculated rates are found to agree quite well with the observed rates.

The rate of char-$CO_2$ reaction is found to have no direct relation with the total surface area of the pores. The study indicates that only a fraction of the total surface area which is occupied by pores above a certain diameter is available for reactions.

## Notation

| | |
|---|---|
| $A$ | Pyrolysis rate constant, 1/min |
| $A_p$ | Pore surface area, $m^2/g$ |
| $B$ | Activation energy of pyrolysis, cal/cmole |
| $C_A$ | Concentration of gas; $C_{As}$ that at the outside surface of solid, $mole/cm^3$ |
| $C_{So}$ | Initial solid concentration, $mole/cm^3$ |
| $D_e$ | Effective diffusivity, $cm^2/min$ |
| $d_{ps}$ | Micropore diameter; $\bar{d}_{ps}$ surface average micropore diameter, Å |
| $f$ | Total fraction conversion due to pyrolysis |
| $k_v, k_{v_o}$ | Second stage reaction rate constants, $cm^3/mole.min$ |
| $R$ | Gas constant, cal/mole.°R |
| $r$ | Radius of solid particle; $r_o$ initial radius, cm |
| $T$ | Temperature, °R |
| $t$ | Time, min. |
| $x$ | Fraction conversion of solid |
| $\beta, \nu$ | Physical parameters of the solid defined in Equation 3 |

## Acknowledgment

This work was supported by grants from the Energy Research and Development Administration, Morgantown Energy Research Center. The authors wish to thank Nancy Tsai Wu for measuring some of the pore characteristics presented in this report and also A. G. Panson and G. E. Chidister for char analysis.

## Literature Cited

1. Austin, L. G. and Walker, P. L., Jr., A.I.Ch.E. Journal, 9, 303 (1963).
2. Essenhigh, R. H. and Howard, J. B., Ind. Eng. Chem., 58 (1), 15 (1966).
3. Gray, D., Cogoli, J. G. and Essenhigh, R. H., Amer. Chem. Soc., Division of Fuel Chem. preprint, 18 (1), 135, Dallas (1973).
4. Gulbransen, E. A. and Andrew, K. F., Ind. Eng. Chem., 44, 1039 (1952).
5. Long, F. J. and Sykes, K. W., Proc. Roy. Soc. (London), 193A, 377 (1948).
6. Petersen, E. E., Walker, P. L., Jr., and Wright, C. C., Ind. Eng. Chem., 47, 1629 (1955).
7. Rossberg, M. and Wicke, E., Chem. Eng. Tech., 28, 181 (1956).
8. Turkdogan, E. T., Olsson, R. G. and Vinters, J. V., Carbon, 8, 545 (1970).
9. Turkdogan, E. T. and Vinters, J. V., Carbon, 7, 101 (1969).
10. Walker, P. L. Jr., Foresti, R. J., Jr., and Wright, C. C., Ind. Eng. Chem., 45, 1703 (1953).
11. Wen, C. Y., Bailie, R. C., Lin, C. Y. and O'Brien, W. S., Advances in Chemistry Series, 9, 131 (1974).
12. Wicke, E., Fifth Symp. on Combustion, p. 245, Reinhold, New York (1955).
13. Yoshida, K. and Kunii, D., J. Chem. Eng. (Japan), 2, 170 (1969).

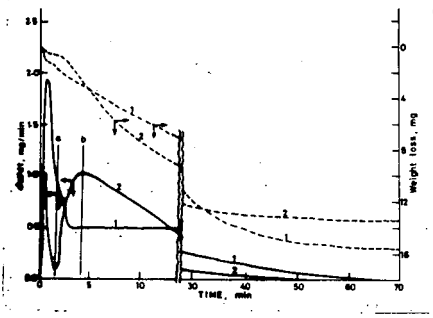

Fig. 1 Reproduction of Two Typical Chart Recordings of the Weight Loss and Rate of Weight Loss Curves
1--Hydrane Char #150, 2--Hydrane Char #49, Temperature: 1875°F.

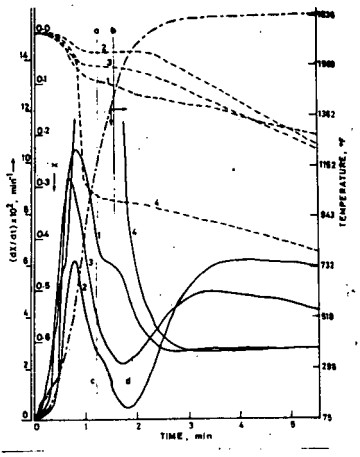

Fig. 2 Typical Rate and Conversion Curves for the Pyrolysis of Coal and Chars,
----Conversion Versus Time Curve
——— Rate Versus Time Curve
-·-·-Temperature Versus Time Curve
1--Hydrane Char #150, 2--Hydrane Char #49, 3--Synthane Char #122, 4--Illinois Coal #6.

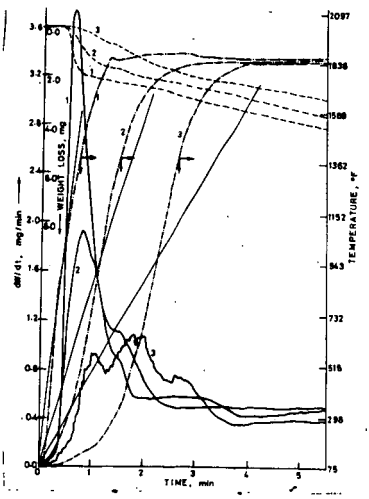

Fig. 3 Effect of Sample Heating Rate on the Pyrolysis of Hydrane Char #150, Sample size: 18.30 mg.

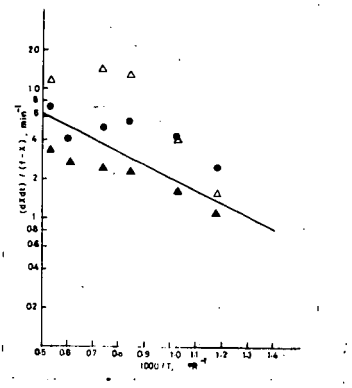

Fig. 4 Arrhenius Plot for the Pyrolysis Stage
▲ Hydrane Char #150, f=0.110
△ Hydrane Char #49, f=0.0369
● Synthane Char #122, f=0.0675

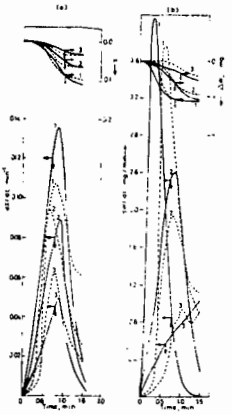

Fig. 5 Calculated (——) and Experimental (- - - -) Rate and Conversion Curves,
(a) For Different Char Samples: 1-Hydrane Char #150, 2-Synthane Char #122, 3-Hydrane Char #49;
(b) For Different Heating Rates for Hydrane Char #150: The numbers 1, 2 and 3 correspond to the heating rate curves shown in Fig. 3.

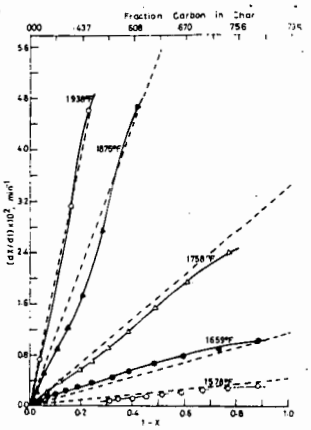


Fig. 6 Gasification of Hydrane Char #49, Rate Versus Conversion Based on Base-Carbon
----Calculated Rates.

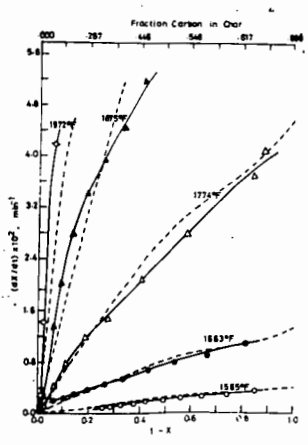


Fig. 7 Gasification of Synthane Char #122, Rate Versus Conversion Based on Base-Carbon
----Calculated Rates.

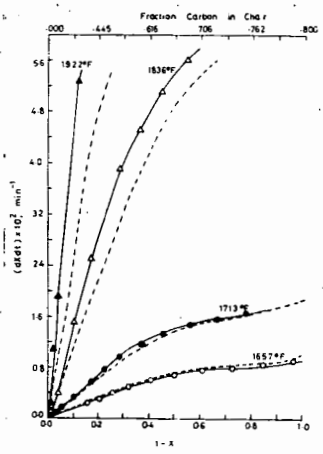


Fig. 8 Gasification of IGT Char #HT155, Rate Versus Conversion Based on Base-Carbon
----Calculated Rates.

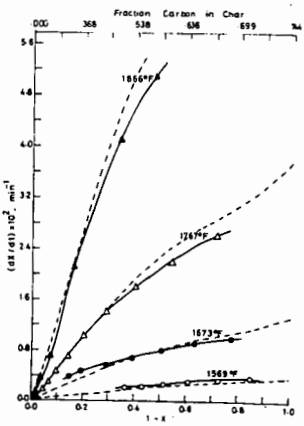


Fig. 9 Gasification of Illinois Coal #6, Rate Versus Conversion Based on Base-Carbon
----Calculated Rates.

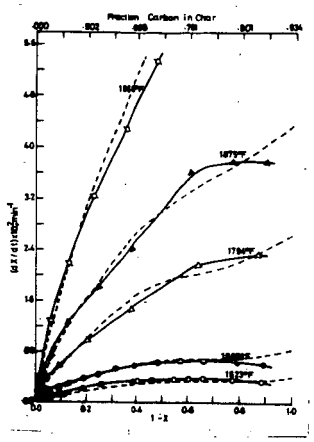

Fig. 10 Gasification of Hydrane Char #150, Rate Versus Conversion Based on Base-Carbon
----Calculated Rates.

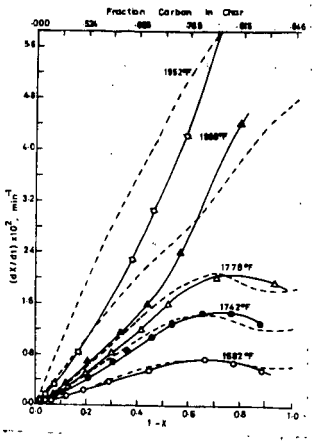

Fig. 11 Gasification of Pittsburgh HVab Coal, Rate Versus Conversion Based on Base-Carbon
----Calculated Rates.

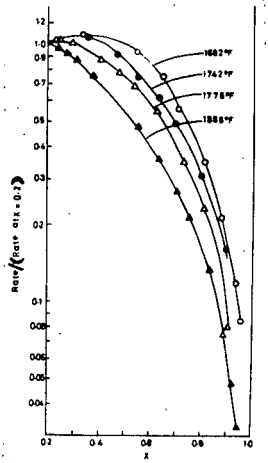

Fig. 12 Normalized Rates Versus Conversions for Pittsburgh HVab Coal.

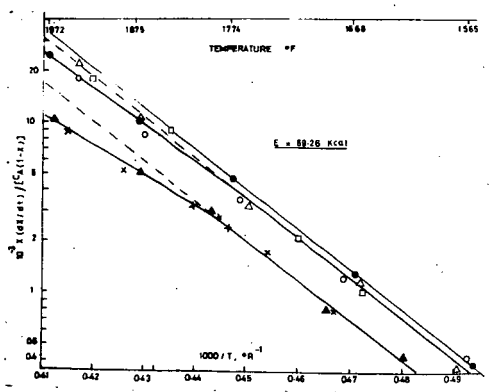

Fig. 13 Arrhenius Plots for Gasification of Coals and Chars

- o Illinois Coal #6
- ● Synthane Char #122
- × Pittsburgh HVab Coal
- Δ Hydrane Char #49
- □ IGT Char #HT155
- ▲ Hydrane Char #150

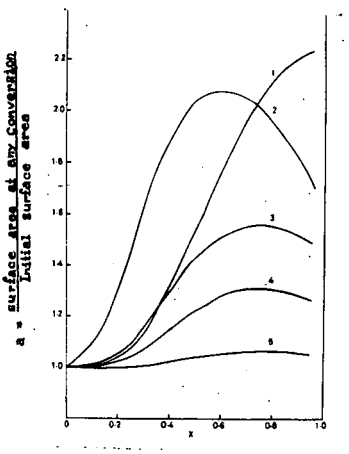

Fig. 14 Relative Available Surface Area Versus Conversion

1. Hydrane Char #150
2. Pittsburgh HVab Coal
3. IGT Char #HT155
4. Illinois Coal #6 & Synthane Char #122
5. Hydrane Char #49.

# Gasification of HYDRANE Char in Reactions with Carbon Dioxide and Steam



Walter Fuchs and Paul M. Yavorsky

U.S. Energy Research and Development Administration
Pittsburgh Energy Research Center
4800 Forbes Avenue
Pittsburgh, Pennsylvania 15213

## INTRODUCTION

During the current efforts, two basic principles for coal gasification have been advanced. One is the production of synthesis gas by reacting the coal with steam under the addition of heat. If this gas should be upgraded to replace natural gas, a methanation step is necessary after the proper ratio of carbon dioxide and hydrogen has been established by a water gas shift reaction. The methanation is highly exothermic. But since it has to be executed at a moderate temperature (400° C), its heat cannot be used (1). The other possibility is to hydrogenate the coal directly under high pressure to obtain methane. This method is more efficient because it eliminates the methanation step. In the real case, direct hydrogasification does not eliminate the methanation completely, because the presence of some hydrogen in the product gas (15 to 20 pct) cannot be avoided; however, the methanation requirements are considerably less.

The HYDRANE process (2) uses the hydrogenation approach and is designed to gasify caking coal without pretreatment by partial oxidation. The caking property of the coal will be removed by feeding the raw coal into a dilute-phase reactor, in which the coal falls freely in contact with a hot gas mixture of hydrogen and methane. If the coal is heated rapidly through the plastic stage (400° C to 700° C) excessive agglomeration of the coal particles can be avoided. After the coal has been devolatilized and partly hydrogasified in the dilute phase reactor, it enters a second stage, which is a fluid bed reactor. In this stage, the solids will be hydrogasified in a hydrogen atmosphere at approximately 900° C and under a pressure of 70 atm. The gas fed to the fluid bed reactor is pure hydrogen; the gas leaving this stage contains approximately 46 pct methane. This mixture is fed to the free fall stage, where the hydrogen-to-methane conversion will continue in presence of the dilute solids phase.

Though the total carbon content of the coal could be gasified in the fluidized bed stage, it is more efficient to hydrogenate the coal only partially, and to use the remaining char for the production of the necessary hydrogen. In this case, the char leaving the fluid bed will be fed into a gasifier, in which, by adding steam and oxygen, the char will be converted into hydrogen rich synthesis gas.

Tests have been made on HYDRANE char to obtain kinetic information concerning the water gas reaction (reaction with steam). By HYDRANE char we mean the residual char rejected from the fluid bed stage of the process development unit at the ERDA Energy Research Center in Pittsburgh. This char contains approximately 50 pct of the initial carbon content of the raw coal.

### Principal Reactions and Kinetics

The overall chemical reaction to be studied is

$$H_2O + \text{Char} \longrightarrow H_2 + CO + CO_2 + \text{Ash} \qquad 1)$$

This is a multistep reaction which , according to (3) and (4) among others, can be

separated into the following principal processes ($C_f$ denotes a free reaction site and $C_o$ an oxidized reaction site at the carbon surface):

$$H_2O + C_f \underset{k_2'}{\overset{k_2}{\rightleftharpoons}} H_2 + C_o \qquad 2)$$

$$C_o \xrightarrow{k_3} CO + \gamma C_f \qquad 3)$$

In addition, there is a competing oxygen exchange reaction

$$CO_2 + C_f \underset{k_1'}{\overset{k_1}{\rightleftharpoons}} CO + C_o \qquad 4)$$

The parameter $\gamma$ in reaction (3) is assumed to be unity. In this case a steady gasification rate will be maintained; a new active site is generated with each carbon atom gasified. The experimental results tend to confirm this assumption. The number of carbon sites available for oxidation depends on the detailed structure of the surface, in addition to the surface area (5, 6, 7, 8, 9). Since the char we are dealing with is very porous, we can assume that the geometrical surface area of the particles can be neglected compared to the internal surface area, i.e., the available surface area is proportional to the total amount of solids in the reactor and independent of the size and shape of the particles.

Denote the fraction of the carbon atoms which can be oxidized (i.e., active sites) by

$$C_t = \frac{\text{Number of active sites}}{\text{Total number of carbon atoms}}$$

which is assumed to be a constant. Then the fraction of the active free sites, $C_f$, and of the oxidized sites, $C_o$, follow the relation

$$C_t = C_f + C_o \qquad 5)$$

Reaction (3) represents the actual gasification step. The gasification rate dn/dt, in mol/s is

$$-\frac{dn}{dt} = N_c = k_3 C_o n \qquad 6)$$

n is the number of carbon atoms present.

The rate constant $k_3$ has the dimension:

$$\frac{\text{moles gasified/second}}{\text{moles of carbon present}}$$

From Equation 6 it is easy to determine the quantity $k_3C_o$:

$$k_3C_o = (1/t)\ \ln\ (n_o/n(t)\ ), \qquad 7)$$

where t is the residence time of the char, and n(t) is the remaining amount of carbon in the reactor after time t. The fractional concentration of oxidized sites, $C_o$, is not known. It depends on the rates of the oxygen exchange reactions.

For experimental purposes we can simplify the system of reactions described above by reacting char with carbon dioxide without the presence of steam. The gasification reactivity, $k_3C_o$, can be determined by measuring the amount of solids converted to gas. In addition, the equilibrium value of $C_o$ approaches very closely that of $C_t$ if the amount of carbon monoxide generated is small compared to the carbon dioxide present; in this case almost all active sites are oxidized. This can be verified theoretically by analyzing reactions (3) and (4).

$$\frac{dC_o}{dt} = k_1 C_{CO_2} C_f - k_1' C_{CO} C_o - k_3 C_o \qquad 8)$$

$C_{CO_2}$ and $C_{CO}$ are the concentrations of $CO_2$ and CO respectively. At the high pressures of interest, the oxygen exchange reactions are very fast compared to the gasification reaction (10). Therefore, the last term of Equation 7 can be dropped. In the steady state $dC_o/dt = 0$. Eliminating the number of free sites and expressing it in terms of the total number of active sites $C_f = C_t - C_o$, we obtain

$$C_o = \frac{C_t}{1 + \frac{x}{K_1}} \qquad 9)$$

where $K_1 = k_1/k_1'$, and $x = C_{CO}/C_{CO_2}$.

Experimental Outline

The experimental system used in this study is basically the same which has been used by S. Friedman et al. (11) (see figure 1). In our application a constant flow of feed gas was maintained, which kept the char in a fluidized state. The pressure (up to 70 atm) was maintained by the supply cylinders, and in case of water, by pressurizing the water reservoir with helium. The gas flow was controlled with needle valves and flowmeters before the gas entered the reactor. A preheater was necessary to maintain a uniform temperature profile along the reactor. The reactor was heated by direct resistance heating, in which the reactor vessel served as the heating element. The heating current of up to 700A was supplied with a stepdown transformer, whose primary voltage could be controlled. The gas leaving the reactor flowed through a steam trap before it was depressurized. A back pressure regulator kept the pressure in the system constant. The gas was metered and flared. Provisions were made to take periodical gas samples for chemical analysis.

The reactor (figure 2) consisted of a 1.78 m long stainless steel tubing with an inner diameter of 0.8 cm (5/16") and a wall thickness of 0.4 cm. Two disks of porous stainless steel confined the char sample within the reaction zone, which was 1 m long. In the non-fluidized state a charge of 5 g occupies half of the reaction zone. The porous disks were kept in place by pinching the tube from the outside. A new tube had to be provided for each experiment. The temperature was monitored with four chromel-alumel thermocouples peened into the tube wall. At the bottom of the stainless steel tube, a preheater in form of a ceramic rod containing a heating wire raised the feed gas temperature.

For the steam experiments, this preheater was not sufficient to vaporize the water completely. Therefore, in addition to the preheater, heating tapes were wrapped around the water feed line to keep the temperature above the boiling point of the water at the pressure of the experiment. Extra thermocouples at the inlet and exit of the reactor allowed the temperatures to be checked to assure that no condensation has occurred.

## Experimental Procedures

All experiments have been carried out isothermally at constant pressure. For the experiments with carbon dioxide and char, the reactor has been heated up rapidly after the proper gas flow has been established. The heat-up time was always less than a minute, with the run lasting between 20 minutes and 4 hours. At the conclusion of the experiment, the heat was turned off, and the reactor quenched with water. The procedure for the steam-char experiments was different. The system was first pressurized with helium, then heat was applied. After the proper temperature has been reached, the water flow was started. At the conclusion of the run, the water was turned off, and replaced with a flow of dry nitrogen in order to remove all of the steam. The reactor was slowly cooled and eventually gradually depressurized. This was necessary to avoid the condensation of water in the reactor. After the reactor has been cooled to room temperature, the stainless steel rod was cut in the middle to retrieve the residual solids, which were weighed and analyzed for their carbon contents.

Care has been taken to prevent a build up of the product gas concentration near the particle surface. This would unduly favor the back reaction of the oxygen exchange reactions. Tests showed that the superficial gas velocity to avoid this effect had to be larger than 40 cm/s for the carbon dioxide experiments, while for the steam experiments, a velocity of 15 cm/s was sufficient. This probably can be explained with the high diffusivity of hydrogen, which is the principal product of the steam - char reaction. The binary gas diffusivity of the $H_2O$ - $H_2$ system is approximately 6 times that of the $CO_2$ - CO system (12).

## Results

An analysis of the char used for most of the experiments is given in Table 1. This represents the averaged data and their standard deviation errors from eight individual analyses. The batch of char HY-13, from which these samples were taken, was always carefully mixed before a sample was withdrawn. As can be seen, the only major components are carbon and ash. In a few cases char from a different source has been used; this is discussed below.

Carbon dioxide - char reactions:

Since the carbon dioxide - char reaction experiments are less complicated and easier to analyze than the steam - char reactions, they have been carried out first. All pertinent data are listed in Table 2. The temperature ranged from 750° C to 900° C. The pressure was usually 35 atm, and twice it was 18 atm. The feed gas was a mixture of carbon dioxide and helium. In most cases the ratio was 1 part helium to 10 parts carbon dioxide. The partial pressure of the carbon dioxide is given in column 3. The feed was adjusted such that the linear gas velocity for most tests was kept between 0.4 and 0.6 m/s (column 4), requiring a gas flow of up to 0.010 mol/s; this is a very high gas feed compared to the actual conversions, such that more than 99 pct of the effluent gas consists of carbon dioxide and helium. The carbon monoxide production was almost not measurable (<0.5%). However, the solids and carbon conversion was determined. Column 6 gives the fraction of the retrieved solids by weight (i.e., X = weight of residual solids/weight of charge). The fraction of the retrieved carbon has been determined by chemical analysis of the charge and of the residue and is listed in column 7 (i.e., Y = mass of carbon in the residuum/mass of carbon in the charge). In figure 3 the quantity Y is plotted versus X. The graph also contains points obtained from steam experiments. All points are scattered around a straight line intersecting the abscissa at 0.32, which corresponds to the ash content of the original char (see Table 1). One can conclude that, while the ash remains completely inert, the

non-ash components, which consist to 97 pct of carbon, are gasified at the same rate as the fixed carbon. This observation allows to calculate the carbon conversion from the total mass loss, which is determined by weighing and therefore many times more accurate than a chemical analysis of the residual solids. The fractional carbon conversion (equivalent to the quantity Y in Table 2) can be expressed as

$$Y = \frac{X - C_A}{1 - C_A}, \qquad 10)$$

where $C_A$ is the fractional ash content of the charge. The reaction constant in column 8 of Table 2 is calculated according to Equations 7 and 10

$$B = \frac{1}{t_{res}} \ln \frac{1 - C_A}{X - C_A} \qquad 11)$$

where $t_{res}$ is the residence time given in column 5 of Table 2. The results show that the carbon conversion is a first order process with regard to the carbon present. Figure 4 shows no systematic relationship between the rate constant as defined in Equation 7 and the mass loss. The Arrhenius plot in figure 5 shows that the process is also of 0th order with regard to the amount of reactant gas present. Two data points have been obtained from experiments conducted at 18 atm, which is half the usual pressure (see Table 2). The Arrhenius plot yields an activation energy of 54.5 kcal/mol and a frequency factor of $1.14 \times 10^7 s^{-1}$. The plotted quantities represent the rate constant $k_3C_o$ as it is defined in Equation 6. However, as already mentioned, with the low carbon monoxide concentration ($\leq 0.5\%$), the quantity $C_o$ is approaching $C_t$ according to Equation 9. $K_1$ is the equilibrium constant for the oxygen exchange reactions 4, and assumes the values from 0.03 to 0.2 for a temperature range between 750° C and 900° C (4, 13). Using these figures and Equation 10, it has been estimated that the quantity $k_3C_t$ should be in the average 10 pct larger than B, with an activation energy reduced by approximately 2 kcal/mol. But this is within the fluctuation of the experimental data. Table 2 and figure 5 contain 3 points taken on SYNTHANE char at three different temperatures. This material, originally Illinois #6 coal, went through a steam gasification process with 60 pct of its original carbon content gasified. The reactivity of this char cannot be distinguished from the HYDRANE char.

Steam - Char Reaction:

The reaction of the char with steam is a more involved process than the carbon dioxide reaction because now reactions 2 and 4 compete with each other. Also with the existing experimental system, the temperature along the reactor could not be kept as uniform as was the case with the carbon dioxide experiments, causing more scattering of the data. Results of the steam series are listed in Table 3. The arrangement of the columns is the same as in Table 2, except no partial pressure is given because the feed gas consisted exclusively of steam. Since the carbon conversion data from these runs have the same relationship to the total mass loss as was the case with the carbon dioxide experiments, Equation 11 could also be used to calculate the rate constant. An Arrhenius plot of the rate constants is given in figure 6 superimposed on the averaged rate constant for the carbon dioxide - char reaction taken from figure 5. Taking the experimental scattering into account, we see that for both types of reactions the reactivity is similar. Since the steam concentration was always more than 98 pct, the difference between $C_o$ and $C_t$ can be assumed to be

very small, using the same argument as for the carbon dioxide tests. The similarity between the carbon dioxide and the steam data indicate that the gasification reaction, Equation 3, is the rate controlling step, with the same type of reaction sites responsible for both reactions. Also it has been shown that the concentration of the reactant gas has no effect on the reactivity.

Discussion

The reactivities obtained in our experiments refer to the composite quantity $k_3C_t$, where $C_t$ is assumed to be independent of the temperature (within the limits of our experimental conditions). $C_t$ represents the fraction of those carbon atoms in the solid which are available for oxidation. Obviously, the surface area of the material is of prime importance. However, as already mentioned, only a small portion of the surface sites is capable of accepting oxygen. In graphites, this portion is 4 pct (9). Moreover, it was shown that various discrete types of reactive sites do exist on graphon surfaces (5, 6, 7, 8), which in general are activated at different temperature regimes. The accepted notion is that oxidation takes place around crystallographic defects (14). Following these arguments, it should be expected that the gasification reactivities of chars and cokes, with their high surface area and their high structural disorder, should be many times larger than those of graphitized materials. In figure 7 the reactivity constants for gasification, $k_3C_t$, of various graphites and carbons, obtained by Ergun (4) and Mentser and Ergun (10) are plotted together with our results from the carbon dioxide - char reaction experiments.

The activation energy remains the same for all materials. In addition, the activation energy from recent experiments on reactions of petroleum coke and electrode material with carbon dioxide (17) is between 51.3 and 56.6 kcal/mol, in good agreement with our data. This allows the conclusion that the chemical desorption step, which according to Equation 3 is controlled by the quantity $k_3$, is unaffected by the crystallographic state of the reactive surface. However, the fraction of available active sites, $C_t$, varies by more than 2 orders of magnitude, as can be seen from the pre-exponential factors of the Arrhenius plots in figure 7. The lowest $C_t$ is associated with Ceylon graphite, which comes closest to an ideal graphite structure. The reactivity of the materials follows inversely the order of their degree of crystallographic perfection.

The first order characteristic of the carbon conversion process is in agreement with the assumption that, for a particular material, the fraction of the active sites, $C_t$, remains constant during the reaction, or, in other words, that the parameter $\gamma$ in the gasification reaction, Equation 3, in unity. This has been confirmed by surface area measurements, which showed that the B. E. T. surface of a sample before and after the experiment increased only slightly.

A catalytic effect due to the multitude of foreign matter in cokes and chars is possible. However, this should also change the activation energy of the gasification step. Experimental evidence suggests that the activation energy should decrease with catalytic action (15).

Experiments on various types of chars and raw coals under atmospheric pressure have been conducted by C. Y. Wen's group in Morgantown, West Virginia, (16). Figure 8 shows the results as continuous curves. An interesting feature is that the pre-exponential factor depends only on the source of the coal, and not on the treatment for charring. The upper curve describes the reaction behaviors of untreated Illinois #6 coal and three different chars made from Illinois #6 (HYDRANE, SYNTHANE, IGT) the lower curve refers to untreated Pittsburgh Seam coal and to HYDRANE char made from this coal. The bottom curve in figure 8 refers to measurements by Ergun (13) on metallurgic coke. The activation energies of all three curves agree well with the results of this study up to a temperature of approximately 1000° C. Above that

temperature, the activation energies decrease markedly. Various explanations have been suggested for this behavior.

## Conclusion

For temperatures up to 1000° C and within a wide pressure range (from atmospheric to 70 atm), the rate limiting step for the reaction of carbon with steam as well as with carbon dioxide is the desorption reaction, in which an oxidized carbon is released from the carbon surface, forming a gaseous carbon monoxide molecule. This process is governed by an activation energy around 56 kcal/mol. It is suggested that for both reactions, steam - carbon and carbon dioxide - carbon, the same type of atomic carbon sites on the surface are involved. In addition, it has been shown that chars made from Illinois #6 coal exhibit high reactivities compared to other carbonaceous materials. This probably is due to a large surface area and a high crystallographic disorder of the char.

## ACKNOWLEDGEMENT

Fruitful discussions with Dr. S. Ergun are greatly appreciated.

REFERENCES


1. Forney, A. J. and J. P. McGee, 4th Synthetic Pipeline Gas Symposium, Chicago, Illinois, p. 51 (1972).

2. Wen, C. Y., S. Mori, J. A. Gray, and P. M. Yavorsky, 67th Annual AIChE Meeting, Washington, D. C. (December 1974).

3. Reif, A. E., J. Phys. Chem. 56, 785 (1952).

4. Ergun, S., J. Phys. Chem. 60, 480 (1956).

5. Phillips, R., F. J. Vastola, and P. L. Walker, Jr., 3rd Conference on Industrial Carbon and Graphite, London, 1970, p. 257.

6. Bansal, R. C., F. J. Vastola, and P. L. Walker, Jr., Carbon 8, 443 (1970).

7. Phillips, R., F. J. Vastola, and P. L. Walker, Jr., Carbon 8, 197 (1970).

8. Wiesmann, U., Carbon 8, 105 (1970).

9. Walker, P. L., Jr., L. G. Austin, and J. J. Tietjen, Chemistry and Physics of Carbon, Vol. 1 (P. L. Walker, Jr., ed.) Dekker, New York, 1965, p. 328.

10. Mentser, M. and S. Ergun, Bureau of Mines Bulletin 664, Washington, D. C., 1973

11. Friedman, S., P. S. Lewis, R. D. Graves, and R. W. Hiteshue, Bureau of Mines Report of Investigation 7209, Washington, D. C. 1968.

12. Janka, J. C., and R. Malhotra, Estimation of Coal and Gas Properties for Gasification Design Calculations, Institute of Gas Technology, Chicago, Illinois, 1971.

13. Ergun, S., Bureau of Mines Bulletin 598, Washington, D. C., 1962.

14. Thomas, J. M., Chemistry and Physics of Carbon, Vol. 1 (P. L. Walker, Jr. ed.) Dekker, New York, 1965, p. 122.

15. Walker, P. L., Jr., M. Shelef, and R. A. Anderson, Chemistry and Physics of Physics of Carbon, Vol. 4 (P. L. Walker, Jr., ed.) Dekker, New York, 1968.

16. Wen, C. Y., private communication.

17. Tyler, R. J. and I. W. Smith, Fuel 54, 99 (1975).

TABLE 1.- Analysis of HYDRANE char
(HY-13, made from Illinois #6)

| | As received | Moisture and ash free |
|---|---|---|
| **Proximate Analysis** | | |
| Moisture | 3.5 ± 0.4 | |
| Volatile Matter | 3.5 ± 1.5 | 4.2 ± 0.8 |
| Fixed Carbon | 61.1 ± 4.8 | 95.8 ± 0.8 |
| Ash | 31.9 ± 3.8 | |
| **Ultimate Analysis** | | |
| Hydrogen | 1.1 ± 0.1 | 1.2 ± 0.3 |
| Carbon | 61.8 ± 3.1 | 96.6 ± 0.6 |
| Nitrogen | 0.4 ± 0.05 | 0.7 ± 0.05 |
| Oxygen | 3.6 ± 0.2 | 0.6 ± 0.2 |
| Sulfur | 0.6 ± 0.05 | 0.9 ± 0.05 |
| Ash | 32.5 ± 3.4 | |

TABLE 2.- Results of the $CO_2$-char reaction experiments

| Temperature, °C | Pressure Total atm | Pressure Partial atm | Gas velocity, m/sec | Residence time, min | Retrieved solids X | Retrieved carbon Y | Rate constant $10^{-4}$ $sec^{-1}$ | Material |
|---|---|---|---|---|---|---|---|---|
| 750 | 35 | 31.8 | 0.49 | 120 | 0.827 | 0.764 | 0.518 | |
| 750 | 35 | 31.8 | .49 | 120 | .898 | | .228 | |
| 750 | 35 | 31.8 | .49 | 120 | .849 | .825 | .352 | |
| 750 | 35 | 31.8 | .49 | 240 | .728 | .659 | .239 | |
| 750 | 35 | 31.8 | .49 | 360 | .671 | .461 | .309 | |
| 750 | 18 | 16.4 | .49 | 120 | .872 | .818 | .292 | |
| 790 | 35 | 17.5 | .60 | 120 | .748 | .668 | .649 | |
| 795 | 35 | 26.25 | .60 | 120 | .759 | .538 | .613 | HYDRANE |
| 800 | 35 | 31.8 | .50 | 120 | .626 | .442 | 1.122 | char |
| 800 | 35 | 31.8 | .50 | 60 | .818 | .656 | 0.873 | |
| 800 | 35 | 31.8 | .50 | 240 | .489 | .225 | .982 | |
| 800 | 35 | 31.8 | .50 | 180 | .555 | .406 | .997 | |
| 800 | 18 | 16.4 | .49 | 120 | .722 | .589 | .843 | |
| 850 | 35 | 31.8 | .54 | 60 | .534 | .341 | 3.257 | |
| 850 | 35 | 31.8 | .54 | 90 | .442 | .174 | 3.245 | |
| 850 | 35 | 31.8 | .54 | 30 | .677 | .557 | 3.617 | |
| 900 | 35 | 26.25 | .66 | 20 | .553 | | 9.04 | |
| 750 | 35 | 31.8 | 0.49 | 240 | 0.779 | 0.723 | 0.311 | SYNTHANE |
| 800 | 35 | 31.8 | .50 | 60 | .786 | .766 | 1.196 | char |
| 850 | 35 | 31.8 | .54 | 45 | .606 | .394 | 3.829 | |

TABLE 3.- Results of the steam-char reaction experiments

| Temperature, °C | Total pressure, atm | Gas velocity, m/sec | Residence time, min | Retrieved solids X | Retrieved carbon Y | Rate constant, $10^{-4}$ $sec^{-1}$ |
|---|---|---|---|---|---|---|
| 700 | 35 | 0.13 | 120 | 0.8908 | 0.7732 | 0.246 |
| 800 | 35 | 0.15 | 120 | .612 | .412 | 1.193 |
| 800 | 35 | 0.10 | 120 | .640 | .462 | 1.062 |
| 800 | 69 | 0.077 | 120 | .565 | .366 | 1.443 |
| 800 | 18 | 0.28 | 120 | .526 | .306 | 1.691 |
| 830 | 35 | 0.15 | 120 | .454 | .311 | 2.313 |
| 900 | 35 | 0.16 | 60 | .366 | .0583 | 7.892 |
| 900 | 35 | 0.16 | 180 | .356 | .0640 | 2.906 |

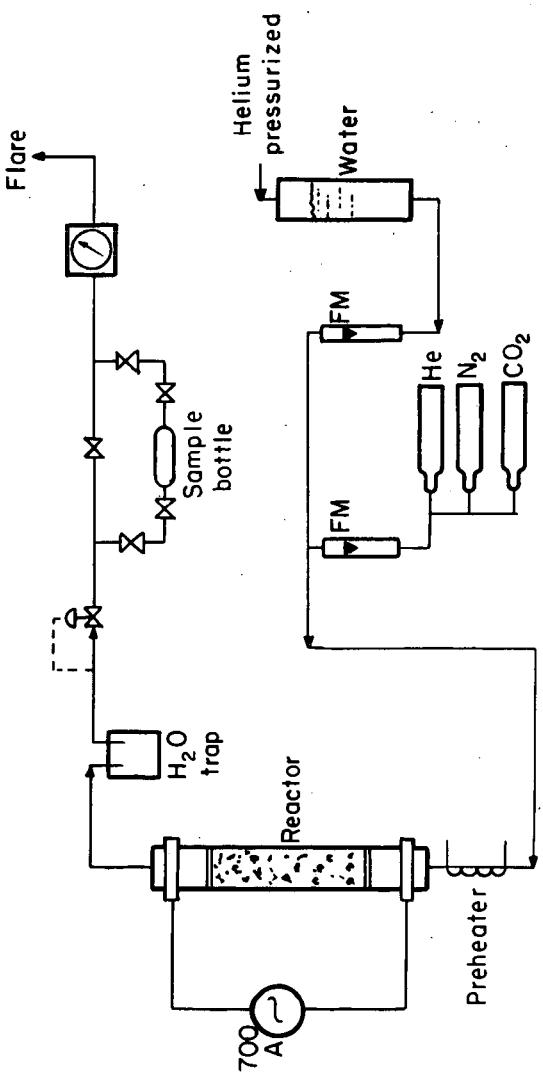


Figure 1— Reaction kinetics experiment simplified flow diagram.

L-14324

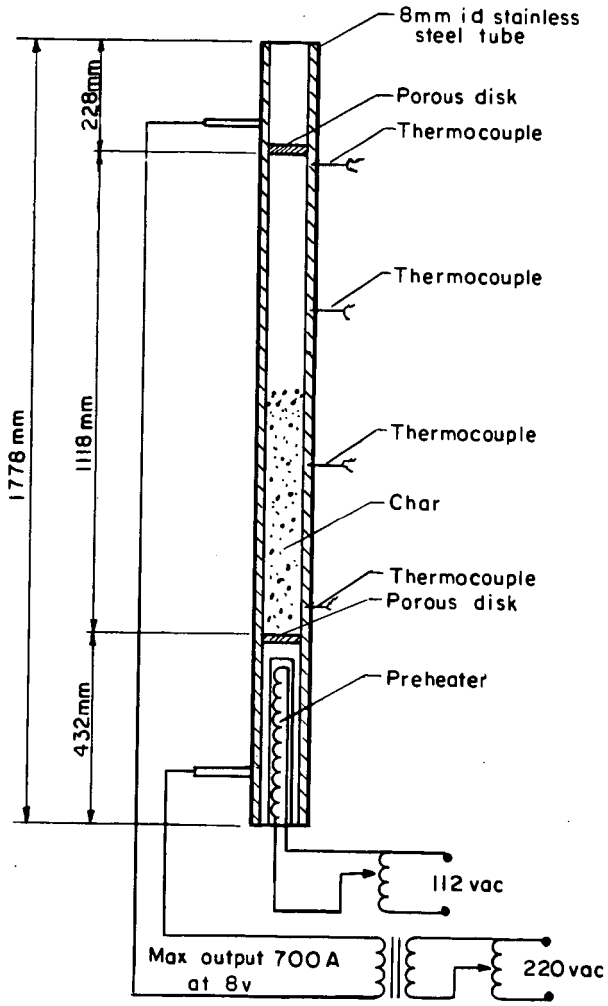


Figure 2—Details of reactor.

L-14325

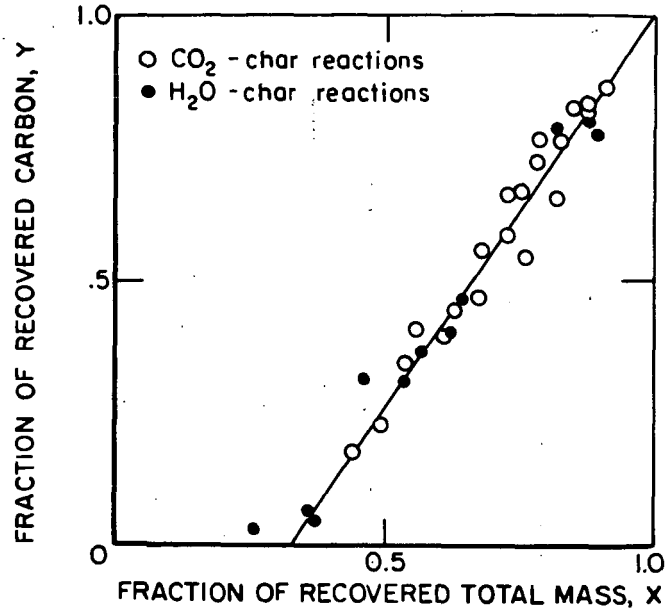


Figure 3—Relationship between the converted carbon and the mass loss

L-14326

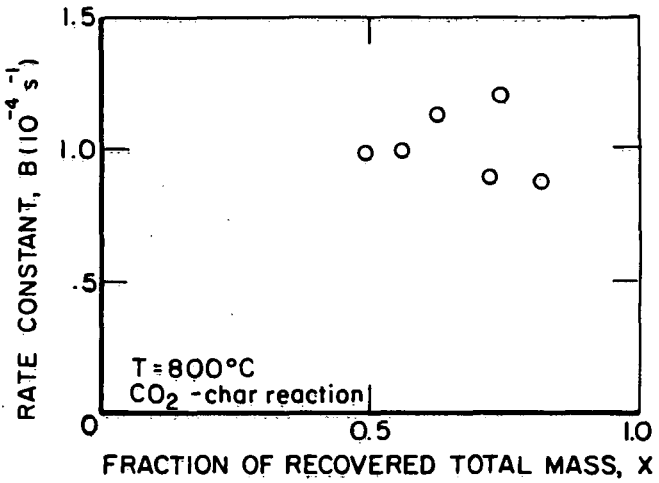


Figure 4—Test for 1st order reaction of the carbon conversion.

L-14327

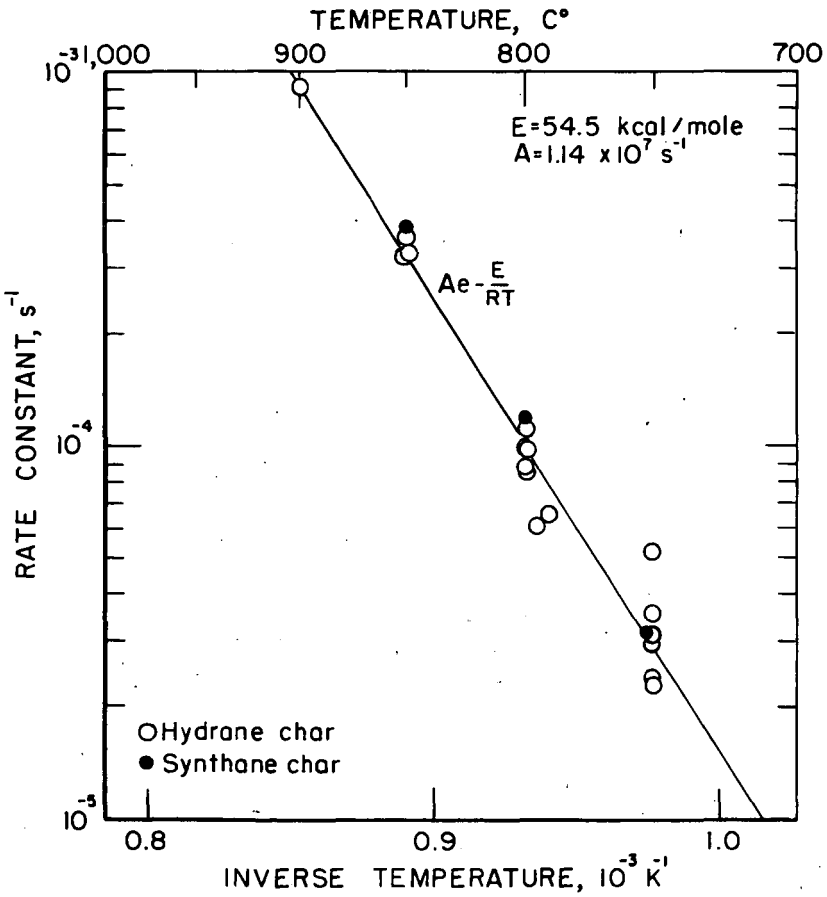


Figure 5—Gasification rate constant for the reaction of $CO_2$ with char.

L-14328

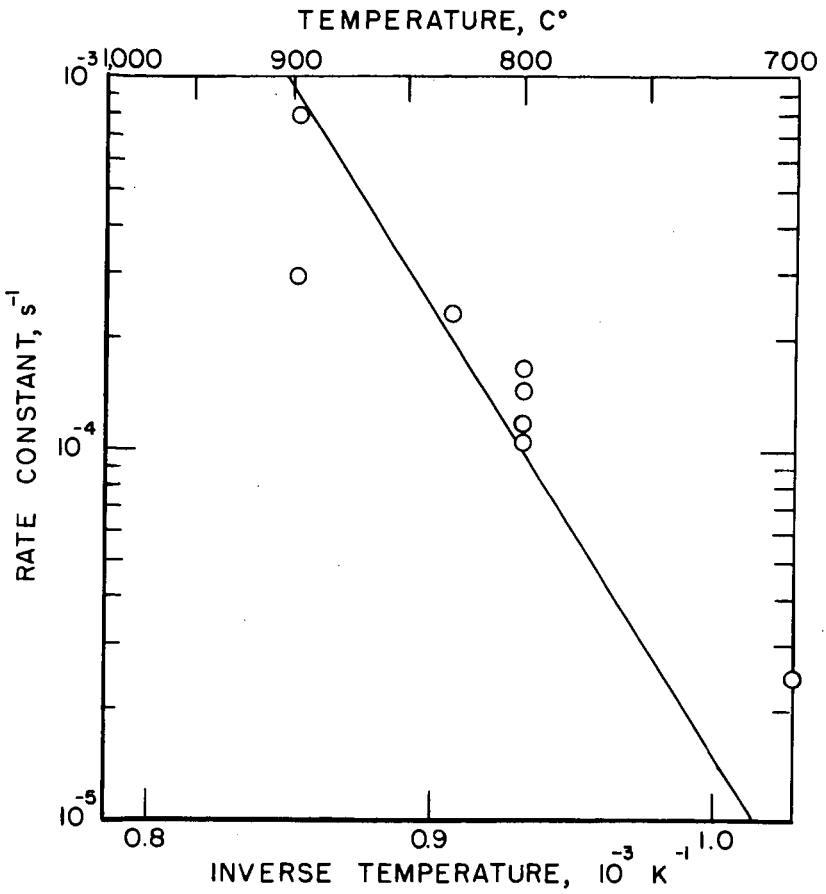


Figure 6—Gasification rate constant for the reaction of steam with hydrane char (The continuous line represents the rate constant for the $CO_2$ char reaction)

L-14329

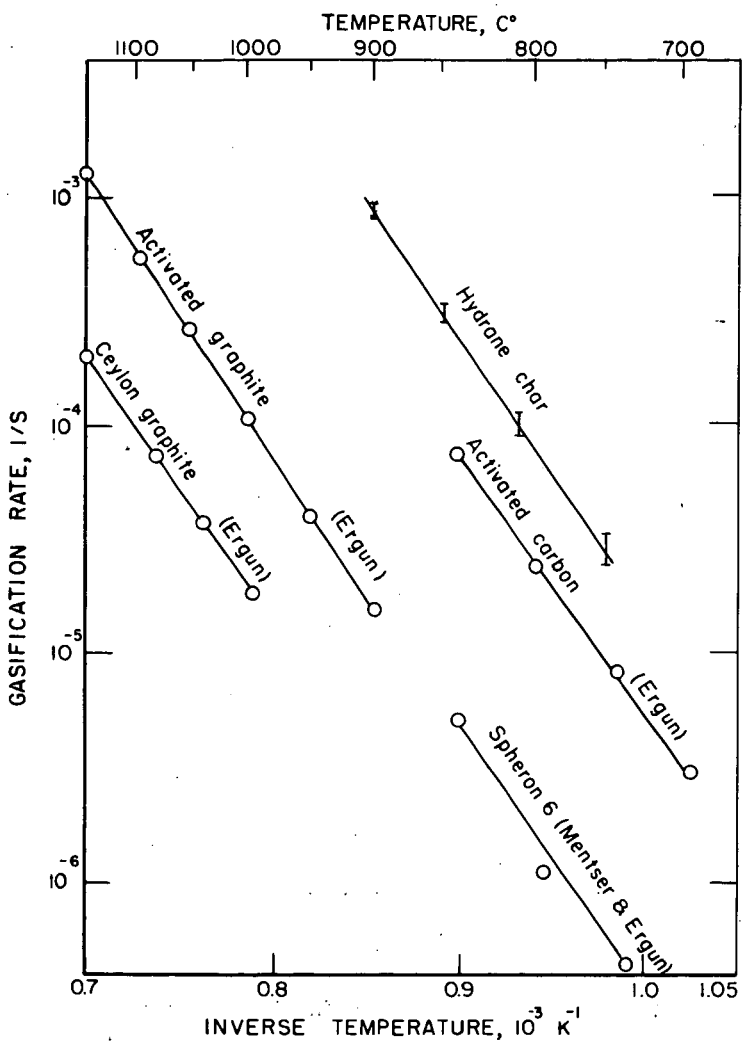


Figure 7 — Temperature variation of gasification rate constants of graphite and carbons.

L-14330

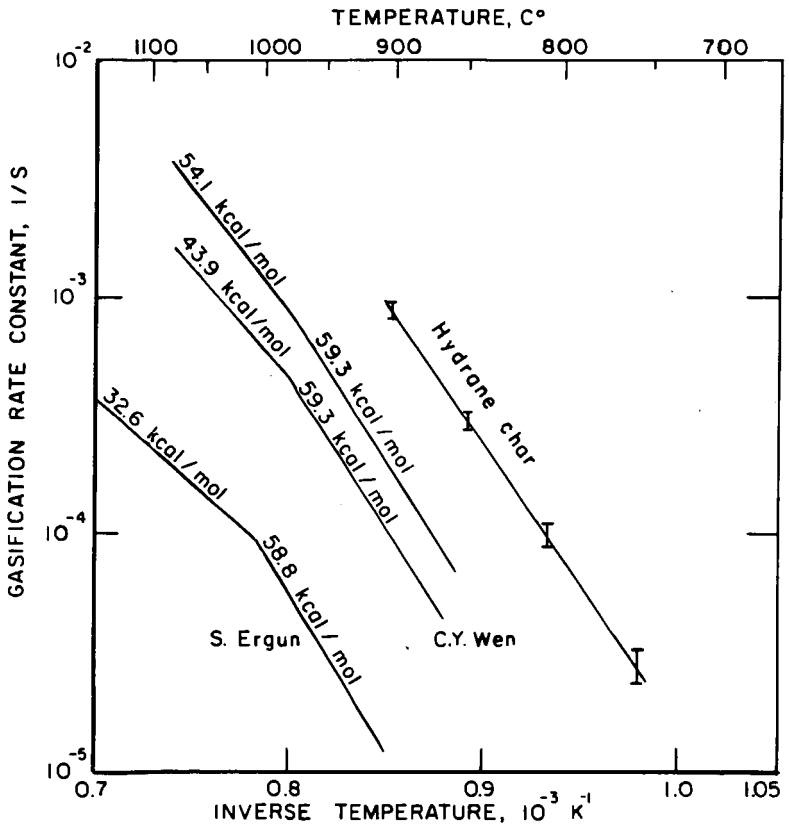


Figure 8—Temperature variation of gasification rate constants of cokes and chars.

L-14331

# PULVERIZED CHAR COMBUSTION IN A LABORATORY SCALE FURNACE

R. H. ESSENHIGH
and
J. G. COGOLI

COMBUSTION LABORATORY
FUEL SCIENCE SECTION
MATERIAL SCIENCES DEPARTMENT
THE PENNSYLVANIA STATE UNIVERSITY
UNIVERSITY PARK, PA. 16802

## INTRODUCTION

Due to the existing energy situation, many different coal gasification and liquefaction processes are in various stages of development at the present time. All these processes produce at least some charbonaceous residues or chars as by-products or perhaps coproducts. In some cases however, the char is used on site internal to the particular coal conversion scheme being employed. Other processes will have a negligible net yield of char for external consumption, and still others may produce char in considerable quantities amounting to as much as 50 percent of the raw coal feed to the plant. A study performed by Battelle Memorial Institute (1) stresses the need for markets to be found for the char produced from conceptual full-scale coal processing plants. They cite as examples yields of 4.4 million tons of char per year from a Consolidation Coal Company liquefaction plant producing 55,000 barrels of liquid petroleum per day at a depth of conversion of 50 percent, and 1.7 million tons per year from an FMC COED plant processing 3.5 million tons of coal per year. The ability to efficiently use these yields of char is of serious concern if full scale plant operation is to become a reality. The long term objective of the present continuing study is to determine the combustion characteristics of various coal chars in order to determine the suitability of the chars produced from various coal conversion processes for use in conventional combustion chambers, especially water-wall utility boiler furnaces.

The work reported here represents only the first stage of this continuing research project, and as such, serves mainly to make some general observations about the combustion of various coal chars and to identify the pertinent questions and research goals that will be examined in future critical detailed experiments.

## EXPERIMENTAL APPARATUS

The experimental flames discussed in this report were generated in a vertical furnace termed the plane-flame furnace. The present version of the furnace is patterned after the one previously used by Howard and Essenhigh (2). The furnace is of square cross section, 16.5 x 16.5 cm inside dimensions, with the chamber walls constructed of insulating brick (6.35 cm thick) and encased in transite sheet insulation (.48 cm thick). The combustion chamber is approximately 2 meters long and is topped by a two-row staggered tube bank of water cooled tubes. On top of the tube bank assembly is a sheet metal mixing chamber, a pyramid in shape and 72 cm high. The pulverized fuel and primary air enter the top of the mixing chamber through a jet directed vertically upward, and the secondary air enters through a jet directly opposed to and impinging on the pulverized fuel and primary air jet. The two air streams and the pulverized fuel mix thoroughly in the mixing chamber and the resulting dust cloud then passes through the staggered tube bank into the combustion chamber below. The tube bank ensures that the dust cloud remains at ambient conditions until it actually enters into the combustion chamber proper and forces the resulting flame to stabilize in the square cross section combustion

chamber. The flames produced in this manner will stabilize with a flat flame front somewhere along the extent of the combustion chamber, with the flame itself extending throughout the remaining portion of the chamber and passing out the flue connecting section to the stack. A set of observation and sampling ports is distributed along the vertical axis of the furnace on the front wall and wall thermocouples, flush with the inside of the furnace wall, are located on the back wall.

The essential feature of the plane-flame furnace is the absence of recirculation currents, i.e., backmix flow in the combustion chamber. Howard (3) verified this fact with detailed helium tracer experiments. No recirculation of hot combustion products means that the history of material gathered at a particular point in the furnace is able to be unambiguously specified.

The flames produced in the plane-flame furnace are stabilized by radiation heat transfer, with conduction and convection playing completely negligible roles. The incoming dust cloud emerges from the tube bank and the fuel particles are heated by radiation from the combustion zone lower in the chamber. The gas is primarily heated by conduction from the hot particles, and when the mixture ignites and proceeds to combust, the hot dust cloud in turn radiates back to the incoming cold cloud and the whole process continues in a selfsustaining manner.

The design and operation of the plane-flame furnace is characterized by the following summary description:

1. No recirculation of combustion gases.
2. All secondary air is added to primary air/fuel mixture before entrance to combustion chamber.
3. No supplementary fuel is fired with the experimental fuel being studied.
4. No preheat of secondary air or primary air/fuel streams.
5. Combustion environment in a utility boiler is simulated.

The last item in the summary above is not obvious since a chamber roughly half a foot on a side and seven feet tall does not seem to resemble a boiler furnace that might be forty feet on a side and perhaps a hundred or more feet high. Both chambers have residence times on the order of 1 second and peak gas temperatures around 1500 - 1600°C. Thus, the plane-flame furnace does simulate quite adequately the combustion environment in a full scale utility boiler.

## PLANE-FLAME FURNACE RESULTS

After the reconstruction of the plane-flame furnace, the first fuel burned in the furnace was a Pittsburgh Seam bituminous coal, in fact, the same fuel that Howard (2, 3) studied. The flame front for the bituminous coal stabilized approximately 5 cm down from the bottom of the tube bank, as Howard had observed. This initial firing on bituminous coal served to verify that the reconstructed furnace behaved similar to Howard's original. As seen in Fig. 1, a variation on particle size was run with one fraction consisting of all particles above 88 microns, another with all particles above 44 microns and the last with all particles below 44 microns. Amazingly, no shift in flame front occured at all, but with a definite shift in wall temperature level present in the case of the smallest size fraction. It should be emphasized that most results presented in this study are displayed as plots of back wall thermocouple temperature versus distance down from the bottom of the tube bank. Suction pyrometer temperatures were obtained for some specific points for various fuels and those readings will be clearly specified as not being the usual wall thermocouple temperatures.

The next fuel burned in the plane-flame furnace was a Bureau of Mines char prepared from a high-volatile bituminous coal (Utah King A mine) in an entrained carbonizer at the Bureau's Grand Forks Station. The VM (volatile matter) content

of this char is 5.1 percent. Only a 20 pound sample of this char was available, meaning that only one short run could be made. In Fig. 2, the wall temperature profiles are shown for two different total air flow rates. The general shape of the profiles is radically different from the bituminous coal profile in Fig. 1. For the higher air flow rate, the flame front was approximately 55 cm from the tube bank, while for the lower air flow rate the flame front stabilized at about 40 cm. Also, it should be noted that the wall temperatures for most of the top half of the chamber become depressed and the ones in the bottom half are elevated with increasing air flow rate. This general tendency will be seen through the presentation of the results here.

The next fuel burned was an FMC COED char with a VM content of around 2.5%, the parent coal being an Illinois No. 6 coal (Peabody No. 10). Fig. 3 shows two wall profiles for this COED char, one for all particles less than 44 microns and the other for about 45 percent (by weight) smaller than 44 microns. The shift in flame front from 55 cm back to 37 cm from the tube bank is quite significant since only a relatively minor change of particle size distribution was involved. Recall that the bituminous coal showed no flame front shift for considerably more radical changes in particle size.

In connection with the study of coal chars, other low volatile fuels, specifically anthracite coals, were burned in the plane-flame furnace. Fig. 4 shows the wall profiles for some anthracite runs. The regular grind anthracite profiles in Fig. 4 correspond to times soon after (early) and about 1 hour after (later) the preheated chamber was switched over to the anthracite coal. This particular anthracite is actually an anthracite silt with about 8.5 percent VM which is fired in utility boilers in the Hunlock Creek Station of the Luzerne Electric Division of U.G.I. Corporation. The silt is very finely ground with about 75% smaller than 44 microns and only 4 percent larger than 88 microns. The wall temperatures fell progressively with time until after about 90 minutes after switchover, the flame extinguished. At no time did the wall temperatures stabilize, thus this run was under strictly transient conditions. Also plotted in Fig. 4 is the profile for an ultra-fine grind Anthracite (5-10 Microns) for approximately the same firing conditions. This profile was stable without a doubt in this case, with the flame front located about 40 cm from the tube bank.

Two different low volatile fuels also became available for experimental purposes after the anthracites were run. These two fuels are Exxon chars produced at the Exxon Baytown Research and Development Division. One char is produced from a Wyodak coal (Wyodak Resources Development Company Mine) and the other from an Illinois coal (Monterey Coal Company No. 1 Mine). Preliminary runs with these chars (7-9 percent VM) indicated that their combustion characteristics were more like bituminous coal than the other low volatile fuels described previously. It was decided to run the previously described COED char and the two Exxon chars under controlled conditions to see how these three fuels would behave under similar experimental conditions.

The conditions chosen for the standarized runs were net heat input close to 100,000 Btu/hr and preset stepped total air flow rates. The proximate analyses, moisture contents, heating values and fuel feed rates are shown in Table 1. (see next page) The total air flow rate values chosen are given below along with their designated symbols: A, 8.76 SCFM; B, 11.55 SCFM; C, 13.76 SCFM and D, 17.79 SCFM. For this series of runs, each fuel was pulverized so that 45 percent was finer than 44 microns. Figures 5 - 7 represent the wall temperature profiles for the COED, Exxon Wyodak and Exxon Illinois chars respectively. Figure 5, the FMC COED plot, contains plots for only conditions A and B, the other conditions could not be stabilized. However, in Figure 5 the same COED type profile is seen as in Fig. 3 discussed earlier. Again the flame front positions are quite far removed from the

TABLE 1

EXPERIMENTAL CONDITIONS FOR STANDARDIZED CHAR RUNS

| CHAR TYPE | FMC | EXXON WYODAK | EXXON ILLINOIS |
|---|---|---|---|
| % VM | 2.97% | 8.84 | 7.83 |
| % FC | 76.03% | 69.91 | 68.17 |
| % ASH | 21.00% | 21.25 | 24.00 |
| % MOISTURE | 2.23% | 6.18 | 3.51 |
| LHV (BTU/LB) | 11,362 | 10,446 | 10,094 |
| FEED RATE (LB/HR) | 8.65 | 10.36 | 10.22 |
| NET HEAT INPUT (BTU/HR) | 98,280 | 108,220 | 103,160 |
| STOICHIOMETRIC AIR FLOW (SCFM) | 15.92 | 14.85 | 17.93 |

tube bank and a region of nearly linear wall temperature rise is followed by an almost isothermal zone. Samples of particulates were taken at a port 123 cm from the tube bank to obtain an estimate of the extent of particle burnoff. Table 2 has the burnoff values tabulated for all three chars.

TABLE 2

BURNOFF PERCENTAGES FOR STANDARDIZED CHAR RUNS (POSITION 123 cm)

| CHAR TYPE | FMC COED | EXXON WYODAK | EXXON ILLINOIS |
|---|---|---|---|
| % BURNOFF CONDITION A | 18.63 | 29.35 | 15.84 |
| % BURNOFF CONDITION B | 31.67 | 53.10 | 19.92 |
| % BURNOFF CONDITION C | -- | -- | 41.17 |
| % BURNOFF CONDITION D | -- | 77.43 | 47.47 |

Profiles for the two Exxon chars are plotted in Figures 6 and 7. Here the wall profiles look more like bituminous coal profiles at low air flow rates and tend to become more like the COED profiles at the highest flow conditions. For both the Exxon chars, the flame never moved more than 23 cm down from the tube bank.

One addition solid sample measurement was taken for the Wyodak char under condition A. A sample was taken just above the visible flame front (3 cm from tube bank) and the resulting burnoff value obtained from this sample was 2.37%. Due to the minute fluctuations of the flame front with time, a 5 minute sample might be expected to show some burnoff slightly greater than zero.

Also several suction pyrometer temperature measurements were taken during these standardized runs. The first reading was for COED (A) and showed the flame temperature 330 degrees above the local wall temperature of approximately 1250°C. A pair of suction pyrometer readings was taken at distances of 2 cm above and below the visible flame front for the Wyodak (C) char. A difference of about 400 degrees in flame temperature was observed in moving a total distance 4 cm across the flame front.

## DISCUSSION

The first point to be treated here is the use of the plane-flame furnace as a qualitative tool to order fuels according to their suitability for combustion purposes. As was mentioned earlier, the regular grind anthracite silt as burned by UGI failed to stabilize, while the COED char can be stabilized at low air flow rates. Taking account of this experimental fact, FMC and UGI arranged a full scale COED char firing of one of UGI's anthracite burning boilers (4). The parent coal of this char is a Utah high volatile - B bituminous coal from the King Mine. The tests were successful with the essential result being that when firing the COED char 8 percentage points in boiler efficiency were gained (73 percent to 81 percent) even with the minimum excess air limited to 45 percent due to the boiler control system. At lower values of excess air, the gain in efficiency might have been still greater. Thus, the plane-flame furnace has already been used as a test to order fuels according to combustion suitability.

It should be noted that the Bureau of Mines has burned the 5 percent VM Bureau of Mines char and the 2.5 percent FMC COED char in their 500 pound per hour experimental furnace. They found in the case of the COED char (6) that for a secondary air preheat temperature of 600°F, 14 percent of the furnace heat input had to be supplied by auxillary natural gas at a primary air/char preheat temperature of 250°F to obtain stavility, decreasing to no natural gas at a primary air/char temperature of 450°F. For the 5 percent Bureau of Mines char approximately 15 percent of the heat input had to be supplied by natural gas with no primary stream preheat and a 700°F secondary stream preheat for a stable combustion condition. As mentioned earlier, the plane-flame furnace uses no preheat of either input stream and no supplefuel. Based on arguments based on radiative heat transfer scaling effects, the small ceramic-walled plane-flame furnace tends to be a better utility boiler simulation than the medium sized (12 ft x 7 ft x 5 ft) water-cooled Bureau of Mines furnace.

Secondly, the subject of particle size was mentioned several times in the previous section. The fact that the regular grind UGI anthracite (75 percent finer than 44 microns) could not be stabilized and that the ultra-fine grind anthracite did stabilize is of general importance in the area of low volatile fuel combustion. Smith and Tyler (5) have studied the reaction of a semi-anthracite with oxidizing atmospheres with four distinct size fractions being used. Only when they dealt with their 6 micron size fraction did the results indicate complete penetration of oxidant into the pore structure. This fact together with

the 40 kcal/mole activation energy for the 6 micron fraction versus the 20 kcal/mole value for the 22, 49 and 78 micron size fractions clearly points to the value of around 6 microns where pure chemical control takes over from the combined chemical and pore diffusion region. This size limit for coals of similar microstructure seems to account for the difference in behavior between the two anthracite samples burned in the plane-flame furnace.

Certainly, the most important topic of discussion here is the extreme difference in the combustion behavior displayed by the two Exxon chars and bituminous coal on the one hand and the anthracites and the other chars on the other. The key point in characterizing the combustion behavior of fuels in the plane-flame furnace is the distance between the flame front and the water-cooled tube bank. The argument behind this decision is based on the thermal ignition theory of flowing systems as first proposed by Vulis (8). In this theory the position of the flame front is determined by the heat balance criterion being simultaneously applied to a set of control volumes composing the flowing mixture from the cold inlet to the chamber exit. For a given stoichiometry, set of reaction kinetics and flow conditions, the temperature profile of the entire flame can be solved for by the simultaneous solution of all the heat balances of the elemental volumes in the system. The solution of these equations must be iterative because each volume element is coupled by radiation to every other volume element in the chamber and to every element of surrounding wall area. A computer simulation of plane-flame furnace behavior has been tested in a simplified form using the char kinetics of Field (9,10) and the Hottel zone method of radiative analysis (11). Preliminary solutions do mirror the effects of increased air flow rates on lowering the earlier temperatures in the flame, displacing the flame front from the tube bank, and elevating the later temperatures in the chamber. Reactivity variations show the trend that higher reactivity fuels will stabilize closer to the tube bank. This fact should be expected because a highly reactive fuel can release more heat per unit volume at a given temperature and consequently for the same rate of heat loss to a cold heat sink. Thus, flame front position is a sound basis on which to compare fuel reactivities on a semi-quantitative basis.

The major question is why do the two Exxon chars behave differently than the other low volatile fuels. The historical approach to characterizing fuel reactivity by simple testing has been by proximate analysis, specifically volatile matter. On a dry ash free basis, the chars and anthracites have the following VM values: ultra-fine anthracite, 10.1%; U.G.I. anthracite silt, 6.9%; Bureau of Mines char, 5.9%; Exxon Wyodak char, 11.2%; Exxon Illinois char, 10.3%; and FMC COED char, 3.8%. The VM content concept obviously cannot explain the observed differences in combustion behavior since all the values tend to be very closely grouped and the lower reactivity fuel will sometimes have the higher VM content of a pair of these fuels.

For the chars, the quantity known as the fixed carbon conversion percentage is a quantity of usual interest. This percentage is defined as the absolute change in fixed carbon content from raw coal to char based on a unit weight of dry coal divided by the original absolute weight of the fixed carbon content of a unit weight of dry raw coal. The fixed carbon (FC) conversion figures for the chars are as follows: Exxon Illinois char, 45.1%; Exxon Wyodak char, 45.7%; Bureau of Mines char, 30.5%; and FMC COED char, 16.4%. As a comparison, Stacy and Walker (12) studied five FMC COED chars whose FC conversion percentages ranged from 9% to 23%. Thus, the COED char studied here can be considered typical. A pattern starts to emerge from the above values for the chars. The two Exxon chars have received quite heavy gasification treatment, the Bureau of Mines char probably an intermediate treatment and the COED char only very light treatment. The COED process is known to involve multistage pyrolysis in fluid bed reactors at temperatures from 320 °C to 870 °C and a light partial combustion (about 10% by weight combustion loss) to heat the pyrolysis stages (12). Only when the FC conversion concept is linked to the concepts of available surface area and pore size distribution does it take on any physical significance in relation to char reactivity.

Two different gas adsorption areas have come into common use to characterize

particulate fuels. The area calculated from nitrogen adsorption at 77 °K is considered to represent the external area of the particle plus the areas in pores larger than about 5 Angstroms, while the area calculated from carbon dioxide adsorption at 298 °K is considered to be the best approximation to the "total surface area of coals" (13). Stacy and Walker (12) report that for the COED chars they tested, the nitrogen areas were typically lower by about 400 $m^2/gm$ than the carbon dioxide areas. Typical values reported are 100 $m^2/gm$ for nitrogen and 450 $m^2/gm$ for carbon dioxide. Other chars tested in the same study (HYGAS and $CO_2$ Acceptor) had both adsorption areas of comparable values averaging around 400 $m^2/gm$ . The two Exxon chars are reported to have nitrogen areas in the 300-425 $m^2/gm$ region for typical char products (14). Thus, the COED chars have far smaller nitrogen areas than carbon dioxide areas, and the Exxon chars have nitrogen areas that are 3 to 4 times the COED nitrogen areas. At the present time carbon dioxide areas for the Exxon chars are not readily available, but this does not hinder the logical pattern described above. Based on the above area figures, the two Exxon chars would be expected to be much more accessible to the attack of reactant gases than the more highly microporous COED char.

Considering anthracite coals, Gan et. al. (15) have recently shown that for all high rank raw coals (percent carbon on daf basis greater than 83% or from HVA to anthracite) the nitrogen areas are certainly less than 10 $m^2/gm$ with corresponding carbon dioxide areas of 200 to 450 $m^2/gm$ . On a surface area basis, it would be reasonable to assume that the regular grind U.G.I. anthracite would not be able to stabilize in the plane-flame furnace when other low volatile fuels with much less pore volume percentages contained in micropores were having some difficulty in stabilizing. Quantitatively, anthracites have been established as having 75% or more of their open pore volumes contained in micropores, with the remaining volume split between the transitional and macropores (15). The COED are reported to only have about 30% of their open pore volume contained in micropores and apparently negligible transitional porosity (12). Therefore, adsorption surface areas and pore size distributions seem to give some solid physical background to the observed reactivity differences found when the low volatile fuels are burned in the plane-flame furnace.

In support of this viewpoint, scanning electron micrographs have been taken as part of this low volatile fuel research project. The Exxon chars, the FMC COED char and the ultra-fine grind anthracite were photographed at magnifications of up to 10,000X. The Exxon chars have voids in the particles which are of the same order of magnitude as the particle dimensions themselves and some lacy fan-like structures have been observed. The COED char shows some voidage, but the apparently solid areas on the particle exteriors are flat planar surfaces with sharp corners and definite clevage edges. The Exxon chars are seen to be almost completely amorphous structures, while the COED char appears to have a high degree of order and organization in some of regions of the particle exterior. The ultra-fine anthracite shows no surface details even down to a scale as small as 500-1000 Angstroms. The SEM results seem to agree quite well, at least in a qualitative sense, with the surface area and pore size distribution argument presented above.

Although it has been recently shown that a strong correlation exists between the reactivity of chars prepared by a thermal treatment in a nitrogen atmosphere and the rank of the parent coal (16), the Exxon Illinois char has completely different characteristics than the FMC COED char which was also prepared from a similar Illinois parent coal. This fact suggests that the precise method of activation of a coal char in a process other than simple heating in an inert atmosphere can have a dominating influence on the reactivity of the resultant char. Although, it has been demonstrated that parent coals of high rank tend to yield highly microporous chars even with activation treatments that tend to open up the pore structures of much lower rank materials (16). Therefore, eventhough preparation method can be the dominating influence on a resultant char's reactivity, high rank parent coals usually will cause severe problems if a highly reactive char is desired.

At this point, some details about the standardized char runs shown in Figs. 5-7 will be brought out to make their meaning a little clearer. As stated previ-

ously, the aim of the set of experiments is to run all three chars at equivalent values of net heat input and total air flow rate. The nominal net heat input was chosen to be 100,000 Btu/hr and the stepped air flow rates are 8.76,11.55, 13.76 and 17.79 SCFM, as stated previously. In Table 1 it can be seen that the net heat inputs ranged from 98,280 to 108,220 Btu/hr. It is regretable that this nonuniformity exists. but it does not alter the conclusions based on the results of the standardized runs. Also, the values of the theoretical air needed for complete combustion of each char are tabulated in Table 1. Here the Exxon Illinois char has the highest value of 17.9 SCFM, the Exxon Wyodak char requires 14.9 SCFM and the COED char value is 15.9 SCFM.

Flame front position again was the major difference between the Exxon chars and the remaining fuel, in this case, the COED char. Even with the highest values of total air flow used, the Exxon Illinois and Wyodak chars moved no further than 20 and 23 cm respectively from the tube bank. The COED char on the other hand, could not be stabilized any closer than 54 cm from the tube bank at the lowest air flow rate. For condition B (11.55 SCFM air flow rate) , the COED flame front moved to 75 cm from the tube bank and for condition C (13.76 SCFM air flow rate) the wall temperatures fell continually at all thermocouple locations, indicating imminent extinction. All three chars showed the effect of increasing maximum wall temperature with increased air flow rate.

Table 2 contains the burnoff data based on particulate samples collected 123 cm from the tube bank. For all chars the burnoff values increased with increasing air flow rate. Some care must be used in comparing burnoff levels of different chars. As mentioned previously, the theoretical air requirements for the chars are somewhat different. The burnoffs for the COED char versus those for the Exxon Illinois char are higher than would normally be expected until the difference in theoretical air requirements is taken into consideration. The Wyodak char has the highest burnoff values and also has the lowest theoretical air requirement. This fact makes interpretation of the burnoff data rather difficult when comparing any two chars. However, it can be noted that for condition D (17.79 SCFM air flow rate) the Exxon Wyodak char has 77.43% burnoff at about 19%excess air, while the Exxon Illinois char yields 47.47% burnoff at nearly stoichiometric conditions. Another observation that can be made is that for the Exxon chars, only when the air flow rate approaches stoichiometric conditions does the early portion of the wall temperature profile become appreciably depressed and sloped, similar to the COED type profile. The added air flows experienced in going from condition A to conditions B and through to D permit combustion to take place appreciably downstream of the tube bank, as evidenced by the flatter wall profiles recorded. Although the total air flow was increasing from condition A to condition D, the chamber residence time was decreasing due to the increase of cold inlet flow and the higher gas velocities present at the higher resultant gas temperatures. Future furnace runs with detailed burnoff profiles obtained along the axis of the furnace at many different locations would establish exactly where the burnoff is taking place, and burnoff rates based on segment residence times could be calculated. Accompanying suction pyrometer reading profiles at the same locations would allow reasonable gas temperatures to be obtained simultaneously.

## CONCLUSIONS

The preliminary data and discussions presented here have demonstrated that coal chars can posses significantly different combustion characteristics, with the differences being due to parent coal rank, method of preparation, etc. It has also been shown that the plane-flame furnace has superior potential for char combustion research due to its unique design. In conclusion, if the use of coal chars in full scale combustion chambers is to become a technical reality, precisely designed critical experiments,based on the qualitative behavior reported here must be performed to put even preliminary design procedures on firm scientific foundations.

## Acknowledgments

We acknowledge support for this project from the Cooperative Combustion Laboratory Fund (Contributors: Alcoa, Babcock and Wilcox, Combustion Engineering, Inc., Exxon Research, General Electric Corp., Mobil Oil Corp., PPG Industries and Wingaersheek Corp.). Additional support also came from the Middle Atlantic Power Research Committee and NSF ERG Traineeship (awarded to J.G.C. 1973/1975). Acknowledgments for the supply of experimental fuels are made to: Exxon Research (Baytown, Texas),FMC Corp., Princeton, N.J., Bureau of Mines, Pittsburgh, Pa., U.G.I. Corp., and Dr. P. L. Walker, Jr., Material Sciences Dept., Penn. State University.

## References

1. Battelle Memorial Institute, "Study of the Identification and Assessment of Potential Markets for Chars from Coal Processing Systems", U.S.D.I. Contract No. 14-01-0001-1190.

2. Howard, J. B. and Essenhigh, R. H., Symp. (Intern.) Combust., 11th, Pittsburgh, p. 399,1967.

3. Howard, J. B., Ph.D. Thesis, The Pennsylvania State University, 1965.

4. FMC Corp., "The Combustion Performance of COED Char", ERDA Contract No. 14-32-0001-1212, R & D Report No. 73 - Interim Report No. 4.

5. Smith, I. W. and Tyler, R. J., Fuel, 51 , 312, 1972.

6. Demeter, J. J., McCann, C. R. and Bienstock, D., ASME Paper No. 73-WA/Fu-2, 1973.

7. McCann, C. R., Demeter, J. J., Orning, A. A. and Bienstock, D., Am. Chem. Soc. Div. Fuel Chem.,15, 96, 1971.

8. Vulis, L. A., "Thermal Regimes of Combustion", McGraw Hill, 1961.

9. Field, M. A., Combustion and Flame, 13, 237, 1969.

10. Field, M. A., Combustion and Flame, 14, 237, 1970.

11. Hottel, H. C. and Sarofim, A., "Radiative Transfer", McGraw Hill, 1967.

12. Stacey, W. O. and Walker,P. L., Jr., "Structure and Properties of Various Coal Chars", Report to Office of Coal Research, August 25, 1968, Contract NO. 14-01-0001-390.

13. Walker, P. L., Jr. and Kini, K. A., Fuel, 44, 453, 1965.

14. Private communication from Exxon Research, Baytown, Texas to J. G.C.

15. Gan, H., Nandi, S. P. and Walker, P. L., Jr., Fuel, 51, 272, 1972.

16. Jenkins, R. G., Nandi,S. P. and Walker, P. L., Jr., Fuel, 52, 288, 1973.

Fig. 1 -- Wall Temperature Profiles for Bituminous Coal

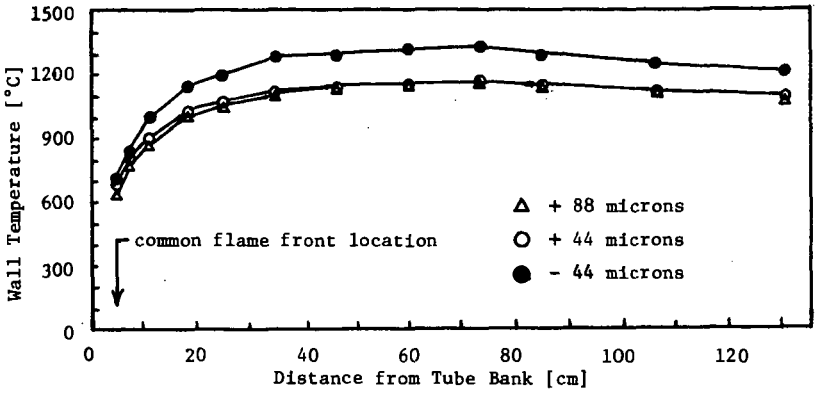


Fig. 2 -- Wall Temperature Profiles for Bureau of Mines Char

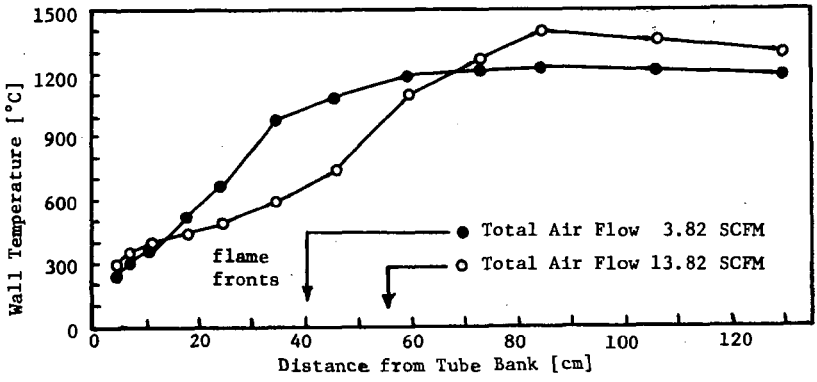


Fig. 3 -- Wall Temperature Profiles for FMC COED Char

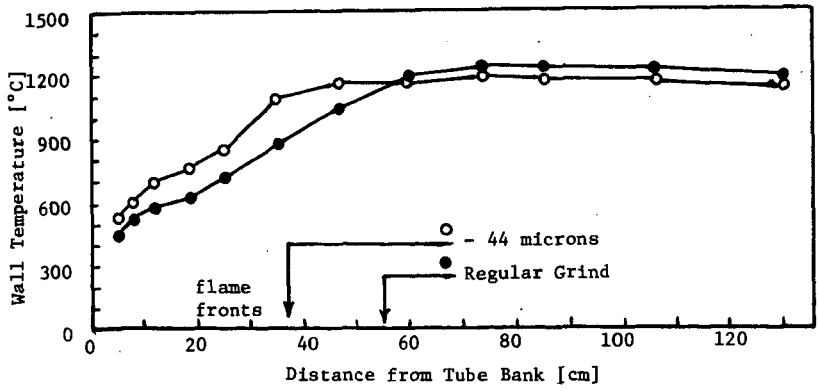

Fig. 4 -- Wall Temperature Profiles for Anthracite Coals

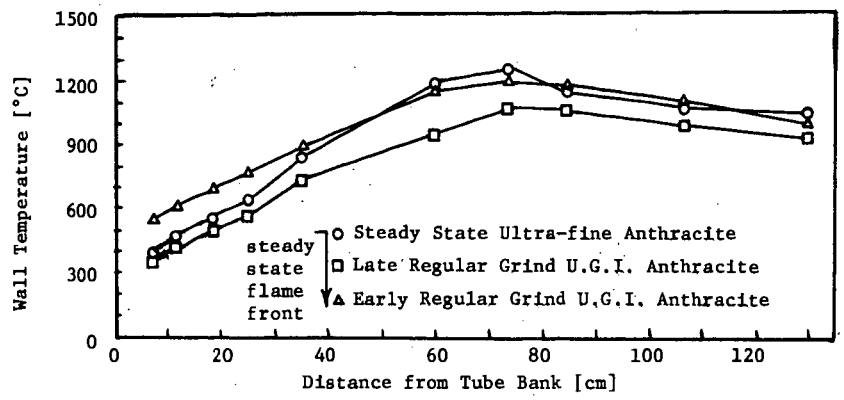


Fig. 5 -- Wall Temperature Profiles for Standardized COED Char Runs

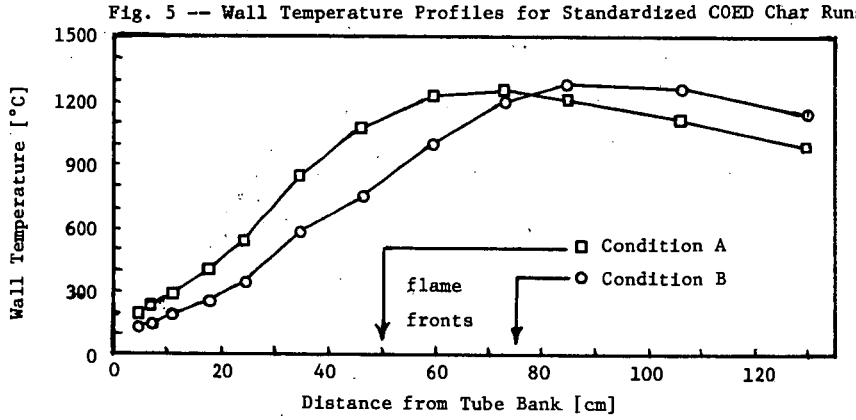


Fig. 6 -- Wall Temperature Profiles for Standardized Exxon Illinois Char Runs

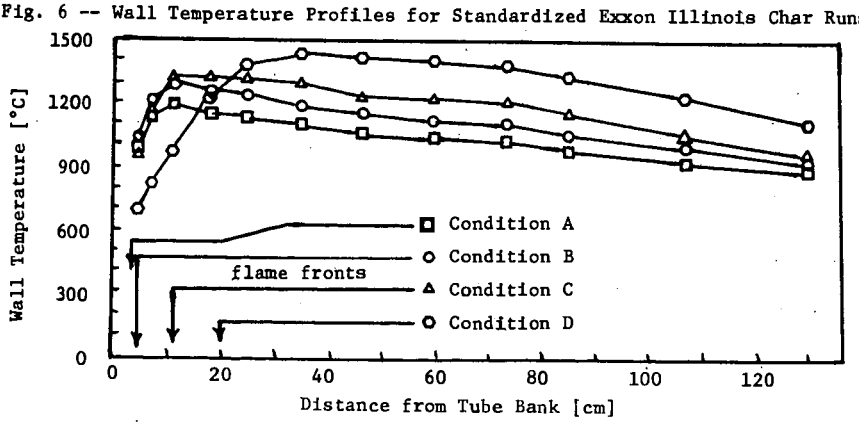

Fig. 7 -- Wall Temperature Profiles for Standardized Exxon Wyodak Char Runs